A TRIDENT SCHOLAR PROJECT REPORT

NO. 268

The Effect of Externally Retrofitted Carbon Fiber Reinforced Polymer Composites on the Ductility of Reinforced Concrete Beams

UNITED STATES NAVAL ACADEMY
ANNAPOLIS, MARYLAND

REPORT DOCUMENTATION PAGE

Form Approved
OMB No. 074-0188

1. AGENCY USE ONLY (Leave blank)

2. REPORT DATE
4 May 1999

3. REPORT TYPE AND DATE COVERED

4. TITLE AND SUBTITLE
The Effect of Externally Retrofitted Carbon Fiber Reinforced Polymer Composites on the Ductility of Reinforced Concrete Beams

5. FUNDING NUMBERS

6. AUTHOR(S)
Simmons, Duane K.

7. PERFORMING ORGANIZATION NAME(S) AND ADDRESS(ES)
U.S. Naval Academy
Annapolis, MD

8. PERFORMING ORGANIZATION REPORT NUMBER
USNA Trident Scholar project report no. 268 (1999)

9. SPONSORING/MONITORING AGENCY NAME(S) AND ADDRESS(ES)

10. SPONSORING/MONITORING AGENCY REPORT NUMBER

11. SUPPLEMENTARY NOTES
Accepted by the U.S. Trident Scholar Committee

12a. DISTRIBUTION/AVAILABILITY STATEMENT
This document has been approved for public release; its distribution is UNLIMITED.

12b. DISTRIBUTION CODE

13. ABSTRACT: This study investigates the effect of externally bonded carbon fiber reinforced plastic (CFRP) laminates on the ductility of reinforced concrete beams. Reinforced concrete structures deteriorate over time due to environmental aging, fatigue, excessive loading, chemical attack, and other factors. Strengthening and rehabilitating these concrete structures by externally bonding carbon laminates is one of many economical engineering solutions. Eight rectangular beams with varying internal steel reinforcement were retrofitted with CFRP strips on the tension faces and tested under four-point bending. The beams were instrumented to monitor strains, deflection, and curvature over the entire spectrum of loading, and determine the structural response of the beams. A computer-based method using strain compatibility and force equilibrium was developed to provide theoretical load-deflection and moment-curvature curves, and a basis for determining ductility and beam failure modes. An existing analytical model using the discrete yield and ultimate values of the load-deflection and moment-curvature curves was modified to an energy-based model and used to predict the ductility of the beams. Numerical results indicated an increase in strength, a decrease in ductility, and validated the analytical model. Ultimately, this study will aid in the development of design guidelines governing the use of CFRP.

14. SUBJECT TERMS
Fiber reinforced plastics, Deflection, Reinforced Concrete, Rehabilitation, Ductility

15. NUMBER OF PAGES

16. PRICE CODE

17. SECURITY CLASSIFICATION OF REPORT

18. SECURITY CLASSIFICATION OF THIS PAGE

19. SECURITY CLASSIFICATION OF ABSTRACT

20. LIMITATION OF ABSTRACT

U.S.N.A — Trident Scholar project report; no. 268 (1999)

The Effect of Externally Retrofitted Carbon Fiber Reinforced Polymer Composites on the Ductility of Reinforced Concrete Beams

by

Midshipman Duane K. Simmons, Class of 1999
United States Naval Academy
Annapolis, Maryland

D. Kevin Simmons
(signature)

Certification of Advisors Approval

Associate Professor Sarah E. Mouring
Department of Naval Architecture, Ocean and Marine Engineering

Sarah E. Mouring
(signature)

3 May 1999

Associate Professor Oscar Barton Jr.
Department of Mechanical Engineering

Oscar Barton Jr.
(signature)

4 MAY 1999

Acceptance for the Trident Scholar Committee

Professor Joyce E. Shade
Chair, Trident Scholar Committee

J. E. Shade
(signature)

4 May 1999

USNA-1531-2

ABSTRACT

This study investigates the effect of externally bonded carbon fiber reinforced plastic (CFRP) laminates on the ductility of reinforced concrete beams. Reinforced concrete structures deteriorate over time due to environmental aging, fatigue, excessive loading, chemical attack, and other factors. Strengthening and rehabilitating these concrete structures by externally bonding carbon laminates is one of many economical engineering solutions. Eight rectangular beams with varying internal steel reinforcement were retrofitted with CFRP strips on the tension faces and tested under four-point bending. The beams were instrumented to monitor strains, deflection, and curvature over the entire spectrum of loading, and determine the structural response of the beams. A computer-based method using strain compatibility and force equilibrium was developed to provide theoretical load-deflection and moment-curvature curves, and a basis for determining ductility and beam failure modes. An existing analytical model using the discrete yield and ultimate values of the load-deflection and moment-curvature curves was modified to an energy-based model and used to predict the ductility of the beams. Numerical results indicated an increase in strength, a decrease in ductility, and validated the analytical model. Ultimately, this study will aid in the development of design guidelines governing the use of CFRP.

Keywords: Fiber Reinforced Plastics, Deflection, Reinforced Concrete, Rehabilitation, Ductility

ACKNOWLEDGMENTS

There are many individuals without whom this project would not have been possible. First and foremost, I acknowledge the assistance of Associate Professor Sarah Mouring and Associate Professor Oscar Barton, who directed and guided me through every step of the project. I am also grateful to Larry Clemens at the Naval Academy's Nimitz Library for his tireless efforts to keep me supplied with the most obscure and difficult-to-locate journals and articles I requested.

The work presented here is part of a program of research into the ductility of reinforced concrete beams fiber retrofitted with reinforced plastic being conducted at the United States Naval Academy and the National Institute of Standards and Technology (N.I.S.T). The writer is a member of the Trident Scholar Program, an independent research program sponsored by the United States Naval Academy. The experimental research outlined herein was partly funded by the Structures Division of the Building and Fire Research Laboratory of N.I.S.T. The writer wishes to acknowledge the contributions of Dr. Nicholas J. Carino and Dr. Dat Duthinh of NIST, as well as the contributions of Dr. Hota V. GangaRao of the Constructed Facilities Center at West Virginia University who was never too busy to entertain questions or even a visit. Also acknowledged are Frank Davis, Steve Johnson, Max Peltz, and Andre Witcher of the NIST Structures Laboratory for their guidance in preparing the test specimens and Mr. William Beaver of the USNA Technical Support Division whose genius helped to make the presentation a success.

TABLE OF CONTENTS

LIST OF TABLES

LIST OF FIGURES

NOMENCLATURE

The following symbols are used in this paper:

A_s = tensile steel reinforcing area

A_{com} = CFRP laminate reinforcing area

b = nominal width

d = beam effective depth

c = depth to the neutral axis

h = nominal depth

E = elastic modulus of steel (Young's modulus of steel)

E_c = elastic modulus of concrete

E_l = elastic modulus of CFRP laminate

f'_c = compressive strength of concrete

f_y = yield strength for steel

f_{ult} = ultimate strength of laminate

M_a = applied moment

M_n = nominal strength

n = the ratio of ultimate laminate strength to steel yield strength

ρ = reinforcement ratio

ρ^* = adjusted reinforcing ratio

μ_Δ = deflection ductility index

μ_ϕ = curvature ductility index

Δ = deflection

Φ = curvature

ε = strain

α = Compositeness Reduction Factor

ε_{cu} = ultimate concrete strain

a = depth to the resultant compressive force

CHAPTER 1
INTRODUCTION

1.1 Background

Constructed infrastructure is essential for the development and progress of commerce and industry in all countries. It is well known that the national infrastructure is in need of major repair and rehabilitation since many buildings, highways, bridges, airports, and transit systems are deteriorating at a rapid rate. The increasingly rapid deterioration of infrastructure is becoming a principal problem facing construction industries worldwide, and finding a solution to this problem has become a challenge facing both researchers and engineers in the construction industry. Engineers are confronted with the continuous challenge of developing new methods to repair, replace or rehabilitate existing structures.

Traditionally, steel and concrete have been the most commonly used materials in civil infrastructure for a number of years. However, the deterioration of reinforced concrete structures has become a serious problem in the last decade specifically as a result of the corrosion of steel reinforcement in concrete structures. As time passes, corrosion produces deep pitting and a severe loss of cross section of reinforcing steel. This condition usually results in expensive repairs or catastrophic failure. The strengthening or upgrading of damaged steel members in predominantly steel structures is relatively simple. Through the use of welding or mechanical connections, additional steel can be added to increase the load-carrying capacity of a beam or girder. Unfortunately, this is not so easily accomplished with reinforced concrete structures.

The last decade has been marked by numerous repairs of concrete infrastructure made necessary mainly by the corrosion of steel reinforcement. In Canada, it is estimated that the repair cost of parking garages is in the range of $6 billion while in Europe, steel corrosion has been estimated to cost about $3 billion per year. The United States Federal Highway Administration has determined some 40% of the 575,000 bridges in the United States to be structurally deficient or functionally obsolete (Childs 1999) and that the estimated repair cost for existing highway bridges to be $50 billion. The estimated cost to repair all of the damaged concrete structures in the United States was $3 trillion in

1990. Much of the cost stems from corrosion of steel reinforcement inside concrete structures (Childs 1999). This situation has been accelerated in parking garages and bridge decks due to the use of de-icing salts and significant fluctuations in temperature. The extensive use of deicing chemicals on concrete bridge decks and the exposure of reinforced concrete infrastructure to chemicals (e.g., in parking garages, chemical plants, and water and wastewater treatment facilities) and marine environments encourages corrosion of the reinforcing steel in concrete structures. Deterioration in all types of reinforced concrete structures is further aggravated by excessive concentrations of chlorides in construction materials, by high humidities and temperatures, and by marine environments. The construction industry is urgently in need of non-corrosive materials as alternatives to steel reinforcement.

To remedy this problem, various solutions ranging from replacement of the structure to strengthening with a variety of techniques have been proposed. In addition, many methods to counter the threat of corrosion in steel reinforcement such as epoxy coatings, cathodic protection, increased concrete cover thickness, and polymer concrete have been tried, but none of these measures has provided a long-term solution. For example, one of the methods presently used to strengthen concrete beams is the addition of epoxy bonded steel plates to the tension flange of the beam. Bonding steel plates to the tension flange increases both the strength and stiffness capacity of the member and reduces cracks; however, a severe disadvantage of this technique is the corrosion of the steel plate. Corrosion damages the bond and eventually results in the failure of the structure. Until recently, there has not been a reliable and economical method of repairing or upgrading steel reinforced concrete beams, short of demolition and replacement. Civil engineers have begun to explore the use of advanced composite materials (ACMs) initially used in aircraft technology because of their high strengths and stiffnesses, as promising solutions to the corrosion problem.

In general, a composite can be defined as a combination of two or more materials, essentially without chemical interaction and insoluble into one another, such that some specific properties of the combination are better than those of the individual constituents. Fiber reinforced composites have a basic advantage in that they can be fabricated from a wide variety of reinforcement and matrix materials, so that a designer can choose and

tailor constituents based on specific design requirements/considerations. The mechanical properties such as strength, stiffness, toughness, and fatigue strength of the "composite" are generally significantly different from those of the matrix and fibers themselves. These properties depend on the volume of the fibers used in the composite, and can be obtained based on a mechanics of materials approach.

The term fiber reinforced plastic/polymer (FRP) describes a group of advanced composite materials composed of synthetic or organic fibers embedded in a resin. In advanced composite materials, the fibers are oriented at high volume fractions in the directions of significant stress in order to maximize the utility of the fibers. The most common FRPs consist of continuous fibers of glass, aramid, or carbon embedded in a polymer resin matrix such as polyester, epoxy, or vinylester and are called carbon FRP (CFRP), aramid (AFRP), and glass FRP (GFRP).

1.2 State of the Art

In recent years, there has been a surge of activities in the civil engineering research community to test and demonstrate the viability of these new materials for the construction of more durable structures and for the repair and rehabilitation of existing structures. Many creative applications of fiber composites have been developed by researchers around the world, such as reinforcing and prestressing concrete structures, seismic retrofitting of concrete and unreinforced masonry structures, and strengthening of buildings and bridges etc. The efforts of these researchers have resulted in many successful demonstration projects.

Significant advancements in the use of composites have been made not only in the research sector, but also in other specialized sectors of the construction industry over the last few years. If correctly applied in the infrastructure area, composites can result in significant benefits related to both overall cost and durability. Composites offer engineers many other advantages such as high tensile strength and stiffness-to-weight ratios, low weight, resistance to electrochemical corrosion and chemical attack, controllable thermal expansion, high fatigue strength, high damping characteristics, and electromagnetic neutrality. These advantages can lead to increased safety and life cycle, as well as provide savings in fabrication, equipment, and maintenance costs. It is now

generally recognized that the use of CFRP sheets, as externally bonded non-metallic reinforcement, is a practically efficient and technically sound method of strengthening and upgrading structurally inadequate or otherwise damaged or deteriorating load-bearing members (Saadatmanesh and Ehsani 1991; Ritchie et al. 1991). CFRP is a high strength, lightweight composite material that consists of high strength carbon fibers continuously bonded to a polymer resin matrix.

The use of fiber reinforced plastics (FRP) for structural repair presents several other advantages which are being investigated internationally (Saadatmanesh and Ehsani 1991a, b; Chajes et al. 1994; Meier and Kaiser 1991; Baaza et al. 1996; Arduini and Nanni 1997). Thus far, these investigations have focused primarily on the strengthening properties of FRP on virgin reinforced concrete beams; however, recent studies have raised questions such as whether the application of FRP changes the mode of failure of a flexural member from ductile to brittle (Arduini and Nanni 1997).

In spite of the recent successes in the limited use of fiber composites in the construction industry, a thorough knowledge of the behavior of these materials is a prerequisite for continued and successful application of these materials. Although the use of advanced composite materials in construction is expanding, the general civil/structural community lacks knowledge regarding new ACM applications and future applications under development. In order to expand the use of ACMs, more needs to be done to educate the general engineering community about them. A definite obstacle to eliminating the present lack of familiarity with ACMs and for the more widespread acceptance of ACMs by civil engineers is the lack of national standards, codes, and guidelines covering the design and fabrication of ACM structural components. Until a set of definitive design standards, codes, and guidelines comparable to those for concrete, wood and steel is developed, civil/structural design engineers will remain hesitant to use ACMs.

Recently, the American Concrete Institute (ACI) has put together Committee 440H, a task force to develop a set of guidelines for design with FRP. These guidelines are targeted for publication by early 2000. This paper presents the results of experimental and analytical studies on the question of ductility to aid in the development of this ACI FRP design code.

1.3 Essence of the Problem

The nature of concrete is such that it naturally undergoes catastrophic brittle failure. Unlike concrete, tension steel undergoes plastic deformation past its yield point. Typically, in a reinforced concrete beam, the steel yields before the concrete crushes in compression and the beam fails in a controlled, observable, ductile manner. However, like other advanced composites, CFRP is unlike steel because it does not have a yielding plateau or region. It is a brittle material and shows totally linearly elastic behavior until failure, thus making it difficult to incorporate into a system and still achieve ductile behavior. Tests on reinforced concrete beams with CFRP sheets bonded to the tension face show that although the CFRP reinforcement is effective in enhancing both stiffness and strength, catastrophic failure occurs when the beam load capacities are reached (Ritchie et al. 1991, Spadea et al. 1998).

There are three principal classifications of the failures in reinforced concrete beams. They are dependent on the amount of steel or tension reinforcement in the beam. If there is insufficient steel to carry the tensile load, the steel will yield before the concrete crushes. This is a tension or ductile failure. If there is an excess of tension reinforcement, the concrete crushes suddenly and explosively before the steel yields. This undesirable mode of failure is called a compression or brittle failure. A balanced failure is said to occur at the transition point between a tension and compression failure. In this case the concrete crushes at the same time the steel yields.

The reinforcement ratio, ρ, is defined as the area of steel in tension, divided by the area of concrete in compression. Existing American Concrete Institute (ACI) building codes specify that ρ must fall between two limits dependent upon the yield strength of the reinforcing steel, f_y, and concrete compressive strength, f'_c, in order to achieve safe ductile failure. In this fashion, ρ has commonly been used as an indicator of failure mode and hence ductility in reinforced concrete beams. However, due to the introduction of brittle FRP as additional tension reinforcement in reinforced concrete beams, ρ as conventionally defined can no longer be used to predict failure mode and ductility. The effect of FRP on the reinforcement ratio, failure mode and ductility is still unknown. This research investigates the effect retrofitted FRP has on the ductility of a reinforced concrete beam.

1.4 Research Significance

The continuing deterioration of the nation's infrastructure highlights the need for effective means of rehabilitating structures. One possible solution is to replace or supplement existing steel with non-corrosive materials like FRP, but most engineers are hesitant to design with FRP because: (1) they are not familiar with FRP, (2) there is no existing design code, and (3) a new design philosophy different from that governing steel reinforcement would be needed. Since no codes or construction guidelines currently exist for the design of structural members with FRP, this research provides important information on the ductile response of FRP repaired beams to assist in the development of design guidelines. This research demonstrates the feasibility of reinforcing concrete beams externally using FRP laminates and provides additional support for the use of ACM's in civil infrastructure.

1.5 Approach

This study is conducted using three approaches. A brief summary of each of the three approaches follows. More detailed descriptions are included in chapters 2-9.

1. The objectives of the literature study are threefold: (1) to acquire reasonable knowledge in FRP research for civil engineering applications, (2) to gather information on experimental techniques and analytical models, and (3) to identify existing models of ductility in the literature.
2. The objective of the experimental study is to gather data to support the analytical study.
3. The objectives of the analytical study are twofold: (1) to formulate a computer-based method to predict the moment-curvature relationship of retrofitted reinforced concrete beams and (2) to assess the ductility of FRP retrofitted beams from experimental data.

1.6 Scope of Study

As noted, externally bonded CFRP has been successfully used both in the laboratory and in field trials to strengthen reinforced concrete beams. In contrast, little research has been performed to determine the effect such strengthening has on the ductility of the reinforced concrete beam.

This report describes the experimental and numerical investigations carried out to determine the effect retrofitting reinforced concrete beams with CFRP has on the ductility of the beam. Information gathered in the literature study is described in Chapter 2. Theoretical considerations in the study are described in Chapter 3. The overall test program is presented in Chapter 4. Information related to materials used in the study is described in Chapter 5. Chapter 6 introduces the raw data while descriptions of data analysis methods are detailed in Chapter 7. Test results and discussion are summarized in Chapter 8, and Chapter 9 contains the conclusions from the study. Graphical representations of the test results, beam design procedure and results of the computer programs are included in Appendices A1 - A11 for completeness.

CHAPTER 2
LITERATURE STUDY

2.1 Introduction

A large number of constructed structures have reached their design service lives and are in need of repair and rehabilitation. Recent advancements in materials science have provided new materials such as FRP composites, that can be used in many areas of civil infrastructure when traditional materials have failed. The interest in FRP composites for construction applications is growing very rapidly within the research community, the government, and private industry as a result of their excellent mechanical properties, among them extremely high strength-to-weight ratios and resistance to electrochemical corrosion. The following chapter is a summary of an extensive survey of the literature conducted by the author to gather information on this particular use of FRP.

2.2 FRP Research History

The use of fiber reinforced materials in structural engineering is in no way a new technology. It can be traced back to the Israelites in 800 B.C., who used straw to reinforce their bricks. In more recent times, lightweight fiber reinforced composite materials have been investigated for possible use in framing (McCormick 1978), walkways and bridges in corrosive environments such as chemical and water treatment plants (Hull 1981, Starr 1983), cooling towers (Sims et al. 1987), and non-electromagnetic interference buildings (Bakeri 1989). Of these modern pioneers, the first to investigate FRP use with reinforced concrete systems was Dr. Urs Meier of the Swiss Federal Laboratories for Material Testing and Research, considered by many to be the leading researcher of FRP in civil engineering today. He was the first to successfully test full-scale reinforced concrete with carbon FRP (Kaiser 1989).

In the 1980's, Meier investigated the feasibility of replacing steel with CFRP for strengthening reinforced concrete beams. Meier and his associates conducted 27 flexure tests in which beams were strengthened by bonding 0.3mm to 1mm thick CFRP plates using epoxy adhesives. The results of the tests indicated that although the strength doubled in some tests, reinforced concrete beams strengthened with 1mm CFRP

laminate, the increase in ultimate load capacity was about 22% (Meier et al. 1992). The study also showed the validity of analyzing cross-sections using the strain compatibility method.

Several possible failure modes were identified by these tests and are shown in Figure 2-1.

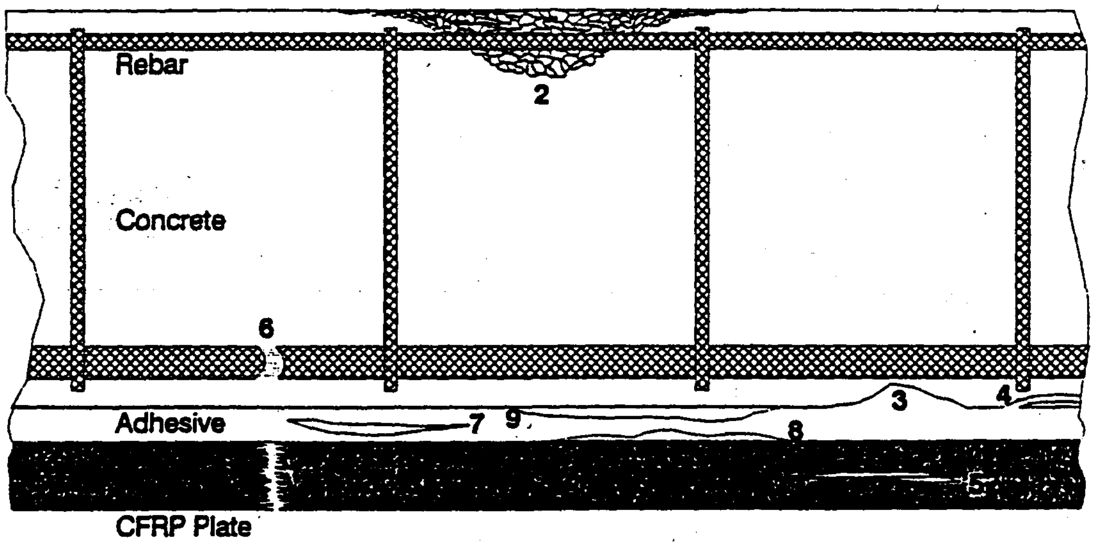

Figure 2-1 Failure Modes in CFRP Reinforced Concrete Beams (Meier et al. 1992)

As identified by the associated numbering, these failure modes are:

(1) Tension failure of the CFRP sheet. The sheets failed suddenly with an explosive snap. Cracking sounds prior to impending failure.

(2) Concrete compression failure.

(3) Continuous peeling-off of the CFRP sheet due to an uneven concrete surface. An extremely even surface is required for thin sheets (less than 1mm) which were applied using a vacuum bag.

(4) Shearing of the concrete in the tension zone (secondary failure).

(5) Interlaminar shear in CFRP sheet (secondary failure).

(6) Tension failure of reinforcing steel.

(7) Cohesive failure within the adhesive.

(8) Adhesive failure at the CFRP sheet/adhesive interface.

(9) Adhesive failure at the concrete/adhesive interface.

Another of the early studies involving the use of FRP as reinforcement was conducted to determine the effect of FRP on beam strength (Diab et al. 1984). It was found then and is now widely accepted that fiber composite plates can strengthen beams. (Saadatmanesh and Ehsani 1990). Since then, other studies have determined that CFRP offers the greatest potential for strengthening structures compared to glass and aramid FRP (An et al. 1991; Ritchie et al. 1991). Studies have confirmed that the use of epoxy for externally bonding the FRP reinforcement is more advantageous than typical mechanical bonding methods since nuts, bolts, and steel plates are vulnerable to environmental corrosion (Deskovic and Triantafillou 1995). In addition, other studies identified midspan deflection and strain over the entire load spectrum as critical parameters for evaluating the response of a strengthened member (Buyukozturk and Hearing 1998). Strain profiles can be used to calculate the stresses at various locations and are necessary to validate the assumptions of reinforced concrete beam flexure theory (Spadea et al. 1998).

A large portion of the research of FRP applications to civil infrastructure is being conducted in Europe and Japan where design codes governing FRP repair already exist. Extensive experimental and theoretical studies on flexural strengthening with GFRP plates was performed in Germany in the early 1990's at the Institute for Structural Materials, Concrete Construction, and Fire Protection (Rostasy et al. 1992). Similar tests as well as new studies are now being performed across the United States at institutes and universities. Dr. Hamid Saadatmanesh and Dr. Mohammad Ehsani of the University of Arizona and Dr. Hota GangaRao of West Virginia University are among the leading researchers of civil engineering applications of FRP in the United States today.

2.3 FRP Strengthening

The application of FRP as external reinforcement to concrete infrastructure as a strengthening mechanism has received more attention from the civil engineering research community than any other application. FRP has been tested with retrofitted concrete members such as columns, slabs, and beams. Researchers have reported improvements in strength and stiffness of retrofitted members with some of them indicating that the

shear and flexural strength of reinforced concrete beams can be increased by 20% to 100% with retrofitted carbon fiber sheets (Norris et al. 1997). Many of the studies on strengthening effects have been both analytical and experimental investigations. In addition, many of them have researched both the short and long term behavior of reinforced concrete systems (Triantafillou and Deskovic 1991; Triantafillou and Plevris 1992; Triantafillou et al. 1992).

Various techniques of FRP application for strengthening have been widely studied. These include jacketing, external post-tensioning, wrapping, and epoxy-bonding external sheets to the tension flange. The increase in flexural strength of reinforced concrete beams after wrapping with carbon fabric was evaluated with regards to six parameters. These parameters were the increase in nominal flexural strength, increase in stiffness during pre-cracking and post-cracking stages, decrease in steel rebar stress, composite action of wrap, and evaluation of failure modes based on wrap configuration (GangaRao and Vijay 1998). As a result of the information gathered in these studies, many useful field applications have been developed. For example, in California, carbon fiber wrapping of highway bridge and ramp support columns as reinforcement against seismic activity has become standard practice (Figures 2-2 and 2-3).

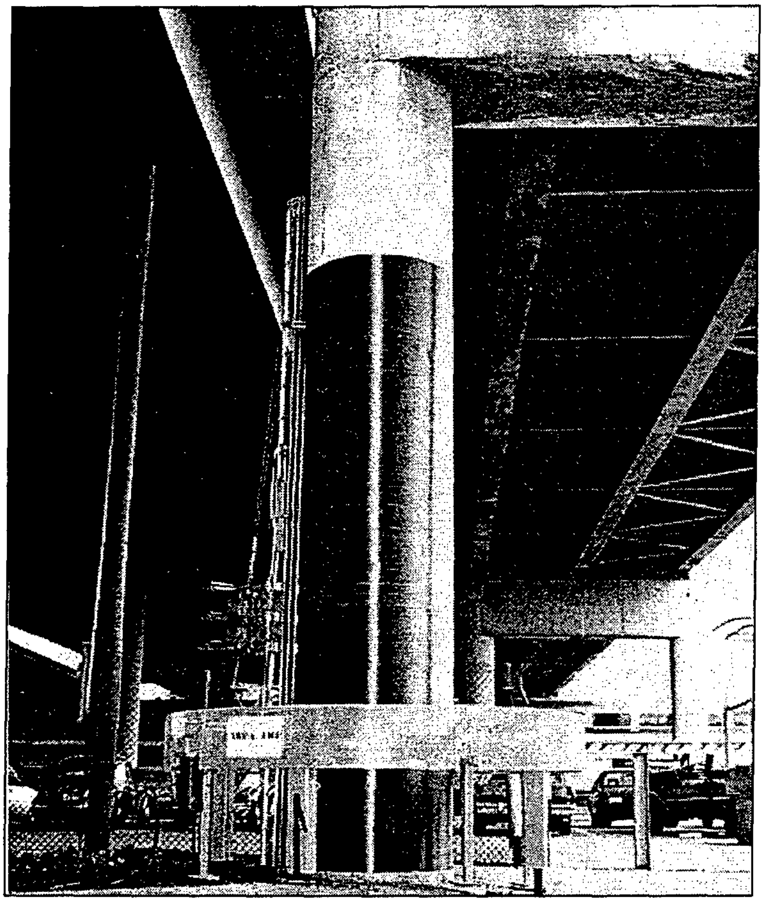

Figure 2-2 Automated Carbon Jacket Installation (ICCI 1996)

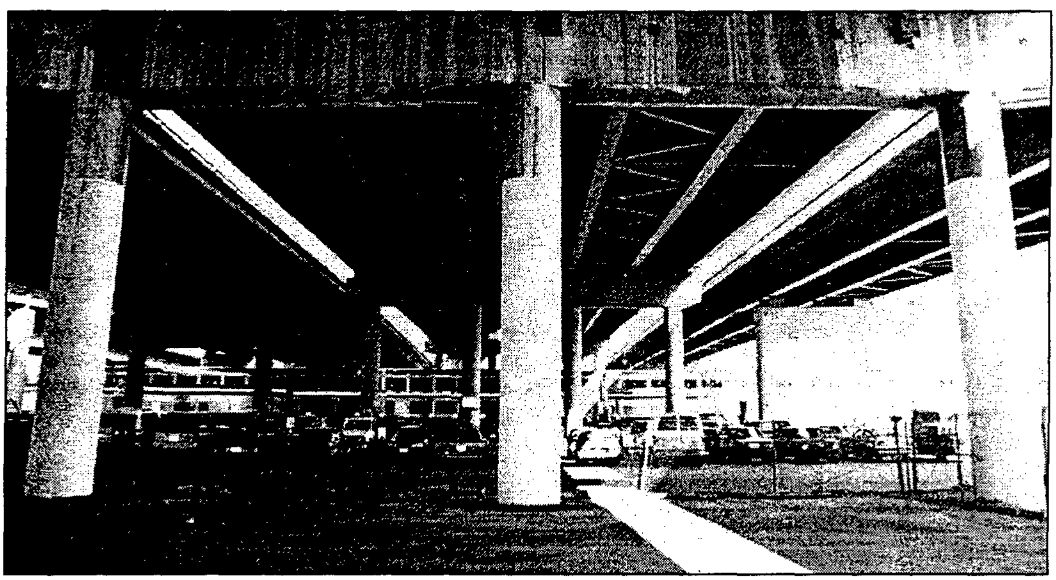

Figure 2-3 Installed Carbon Jacketing on the Santa Monica Freeway (ICCI 1996)

Extensive work has been conducted on the short-term response of concrete beams strengthened in flexure with FRP plates (Saadatmanesh and Ehsani 1991; Ritchie at al. 1991). From their results, a pivotal belief was formed that given the superior properties of CFRP over other composites, CFRP offers the highest potential for strengthening concrete structures. A critical evaluation of all the research data shows that there are still many aspects of material and structural behavior arising from the use of FRP that are not yet clear (Swamy et al. 1996; Bencardino et al. 1996). Continued research into FRP strengthening of reinforced concrete structures is necessary.

2.4 Experimental Methods

The literature survey revealed that certain experimental techniques are repeatedly used in FRP research. For flexural beam investigations for example, the use of four-point bending is widely used and it appears to have become standard practice (GangaRao and Faza 1991; Spadea et al. 1998). This testing configuration ensures that the midspan region of the beam experiences no shear forces and a constant maximum moment regardless of the load (Figure 2-4). This benefits flexural investigations because undesirable shear effects are eliminated.

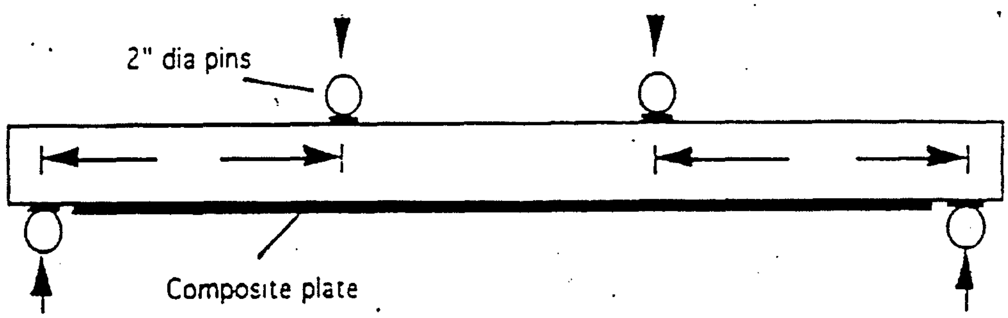

Figure 2-4 Typical Four-point Bending Configuration (ICCI 1996)

Another technique appearing often in the literature was the use of the linear variable displacement transformer (LVDT) to gather displacement data. This device has simplified data acquisition. It can be used to determine strain, deflection, and curvature measurements at every instant of loading without interrupting testing. Earlier technologies such as the Whittemore strain gage required frequent interruptions in testing

and could not provide data for every instant of testing (Buyukozturk and Hearing 1998; Arduini and Nanni 1997).

2.5 Failure Modes

Research has indicated that failure criteria for laminated systems need to be more clearly defined and understood (Buyukozturk and Hearing 1998; Saadatmanesh and Ehsani 1989; Triantafillou and Deskovic 1991). It has been recommended that failure of these systems should occur with yielding of steel and ultimately rupture of the laminate before compressive concrete failures (Meier 1995). Tests on reinforced concrete beams with CFRP sheets bonded to the tension face show that although the CFRP reinforcement is effective in enhancing both stiffness and strength, catastrophic failures occur when the beam load capacities are reached (Ritchie et al. 1991; Triantafillou and Plevris 1992). Failure of FRP strengthened beams may occur by either FRP rupture, steel yield and FRP rupture, concrete compression failure, shear failure, delamination of FRP, or debonding of the composite attachment (Ritchie et al. 1991; Triantafillou and Plevris 1992; Spadea et al. 1998). Some researchers propose that these failures can be predicted and avoided by optimizing the FRP and the steel reinforcement ratio using traditional reinforced concrete design methods (Buyukozturk and Hearing 1998). However, before this occurs, a fundamental understanding of the mechanics and failure mechanisms of the retrofit system must be established.

2.6 Ductility

Only a few studies can be found in the literature which discuss the ductility of FRP retrofitted beams. An investigation into the behavior of concrete slabs reinforced with FRP grids under service and ultimate loading define ductility as the plastic deformation energy and suggests a ductility index, μ, based on energy considerations calculated from the area under the load-deflection curve (Matthys and Taerwe 1995). These results are compared to identical tests performed using concrete slabs reinforced with steel plates and it was reported that the ductility of the FRP repaired slabs was 60% to 75% lower than that of the steel repaired slabs. This study concludes that ductility decreases appreciably with the addition of FRP reinforcement. No related work can be

found in the literature to validate this conclusion.

The area under the moment-curvature curve also has been used to determine the ductility of composite beams (Uy and Bradford 1995). These curves are typically obtained from numerical models based on the load-strain distribution through the depth of the cross section of the beam. The curvature is the quotient of the top-fiber concrete strain measured experimentally and the neutral axis depth determined from the strain distribution by similar triangle methods or lines of best fit. This approach is gaining acceptance as an appropriate method of defining and calculating ductility.

Other groups challenge the conventional definition of ductility as misleading due to the linear stress-strain relationship of FRP that exists until failure (Masmoudi et al. 1997; GangaRao and Vijay 1998). One study adopts a ductility model based on a measure of energy absorption capacity through plastic deformation, and defines the ductility factor of reinforced concrete beams as the ratio of deflection or curvature at ultimate to that at yield (Spadea et al. 1998). Other studies presented ductility using a unified limit state approach to account for deflection limits and crack width limits (Vijay and GangaRao 1996). This approach represents an implied measure of ductility and safety by satisfying the serviceability limits.

2.7 Analytical Modeling

There are many numerical models for the behavior of concrete members repaired with FRP in the literature. They exist to provide benchmarks and predictions of the response of concrete and FRP systems. Analytical models have been suggested for the prediction of various modes of failure for reinforced concrete member systems (Triantafillou and Plevris 1992). These models assume a variety of forms, but there are two forms typically used today.

Many researchers use finite element analysis models to predict the response of reinforced concrete beams with flexural reinforcement plates. This method models FRP as elastic brittle plate or shell elements. This has been performed with a great deal of success (Saadatmanesh and Ehsani 1991c). A nonlinear finite element model was used in pretest analysis of rehabilitated Navy pier decks with CFRP sheets at Port Hueneme, California. It was found that although the average ultimate loads for the investigated

slabs increased by 31%, ultimate deflections (inversely proportionate to stiffness) decreased by 42%. This allowed repair engineers to modify the FRP repaired slabs prior to installation.

Another typical modeling method is based on the compatibility of strain and equilibrium of forces. This method is the theoretical base for the most recent ACI building code, ACI 318-95. It accounts for the variation of strains and stresses through the depth of a reinforced concrete beam by approximating it as a linear function, thus simplifying design and analysis procedures. This model considers also the influence of shrinkage and creep of the concrete on the deflection and strain distribution. In addition, it is applicable to reinforced concrete beams with different cross sections, internal and external reinforcement configurations cracking patterns and different loading sets.

2.8 Field Applications

Apart from laboratory studies, field applications have also been reported in which concrete and timber bridges were strengthened using FRP composites. The Ibach bridge in Lucerne, Switzerland, built in 1969, was accidentally damaged during the installation of traffic signals when a supporting tendon was severed. The repair was carried out overnight using CFRP sheets—two 150 x 5000 x 1.5mm sheets and one 150 x 5000 x 2mm sheet (Sen and Liby 1994). More recently, CFRP laminates proved to be a solution to the problem in the City Hall of Gossau St. Gall, Switzerland (Sen and Liby 1994). In order to add an elevator, a rectangular hole had to be cut in the concrete slab. Prior to the cutting, the slabs bordering the intended hole were strengthened using CFRP laminates. In another renovation, walls in a store were removed to increase the available floor space. As a result, the existing concrete slabs supported by these walls needed strengthening. CFRP laminates were used in this situation (Sen and Liby 1994).

CHAPTER 3
THEORY

3.1 Introduction

In this chapter, the theoretical base of this study is provided in order to facilitate an understanding of the mechanics of retrofitted reinforced concrete systems. In particular, the mechanics of concrete, steel, reinforced concrete, and composite materials are presented with specific details and considerations for each.

3.2 Concrete

Concrete is a composite material composed of coarse aggregate (gravel) and fine aggregate (sand) chemically bonded by hydrated Portland cement. Portland cement is a finely powdered, grayish material which consists chiefly of calcium and aluminum silicates. It provides the adhesive and cohesive properties necessary to bond inert aggregates into a solid mass with adequate strength and durability. This standard type of cement is identified by ASTM (American Society for Testing and Materials) C150 as Type I. Other basic types of Portland cement and their uses are given in Table 3-1.

TYPE	USAGE
I	Ordinary construction where special properties are not required
II	Ordinary construction for moderate sulfate resistance or moderate heat of hydration
III	When high early strength is desired
IV	When low heat of hydration is desired
V	When high sulfate resistance is desired

Table 3-1. Usage of Basic Types of Portland Cement (ACI 318-95)

Since concrete is a mixture of water, cement, aggregate, and air, variations in the properties or proportions of these constituents as well as variations in transporting, placing, and compaction of the concrete lead to variations in the strength of the finished concrete. Among the large number of factors affecting concrete, the most important for

structural concrete are the following:

- Water/cement ratio: A lower water/cement ratio reduces the porosity of the hardened concrete and thus increases the number of interlocking solids.
- Type of cement
- Supplementary cementitious materials and admixtures
- Aggregate: The strength of concrete is affected by the strength and size of the aggregate, its surface texture, and grading.
- Moisture and temperature conditions during curing
- Concrete age: Concrete maturity is a product of the concrete curing temperature and the length of time it remains at the cure temperature.
- Rate of loading

The strength of concrete is denoted in the United States by f'_c which is the uniaxial compressive strength in psi of a standard concrete test cylinder 6in (150 mm) in diameter by 12 in (300 mm) high measured on the 28th day after it is cast. Typical compressive strengths, f'_c, vary from 2000psi to 8000psi (13.8 MPa to 55.2 MPa) at 28 days but 6000psi (41 MPa) is a more common upper limit. All other strength parameters, such as tensile or bond strength, are related to the compressive strength. Since nearly all the behavior of reinforced concrete is related to the 28-day compressive strength, it is important to note that such strength differs depending on the size and shape of the standard test specimen and the manner of testing. Typical stress-strain curves for concrete of various strengths are shown in Figure 3-1.

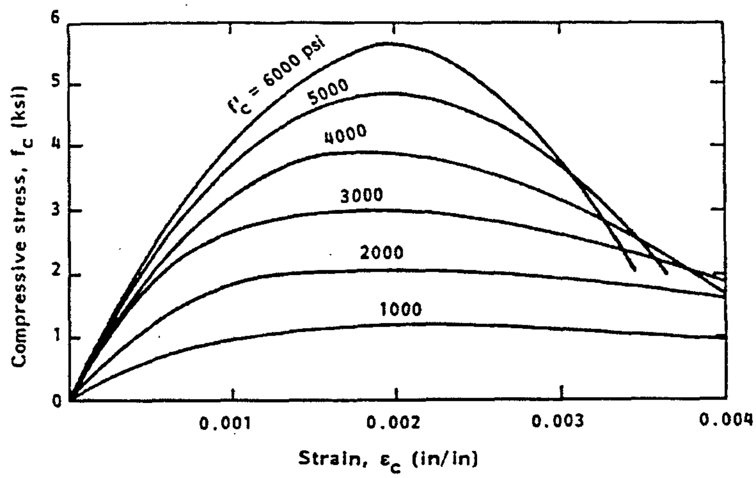

Figure 3-1 Stress-Strain Curves for various strength concretes (MacGregor 1997)

The stress-strain behavior of concrete is dependent on its strength, age at loading, rate of loading, aggregates and cement properties, and type and size of specimens. This shows that lower-strength concrete has greater ductility than higher-strength concrete and the maximum stress is reached at a compressive strain between 0.002 and 0.0025. Ultimate strain at crushing of concrete varies from 0.003 to as high as 0.008; however, the maximum usable strain for practical cases is 0.003-0.004. The ACI Building Code states "Maximum usable strain at extreme concrete compression fiber shall be assumed equal to 0.003."

3.3 Steel Reinforcement

Plain concrete beams are inefficient as flexural members because the tension strength in bending (modulus of rupture) is a small fraction of the compression strength. Due to the fact that the majority of structural applications of concrete require it to withstand large tensile forces, concrete is commonly embedded with steel to carry the tensile forces. Concrete with embedded steel reinforcement is called reinforced concrete. Compared to concrete, steel is a high-strength material. The strength of typical steel in compression is about 15 times the compressive strength of common structural concrete, and the strength of steel in tension is well over 100 times the tensile strength of concrete.

The most common type of reinforcing steel is in the form of hot-rolled deformed steel bars which are designed according to ASTM A 615 specifications for dimensions

and chemical and mechanical properties of round bars. These bars are called *rebars* and are available in a large range of diameters, from about 3/8 to 1 3/8 in (10 to 35 mm). Moreover, the surface is prepared in a wide range of raised patterns (Figure 3-2). This allows the concrete to mechanically bond to the steel and aids the transfer of forces between the concrete and the steel.

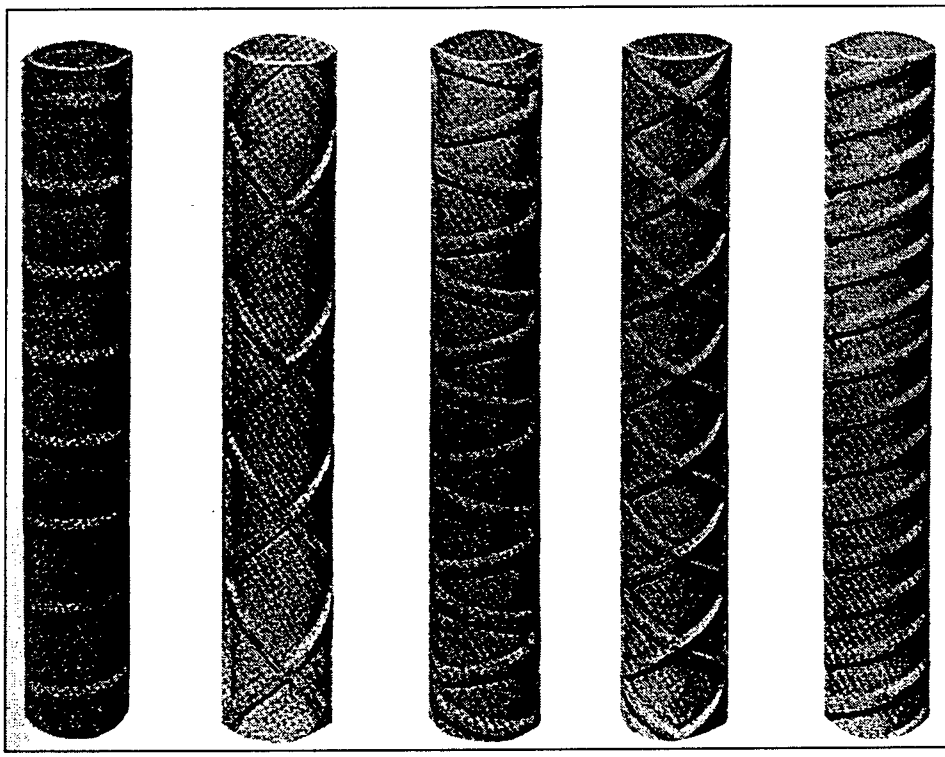

Figure 3-2 Standard Deformed Reinforcing Bars

Bars are classified according to sizes and are identified by a number designation. The numbers correspond to the nominal diameters of the bars in increments of 1/8 inch (3 mm). Hence, a #5 bar has a nominal diameter of 5/8 inch (16 mm). The most common reinforcing bars used to reinforce concrete range from #3 to #11. These bars are available in many grades of steel but, typically, Grade 60 steel rebar is used in the construction industry. Table 3-2 summarizes these bars and their properties for Grade 60 steel.

Bar Designation	Nominal Dimensions		Minimum Yield Strength (ksi)	Minimum Tensile Strength (ksi)
	Diameter (in)	Area (in^2)		
#3	0.375	0.11	60	90
#4	0.500	0.20	60	90
#5	0.625	0.31	60	90
#6	0.750	0.44	60	90
#7	0.875	0.60	60	90
#8	1.000	0.79	60	90
#9	1.128	1.00	60	90
#10	1.270	1.27	60	90
#11	1.410	1.56	60	90

Table 3-2. Standard Reinforcing Bar Dimensions and Strengths

The two chief mechanical properties that are used in the characterization of steel rebar are the yield point, f_y, and the modulus of elasticity, E_s. These can be clearly identified from the stress-strain behavior of the steel. The yield point is important because it corresponds to the largest value of stress for which no plastic deformation results. It can be identified in Figure 3-3 as the point in which the initial linear region changes gradient. Plastic deformation refers to the permanent deformation in the material after it has been stressed beyond its yield point. The modulus of elasticity is the ratio of stress to strain measured in the linear or elastic region of the stress-strain diagram. Figure 3-3 shows two representations of the mechanical response of steel. The solid line indicates the typical response and the dashed line is the ideal response. This idealization is termed an elastic-perfectly plastic response.

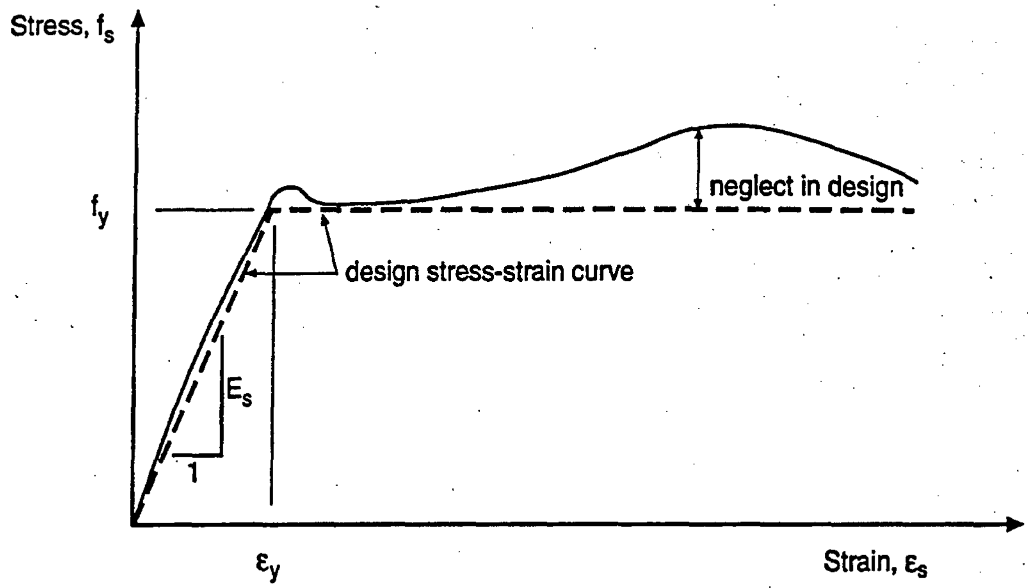

Figure 3-3 Typical Stres-Strain Relationship for Grade 60 Steel (MacGregor 1997)

Figure 3-4 shows the stress-strain relationships for a number of grades of steel. The modulus of elasticity, Es, can be taken as $29x10^6$psi ($2x10^6$ MPa) for all reinforcing bars, however, the yield strength can vary dramatically.

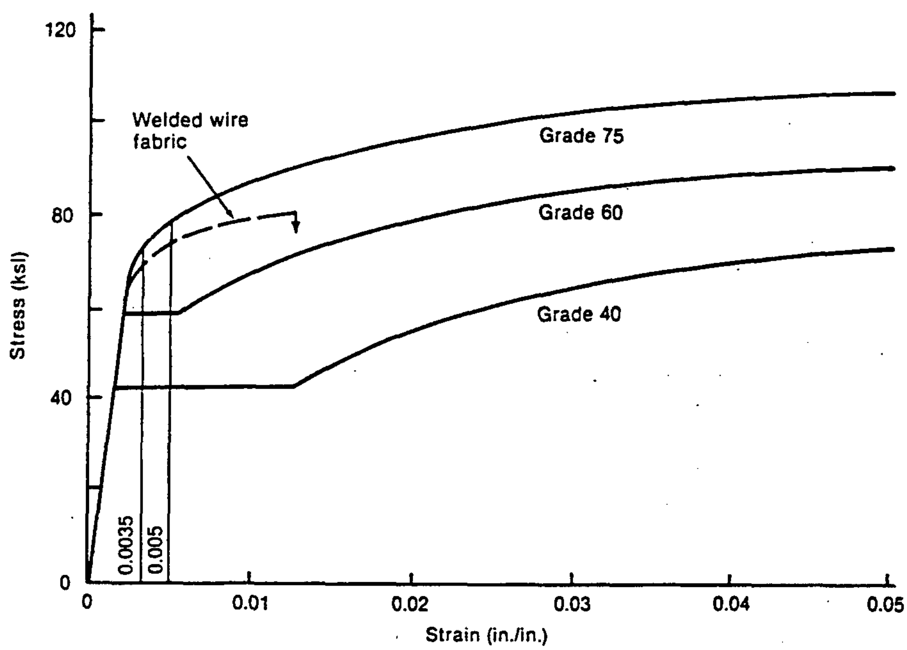

Figure 3-4 Stress-Strain Relationships for Various Steel Grades (MacGregor 1997)

3.4 Composite Theory

The word "composite" in composite material signifies that two or more materials are combined on a macroscopic scale to form a useful material. The need for such a material is to satisfy the performance requirements failed by either constituent. Some of the properties targeted for improvement include strength, stiffness, durability, toughness, and corrosion resistance.

All composite materials are composed of two basic components. The reinforcing material provides a mechanism to improve mechanical performance, and the second, the binder material protects the reinforcing element and provides adhesion to form the system. The reinforcing elements can vary greatly with respect to size, shape, and dimensions. For instance, the reinforcing elements can take the form of fibers which are long with small cross sections, the form of whiskers which are more narrow than fibers, or inclusions which can be spherical or ellipsoid in geometry. The binder, commonly referred to as the matrix, is typically organic, metallic, ceramic, or polymeric. Therefore, fiber reinforced polymer composites are those types of composites that use long fibers as the reinforcing element and polymer materials as the matrix materials. A basic schematic of fibers inside of a matrix material is shown in Figure 3-5.

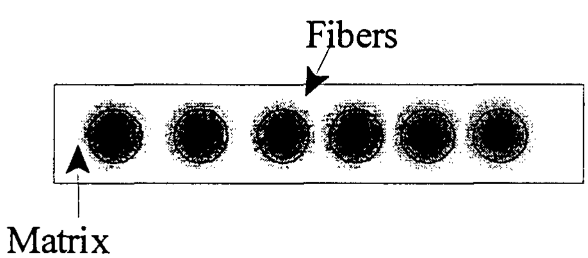

Figure 3-5 Basic Composition of Composite Material

There are three commonly accepted types of composite materials:

1. Fiber/Fibrous composites which consist of fibers in a matrix
2. Laminated composites which consist of layers of various materials
3. Particulate composites which are composed of particles in a matrix

For the remainder of this report, fiber reinforced composites will be emphasized. Primary concern will be with carbon fiber reinforced polymer composites, the class of complex fiber composites, in which non-woven continuous fibers of carbon are deliberately oriented in a polymer matrix in such a way as to increase its structural efficiency.

The basic terminology of fiber-reinforced composites will be introduced in the following sub-sections. For a lamina, defined below, the configurations and functions of the constituent materials, fibers and matrix, will be described. The characteristics of the fibers and matrix are then discussed. Finally, a laminate and its mechanical properties are defined to complete this introduction to characteristics of fiber reinforced plastic composite laminates.

3.4.1 Composite Laminae

The basic building block of a laminate is a *lamina* which is a flat arrangement of unidirectional fibers or woven fibers in a matrix. The fibers are the principal reinforcing or load-carrying agent and are typically strong and stiff. The matrix can be organic, metallic, ceramic, or carbon. Two typical flat laminae along with their principal material axes that are parallel and perpendicular to the fiber direction are shown in Figure 3-6.

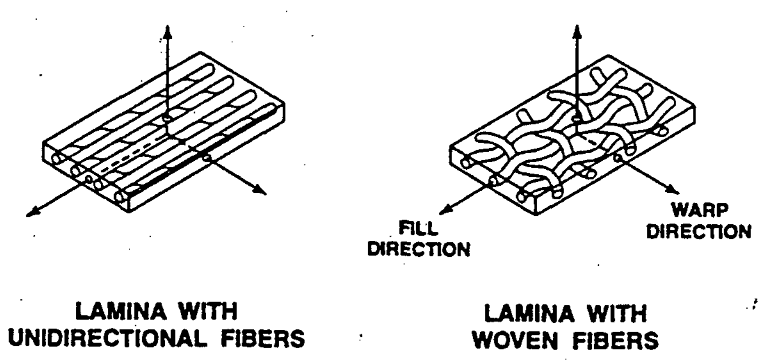

Figure 3-6 Two Composite Laminae with Different Fiber Orientation (Jones 1999)

Modeling of the lamina is governed by micromechanics theory in which behavior of the composite lamina is presented in terms of the behavior of the constituent materials. The important properties include the longitudinal stiffness, transverse stiffness, shear

stiffness, and Poisson's ratio. These properties are essential when relating stress to strain.

3.4.2 Composite Laminate

A composite laminate is a bonded stack of laminae. Figure 3-7 shows a laminate composed of five laminae. Laminate stacking can be arranged in either a symmetric fashion or an anti-symmetric fashion. Each has its merits and is based solely on the desired response of the laminate. The behavior of the resulting structure is governed by the classical lamination theory, and provides one with the ability to predict the response in terms of the materials used, number of laminae, thickness of each lamina, and how each lamina is oriented with respect to a common reference. A major purpose of lamination is to tailor the directional dependence of strength and stiffness of a material to match the loading environment of the structural element.

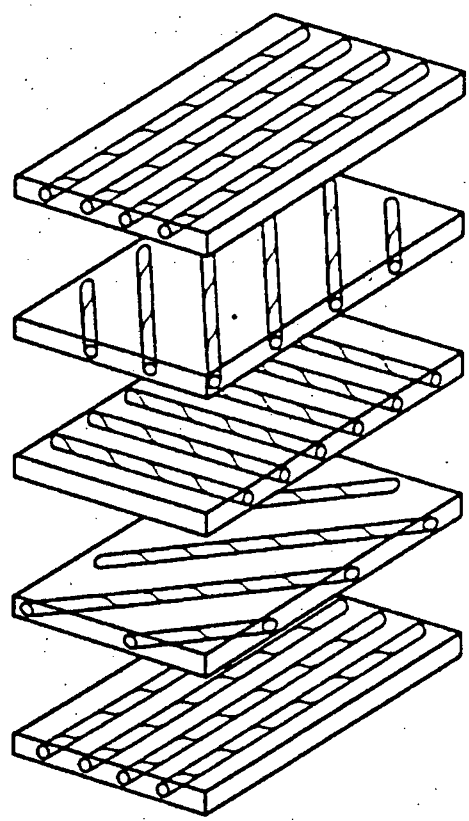

Figure 3-7 Laminae Stacking to form Composite Laminate (Jones 1999)

Finally, fiber reinforced composites generally exhibit linear elastic behavior since

the stiff fibers provide the majority of the strength and stiffness. The stress-strain behavior is typified as one of the classes illustrated in Figure 3-8.

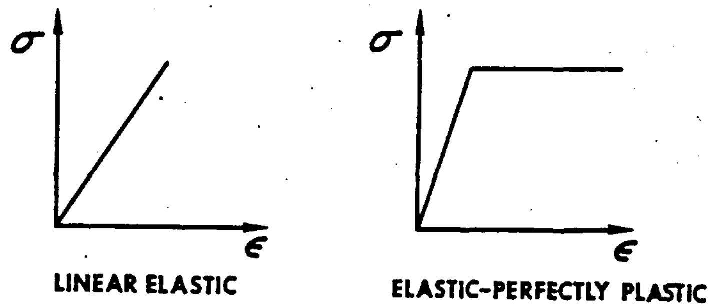

Figure 3-8 Common Stress-Strain Relationships for Fiber Reinforced Composites (Jones 1999)

3.5 Flexure Theory[1]

A beam is a structural member that supports applied loads and its own weight primarily by internal moments and shears. Figure 3-9(a) shows a simply supported beam supporting its own dead weight per unit length, *w*, plus an applied load, P. If the axially applied load, N, is zero, the member is a beam. If N is a non-zero compressive force, the member is a beam-column. For the purpose of this description, N will be restricted to zero.

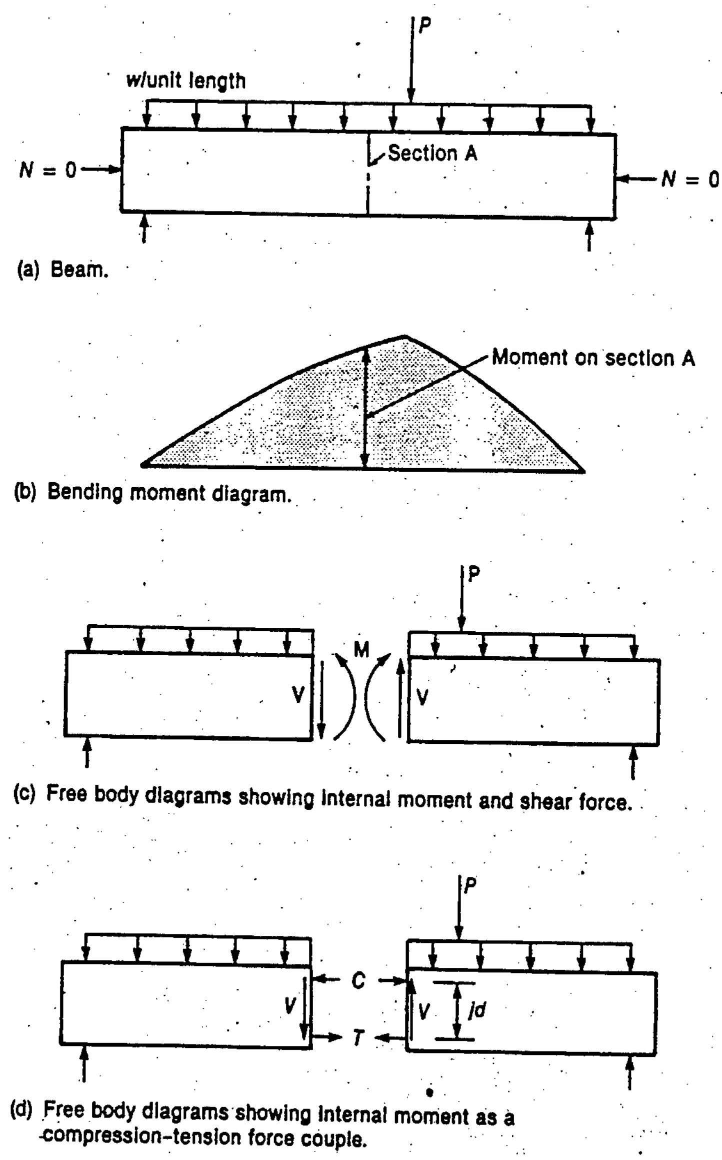

Figure 3-9 Illustration of Beam Bending Theory (MacGregor 1997)

[1] *Reinforced Concrete, Mechanics and Design, 3rd Ed.*, MacGregor, Prentice-Hall, Englewood Cliffs, N.J.

The loads, w and P, cause bending moments distributed as shown above in Figure 3-9(b). The bending moment is a load effect determined from the loads using the laws of statics. For a simply supported beam of a known span and applied load, the moments are independent of the composition and size of the beam.

At any section within the beam, the internal resisting moment, M, is necessary to equilibrate the bending moment (Figure 3-9(c)). An internal resisting shear, V, is also required. This moment, M, results from an internal compressive force, C, and an internal tensile force, T, separated by a lever arm, jd (Figure 3-9(d)). Since there are no external axial loads, N, summation of the horizontal forces gives:

$$C - T = 0 \text{ or } C = T \tag{3-1}$$

Summation of moments about an axis through the point of application of either T or C gives

$$M = Tjd \text{ or } M = Cjd \tag{3-2}$$

Since C = T, these two equations are identical. Equations (3-1) and (3-2) come directly from statics and are applicable to beams made of steel, timber, or reinforced concrete equally.

Conventional elastic beam theory for an un-cracked, homogeneous, rectangular beam without reinforcing gives the distribution of stresses as shown in Figure 3-6. The stress diagram shown may be visualized as having a "volume" and this is what is commonly referred to as the *compressive* and *tensile stress blocks.*

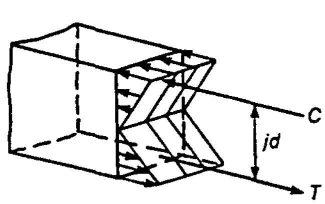

Figure 3-10 Elastic Beam Stress Blocks (MacGregor 1997)

The elastic beam theory cannot be directly used in the design of reinforced concrete beams. Reinforced concrete beams are non-homogeneous in that they are made of two entirely different materials. The methods used in the analysis of reinforced concrete beams are therefore different from those used in the design or investigation of beams composed entirely of steel, wood, or any other structural material. The fundamental principles involved are, however, essentially the same.

3.6 Flexure Theory for Steel Reinforced Concrete[2]

Plain concrete beams are ineffective as flexural members because the tensile strength in bending is a small fraction of the compressive strength. Consequently, such beams fail on the tension side at low loads long before the strength of the concrete on the compression side has been fully developed. For this reason, steel reinforcing bars are placed on the tension side as close to the extreme tension fiber as design codes allow. For simplicity, the following discussion will focus on beams with rectangular cross section only, even though members of other shapes are very common in concrete structures.

3.6.1 Equilibrium of Forces and Compatibility of Strains

Computation of the strength of a member or cross-section by the methods detailed in ACI 318-95 requires that two basic conditions be satisfied: (1) static equilibrium and (2) compatibility of strains.

The first condition requires that the compressive and tensile forces acting on the cross-section at "ultimate" strength be in equilibrium, and the second condition requires that compatibility between the strains in the concrete and the reinforcement at "ultimate" conditions must also be satisfied within the design assumptions permitted by the code.

The term "ultimate" is used frequently in reference to the computed strength of a member; however, it should be realized that the "nominal" strength computed under the provisions of the code may not necessarily be the actual ultimate value. Accordingly, the term nominal strength is used when defining the computed strength of a member. The

"nominal strength" of a beam must satisfy the assumptions given in 10.2 of ACI 318-95.

3.6.2 Assumptions

There are six assumptions which govern the theory of flexure for reinforced concrete beams. They are presented below.

Assumption #1

Strain in reinforcement and concrete shall be assumed directly proportional to the distance from the neutral axis.

In other words, plane sections perpendicular to the axis of bending are assumed to remain plane after bending. This is known as Bernoulli's hypothesis. Many tests have confirmed that the distribution of strain is essentially linear across a reinforced concrete cross-section, even near ultimate strength. The assumed strain conditions at ultimate strength of a rectangular section are illustrated in Figure 3-11.

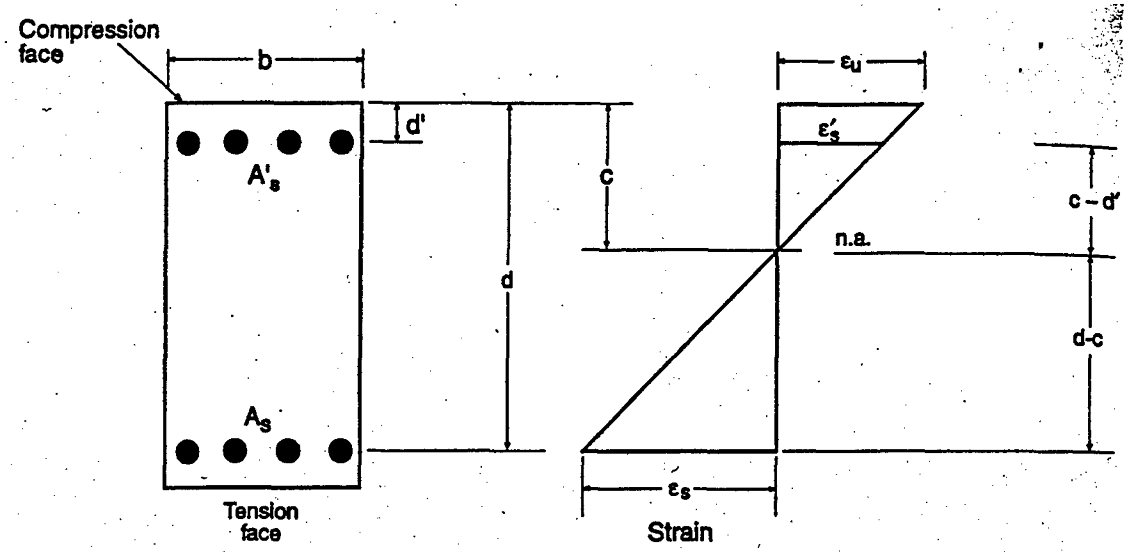

Figure 3-11 Illustration of Bernoulli's Hypothesis (ACI Notes)

Both the strain in the reinforcement and in the concrete are directly proportional to the distance from the neutral axis. This assumption is valid over the full range of loading-zero to ultimate and is of primary importance in determining the strain in the

[2] Notes on ACI 318-95 "Building Code Requirements for Structural Concrete" (1996). Skokie, Illinois

reinforcement. The strain in the reinforcement is equal to the strain in the concrete at the same level. (For external FRP reinforcement, this assumption is expanded to say that there is no slip between concrete and reinforcement)

Assumption #2

Maximum usable strain at extreme concrete compression fiber shall be assumed equal to $\varepsilon_{cu} = 0.003$.

The maximum concrete compressive strain at crushing of the concrete has been measured in many tests of both plain and reinforced concrete members. Test results indicate that the maximum concrete compressive strain varies from as low as 0.003 to as high as 0.008 (Figure 3-13). The maximum strain decreases with increasing compressive strength of concrete.

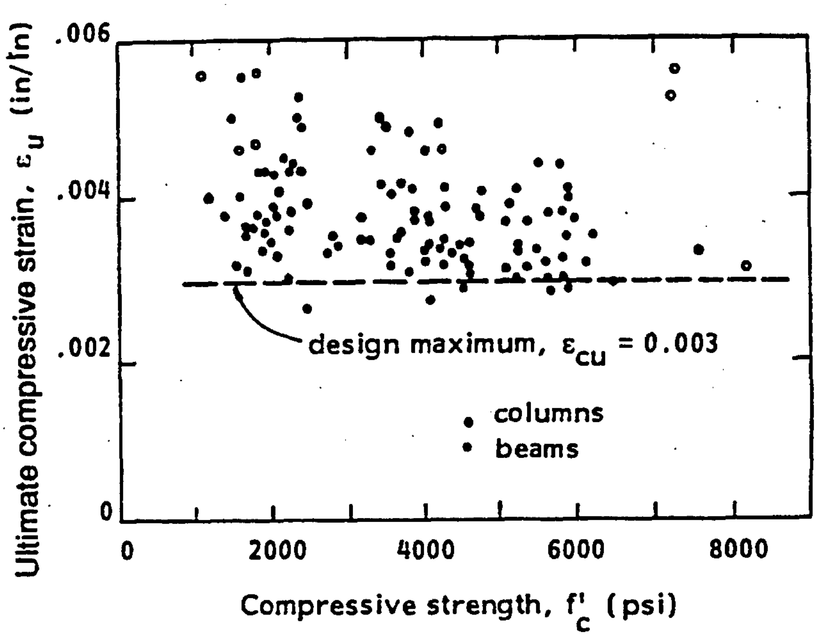

Figure 3-12 Test Distribution of Concrete Compressive Strains (MacGregor 1997)

Strictly speaking, a limiting compressive strain for concrete does not exist; however, design calculations are very much simplified if a limiting strain is assumed. Concrete is assumed to fail when the compressive strain, ε_{cu}, reaches this limiting value. ACI Code

10.2.3 specifies the limiting value, ε_{cu}, to be 0.003 while the European CEB Model Code and Swiss Code takes ε_{cu} to be limited at 0.002 and 0.0035, respectively. This project uses the ACI determined value for analytical predictions and an adjustment of that value of 0.0025 to account for the high strength concrete.

Assumption #3

Stress in reinforcement, f_s, below the yield strength, f_y, shall be taken as E_s times the steel strain, ε_s. For strains greater than f_y/E_s, stress in reinforcement shall be considered independent of strain and equal to f_y.

For deformed reinforcement, it is reasonably accurate to assume that, below the yield stress, the stress in the reinforcement is proportional to strain. The force developed in the tensile or compressive reinforcement is a function of the strain in the reinforcement, ε_s, such that

when $\varepsilon_s \leq \varepsilon_y$ (yield strain):

$$f_s = Es\,\varepsilon_s$$

$$A_s f_s = A_s E_s \varepsilon_s$$

when $\varepsilon_s \geq \varepsilon_y$:

$$f_s = E_s \varepsilon_y = f_y$$

$$A_s f_s = A_s f_y$$

where ε_s is the value from the strain diagram at the location of the reinforcement. The modulus of elasticity of steel reinforcement, E_s, may be taken as $2.9\text{x}10^6$ psi.

Assumption #4

Tensile strength of concrete shall be neglected in flexural calculations of reinforced concrete.

The tensile strength of concrete in flexure, known as the modulus of rupture, is a more variable property than the compressive strength, and is about 10% to 15% of the compressive strength. This assumption simplifies flexural calculations. The tensile force

in the concrete below the neutral axis or axis of zero strain, is small compared to the tensile force in the steel and can be neglected.

Assumption #5

Relationship between concrete compressive stress distribution and concrete strain shall be assumed to be rectangular, trapezoidal, parabolic, or any other shape that results in prediction of strength in substantial agreement with results of comprehensive tests.

This assumption recognizes the inelastic stress distribution in concrete at high stresses. As maximum stress is approached, the stress-strain relationship of concrete is not a straight line (stress is not proportional to strain). The general stress-strain behavior of concrete is shown in Figure 3-1. The shape of the curves is primarily a function of concrete strength and consists of a rising curve from zero stress to a maximum at a compressive strain between 0.0015 and 0.002, followed by a descending curve to an ultimate strain (corresponding to crushing of the concrete) varying from as low as 0.003 to as high as 0.008. The actual distribution of concrete compressive stress is complex and usually not known in practical cases. Research has shown that the important properties of the actual concrete stress distribution (Figure 3-13(a)) can be approximated closely using any one of several different forms of stress distributions (Figure 3-13).

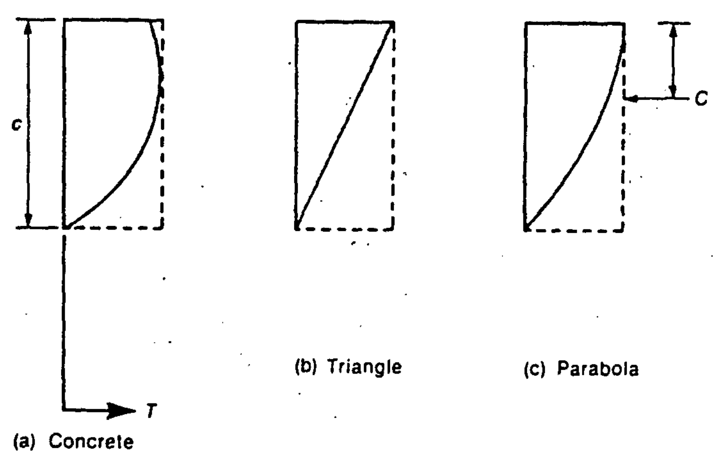

Figure 3-13 Mathematical Approximations to the Compression Stress Block (MacGregor 1997)

One other important point of this assumption is that the maximum strength is assumed to be reached when the strain in the extreme compression fiber is equal to the crushing strain of the concrete, ε_u. When crushing occurs, the strain in the tension reinforcement, ε_{su}, may be either larger or smaller than the yield strain, $\varepsilon_y = f_y/E_s$, depending on the relative proportion of reinforcement to concrete. If the reinforcement amount is low enough, yielding of the steel will occur prior to crushing of the concrete (ductile failure condition). With a very large quantity of reinforcement, crushing of the concrete will occur first, allowing the steel to remain elastic (brittle failure condition). Present ACI code includes provisions which are intended to ensure a ductile mode of failure by limiting the amount of tension reinforcement.

<u>Assumption #6</u>

Requirements of Assumption #5 may be considered satisfied by an equivalent rectangular concrete stress distribution defined as follows: A concrete stress of 0.85f'c shall be assumed uniformly distributed over an equivalent compression zone bounded by edges of the cross-section and a straight line located parallel to the neutral axis at a distance $a = \beta_1 c$ from the fiber of maximum compressive strain. Distance c from the fiber of maximum compressive strain to the neutral axis shall be measured in a direction perpendicular to that axis. Fraction β_1 shall be taken as 0.85 for strengths f'_c up to 4000 psi and shall be reduced continuously at a rate of 0.05 for each 1000psi of strength in excess of 4000 psi, but β_1 shall not be taken less than 0.65.

The code allows the use of a rectangular compressive stress block to replace the more exact stress distributions of Assumption #5. Figure 3-14 shows the actual stress conditions at nominal strength in flexure as a dotted parabola overlaid by the equivalent rectangular stress distribution in solid print. The equivalent stress block assumes a uniform stress of 0.85 f'_c over a depth $a = \beta_1 c$. The constant β_1 is equal to 0.85 for concrete with $f'_c \leq 4000$ psi and reduces by 0.05 for each additional 1000 psi of f'_c in excess of 4000 psi.

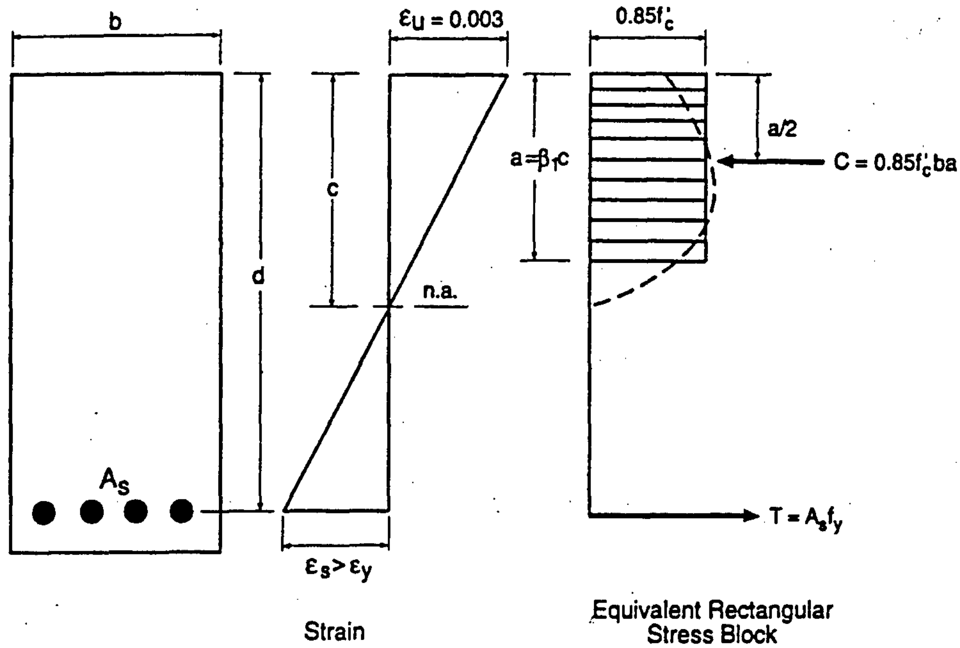

Figure 3-14 Equivalent Rectangular Concrete Stress Distribution (ACI)

Using the equivalent rectangular stress distribution and assuming that the reinforcement yields prior to crushing of the concrete ($\varepsilon_s > \varepsilon_y$), the nominal moment strength M_n maybe computed by equilibrium of forces and moments.

From force equilibrium:

$$C = T$$

or, $0.85\, f'_c\, b\, a = A_s f_y$

so that $a = \dfrac{A_s f_y}{0.85 f'_c b}$

From moment equilibrium,

$$M_n = A_s f_y \left(d - \frac{a}{2} \right) \tag{3-3}$$

3.7 Flexural Behavior of Reinforced Concrete Beams

Two requirements must be satisfied throughout the analysis and design of reinforced concrete beams and columns. These are:

1. **Stress and strain compatibility**. The stress at any point in a member must correspond to the strain at that point. Except for short, deep beams, the distribution of strains over the depth of the member must be linear to satisfy Assumptions #1 and #2 presented earlier.
2. **Equilibrium**. The internal forces must balance the external load effects as illustrated in Figure 3-9 and Equations (3-1) and (3-2).

The interaction between stress and strain compatibility and force equilibrium in reinforced concrete beams depends heavily on the properties of the beam. Such properties include the area of steel in tension, the area of concrete in compression, the yield strength of the steel reinforcement, and the ultimate or crushing strain of the concrete. Depending on the stress-strain and equilibrium conditions, flexural failures in a beam may occur in the three distinct ways:

1. **Tension Failure**. Reinforcement yields before concrete crushes (reaches its limiting compressive strain). Such a beam is said to be *under-reinforced.*
2. **Compression Failure**. Concrete crushes before steel yields. Such a beam is said to be *over-reinforced.*
3. **Balanced Failure**. Concrete crushes and steel yields simultaneously. Such a beam has balanced reinforcement and is also called *over-reinforced.*

Appendix B of the most recent ACI building code has moved away from this traditional terminology and has introduced different terms. According to ACI 318-95, beams in which the strain at ultimate in the extreme steel layer is less than or equal to the tensile yield strain, $\epsilon_y = f_y / E_s$, are called *compression-controlled* beams. Beams with compression or balanced failures, are indicative of this type. Beams having a strain at ultimate in the extreme tension steel layer equal to or greater than 0.005 are called *tension-controlled* beams. Beams with characteristics falling between these two limits are

called *transition* beams. These failure modes are discussed in further detail in the following section.

3.8 Failure Mode Theory

(a) The Balanced Failure Condition

At the balanced strain condition, the maximum strain, ϵ_{cu}, at the extreme concrete compression fiber just reaches its limiting value, say 0.003, simultaneously with the tension steel reaching its yield strain $\epsilon_y = f_y / E_s$ (Figure 3-15). This case, which exhibits brittle failure, marks the boundary between ductile tension and brittle compression failures. A balanced amount of tension steel, A_{sb}, would provide the neutral axis distance, x_b, for this balanced strain condition, so that the strain ϵ_s would be less than ϵ_y when $\epsilon_{cu} = 0.003$. The failure of this beam would be sudden when the concrete reaches the strain 0.003 and the beam will exhibit little deformation (steel does not yield) to warn of impending failure.

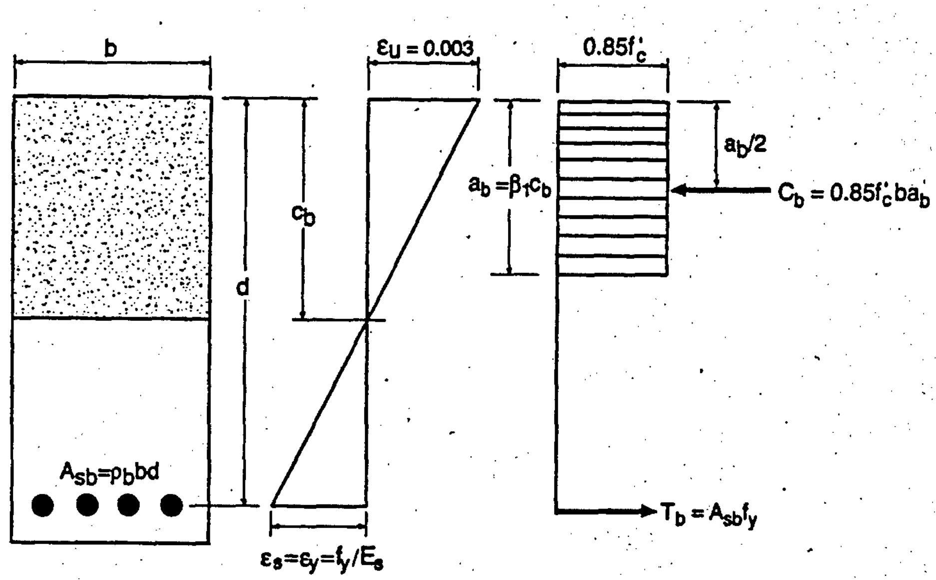

Figure 3-15 Balanced Strain Condition in Flexure (ACI 318-95)

(b) Under-reinforced Condition

When the actual area of steel reinforcement, As, is less than the area of steel in the balanced condition, A_{sb}, the tensile force reduces. The internal force equilibrium reduces

the depth of the compression stress block (and thereby reducing the depth to the neutral axis to less than the depth to the neutral axis at the balanced strain condition) giving a strain, ϵ_s, greater than ϵ_y. In this case, the reinforcement yields before the failure occurs and the beam develops a tension failure. A typical reinforced concrete beam should display similar moment-curvature behavior to the hypothetical plot in Figure 3-16. At failure (E), the curvature at the section of the maximum moment was approximately four times that at the yield point (D). As a result, deflection prior to the concrete reaching the crushing strain of 0.003, the beam will have noticeable extensive deflection. This type of behavior is said to be ductile since the moment-curvature diagram has a long plastic region (D – E). This is the desirable design mode of failure because if a beam in a building fails in a ductile manner, the occupants of the building have warning of the impending failure and have an opportunity to leave the building before the final collapse, thus reducing the consequences of collapse. Note that the yield point was designed to be well past the service or required moment of the beam (C) and well away from the influence of the cracking region (A and B).

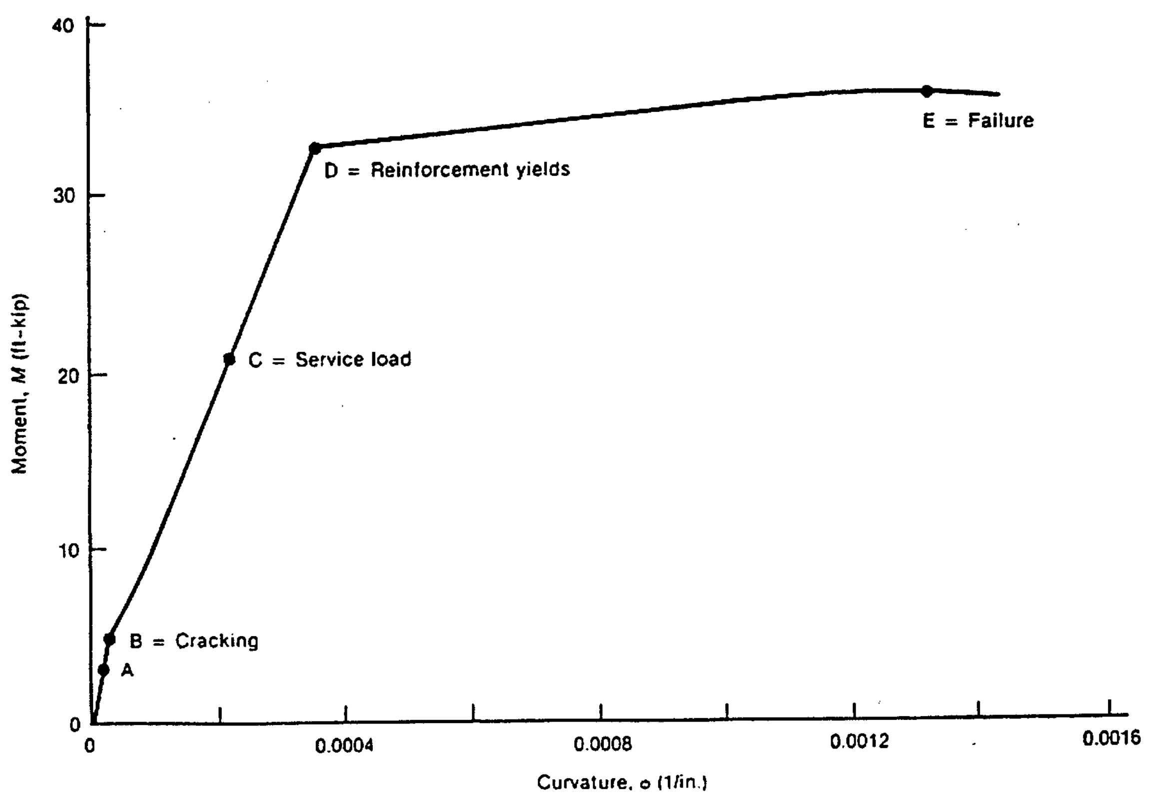

Figure 3-16 Theoretical Moment-Curvature Plot with Annotations (MacGregor 1997)

(c) Over-reinforced Condition

If the actual area of steel reinforcement, As, were greater than that at the balanced strain condition, A_{sb}, the equilibrium of compressive and tensile forces (C = T) would result in an increase in the depth of the compression stress block. The depth to the neutral axis would exceed the depth in the balanced condition. In this case, the concrete in the extreme compression fiber reaches the assumed crushing strain of 0.003 before the steel starts to yield. This is a typical compression failure. The moment-curvature diagram for such a beam does not have the ductile post-yielding response displayed in Figure (3-16) (D-E). Instead, the moment-curvature curve terminates at an unknown point before the yield point (D). This could occur past, at, or even before the service load has been reached (C). Because compression failures are sudden and brittle, a beam in this condition would fail without warning to the occupants of a building. Such a failure may have serious consequences. To avoid this, the ACI Code specifies that all beams are to be designed for the under-reinforced condition, with the tensile steel ratio well below the balanced value.

3.9 Reinforcement Ratio

Due to these differences in behavior, beams are designed such that if failure occurs, it will be by yielding of the steel, not by crushing of the concrete. The relative amount of tension steel compared to that in the balanced strain condition significantly affects the mode of failure. The reinforcement ratio, ρ, may be conveniently used to represent the relative amount of tension steel reinforcement in a beam. It is traditionally defined as the ratio of the area of steel reinforcement in tension to the area of concrete in compression, given by

$$\rho = \frac{A_s}{bd} \tag{3-4}$$

The parameters b and d refer to the width of the beam and the effective depth or depth to the steel reinforcement, respectively. The reinforcement ratio of the balanced strain condition, $\rho_{balanced}$, may be obtained by applying the equilibrium and compatibility

conditions with $\epsilon_u = 0.003$ and $E_s = 29 \times 10^6$ and rewritten in the form of Equation (3-5), given below. (β_1 is a strength reduction factor applied in ACI Code.)

$$\rho_{balanced} = \frac{0.85\beta_1 f_c^{'}}{f_y}\left(\frac{87{,}000}{87{,}000 + f_y}\right) \tag{3-5}$$

In order to have some reasonable assurance for a ductile mode of failure in flexure, ACI 10.3.3 limits the reinforcement ratio to less than 75% of the balanced value, i.e.

$$\rho_{max} = 0.75\rho_{balanced} \tag{3-6}$$

CHAPTER 4
EXPERIMENTAL PROGRAM

4.1 Introduction

In order to satisfy the objectives of this research, a series of test was carried out in which the eight test specimens were loaded past initial cracking of the tension face to simulate service damage. Subsequently, each specimen was repaired in-situ using CFRP laminates and tested to failure under the same loading conditions. This chapter provides pertinent information relating to the series of tests. Details regarding the test specimens, instrumentation, loading, and test procedure are summarized in this chapter. The actual results of the testing are presented in Chapter 6.

4.2 Specimen Details

Eight reinforced concrete beams were designed to represent a typical reinforced concrete beam in service. All specimens were constructed by the author, at the Structures Division of the Building and Fire Research Laboratory (BFRL) at the National Institute of Standards and Technology (NIST). Standard construction techniques were closely followed and the quality of the constructed beams closely mirrored normal construction standards. The beam design requirements were based upon research needs, material availability, and experience. There was relatively easy access to a wide range of rebar (#3 to #9); however, the Tinius Olsen (TO) testing machine would not accommodate a beam with a span over 11 ft. Therefore, the aim was to design beams that would fail in flexure, with a span of less than 11 ft using #3 to #9 rebar. The beams were designed in accordance with ACI 318-95, Building Code Requirements for Structural Concrete. The design procedure is provided in Appendix A1.

The details of the beams are summarized in Table 4-1. Figure 4-1 shows the cross section details of the beams and Figure 4-2 shows a side view of the beams with details on the internal steel reinforcement configuration. All beams had identical nominal dimensions. Each beam was 9½ ft (2.896m) in length, 6 in (1500mm) in width, and had an 18 in (4500mm) nominal depth. The internal longitudinal flexural reinforcement was varied in each bar, as shown in Table 4-1, but the vertical shear reinforcing had a constant

stirrup arrangement as shown in Figures 4-1 and 4-2.

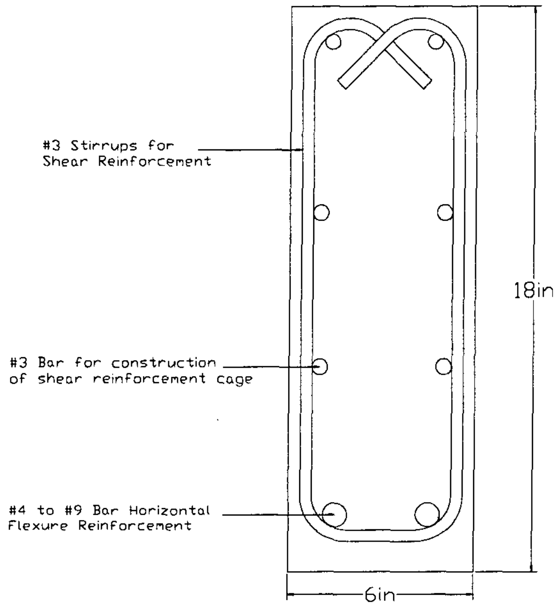

Figure 4-1 Cross Section View of Test Specimen

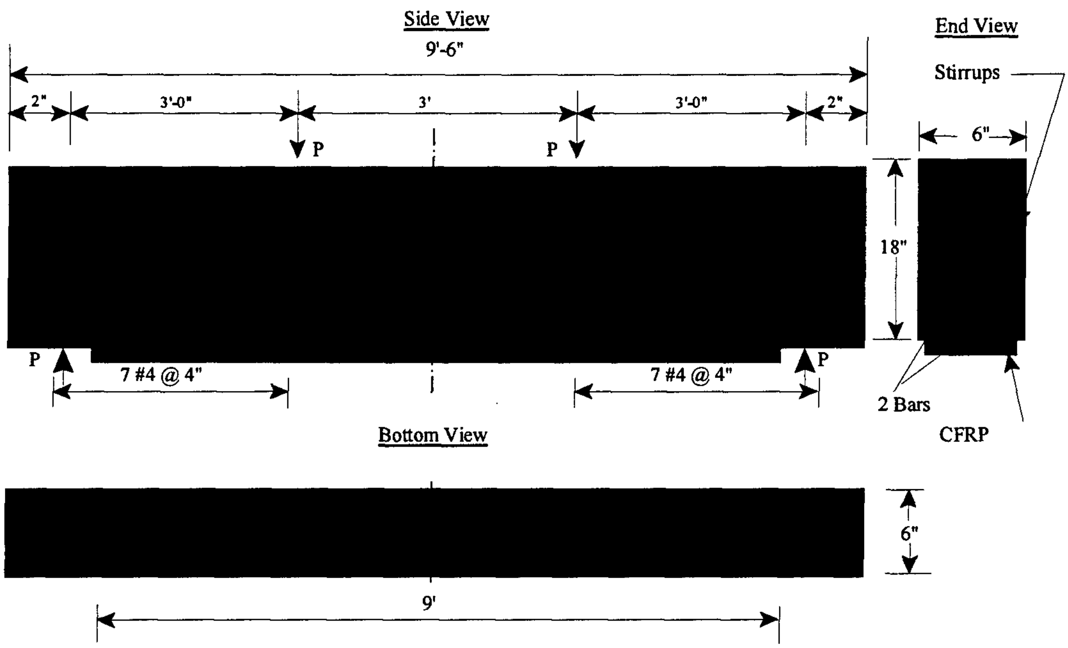

Figure 4-2 Side View of Test Beams Showing Internal Steel Reinforcement

All of the beams were designed to achieve ductile failure in accordance with existing guidelines (ACI 10.2.7.3). All beams were constructed in the Structures Laboratory of the Building and Fire Research Laboratory (BFRL) at the National Institute of Standards and Technology (NIST) by the author. Conventional fabrication, casting, and curing techniques were used. The code used to identify each specimen consists of a number (5 – 8) and in some cases a number and a letter (4A, 4B, 9A, 9B). The number represents the internal steel reinforcement bar size, #4 through #9. Thus, Beam 5 was reinforced with two #5 steel rebars. The letter was either an A or B and differentiated between two beams which had identical internal reinforcement but different external reinforcement. Hence, Beam 4A and Beam 4B were both reinforced internally with #4 steel rebar, but Beam 4B was reinforced externally with S812 CFRP laminate while Beam 4A was reinforced with S512 CFRP laminate.

Beam	Longitudinal Reinforcement				CFRP Type	No. of Strips
	Number of Rebars	Size of Rebars	Area of Steel (in^2)	Reinforcement Ratio (%)		
4A	2	#4	0.40	0.404	S512	1
4B	2	#4	0.40	0.404	S812	1
5	2	#5	0.62	0.626	S512	1
6	2	#6	0.88	0.889	S512	1
7	2	#7	1.20	1.212	S512	1
8	2	#8	1.58	1.596	S512	1
9A	2	#9	2.00	2.020	S512	0
9B	2	#9	2.00	2.020	S512	1

Table 4-1 Specimen Designation and Details

Each beam was designed with an excess of vertical shear reinforcement to reduce the occurrence of shear failure, and hence ensure that failure would result only from bending stresses. Additional horizontal reinforcement was designed and placed directly under each load point in order to reduce bearing effect through localized confinement.

Two types of commercially available CFRP reinforcement were used in the

investigation: Carbodur S512 and S812 manufactured by the Sika Corporation. Each was a pultruded carbon fiber reinforced plastic laminate designed for strengthening concrete, timber, and masonry structures. The CFRP consisted of continuous carbon fibers with a 68% by volume fiber content in an epoxy resin matrix. The sheets were bonded to the tension face of the beam over a length of 9½ ft (2900mm).

The surface of each beam had to be prepared before applying the structural adhesive. The first step in the surface preparation was a light surface chemical cleaning with acetone. Dry sanding was performed using an air-compressed paint chipper until the coarser aggregate was exposed. The average depth of material removed around the coarse aggregate was 0.04 in (2mm). Surface preparation was completed on the designated specimens prior to initial loading. The epoxy adhesive was applied as outlined in the product manual provided by the manufacturer. The epoxy adhesive thickness was maintained constant at 0.04 in. (2mm) for all the beams.

4.3 Test Rig

All beams were tested under four-point bending. Four-point bending is essential because this ensures zero shear and a constant positive moment at the midspan. A Tinuis Olson (TO) testing machine with a maximum rated compressive capacity of 400,000 lbs was used to apply the load. In order to achieve a convenient configuration to repair the beams once cracked, a test rig was designed. In this configuration, the beams were inserted upside down to their typical orientation with the tension face on top instead of at the bottom. The test frame was designed and constructed using steel box beams.

The rig consisted of an 11 ft (3.353m) steel box beam, ½ in (12.7mm) thick resting atop the lower load head of the TO machine. This support beam was double bolted at both ends to an 11 ft structural steel wide flange beam. The wide flange beam acted as a spreader beam to distribute the load. The bolted support beam was used to increase the stiffness of the wide flange beam, as well as provide additional connections as safety measures in the event of an accident. Stiffeners also were added at 3 ft intervals on center to increase the flexural stiffness of the wide flange member. Another steel wide flange was plastered to the floor of the TO machine and used as the base of the test frame. Two additional steel members were welded onto the spreader beam and two onto

the base beam to act as load points. Four 6 in x 1 in steel plates were bonded to the loading points of each beam using HydroCal, a water- based plaster adhesive. The steel plates were used to prevent localized concrete crushing or punching shear resulting from excessive stress concentrations of the point loading. Metal cylinders, 3 inches in diameter, were used to apply the load to the 6 in x 6 in steel plates. The applied load was transmitted directly from the 400 kip hydraulic TO ram to the 11 ft spreader beam. The beam was attached to the stiffener beam to ensure constant contact with the loading ram ensuring the loads were transferred equally to the spreader beam. The test rig schematics and actual set up are shown in Figures 4-3 and 4-4.

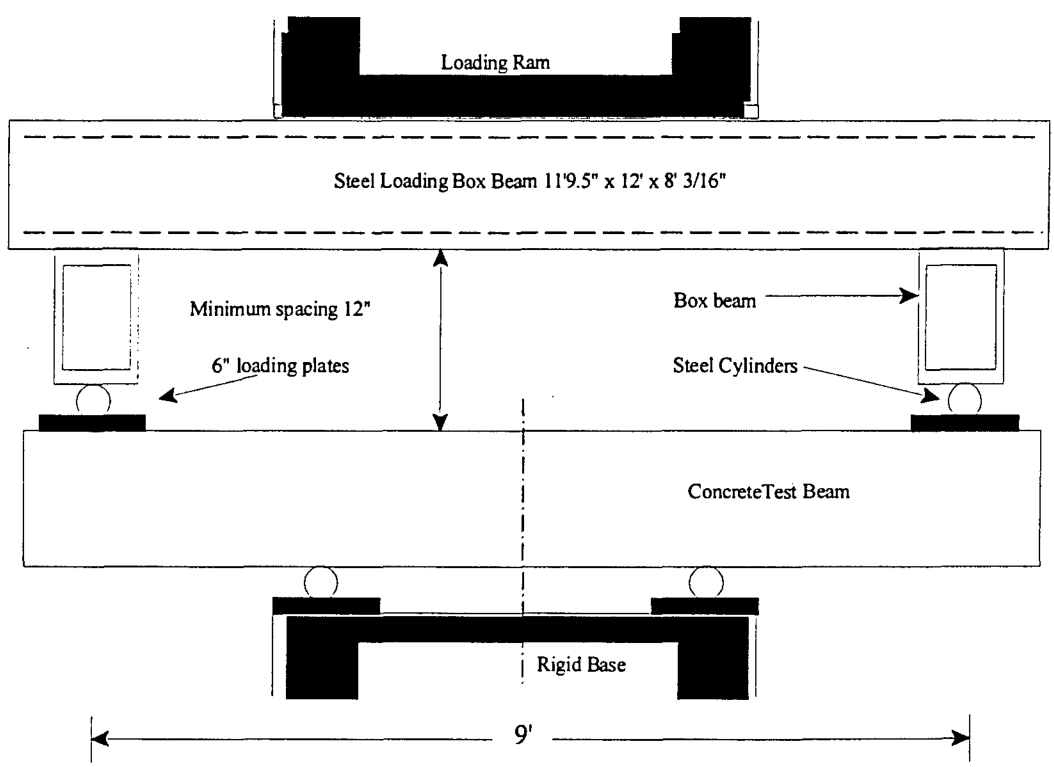

Figure 4-3 Diagram of Testing Rig

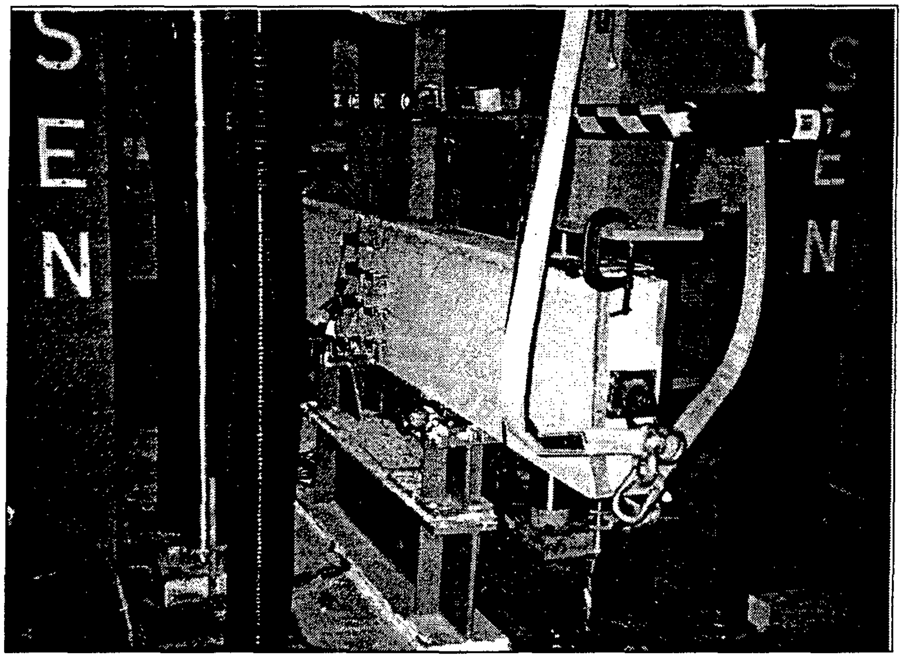

Figure 4-4 Actual Test Rig (Beam 6 Loaded Prior to Testing)

4.4 Instrumentation

Eight extensively instrumented rectangular beams were tested in this study. Beams were instrumented with three vertical linear variable displacement transducers (LVDT) in contact with the tension face. One at midspan and two directly under the outer load points. The concrete surface was instrumented at midspan with a strain gage. Strain gages were bonded with M-Coat J, an epoxy resin, in accordance with manufacturer's specifications. Eight LVDT's were mounted horizontally on the sides of the beams at the midspan, four on each side of the beam at staggered intervals throughout the depth for the purpose of measuring deformations (Figure 4-5). This data was used to calculate strain profiles through the depth.

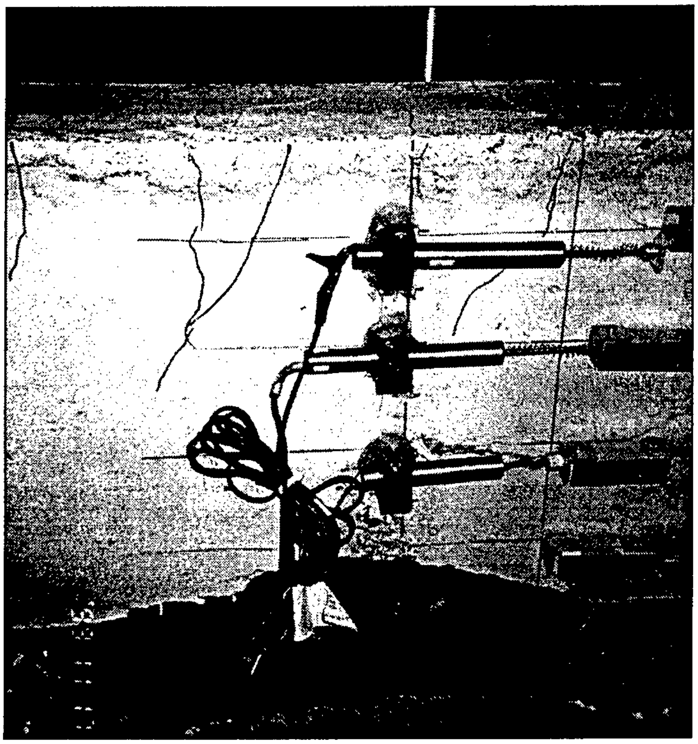

Figure 4-5 Side View of Beam showing Placement of LVDTs

4.5 Test Procedure

The eight reinforced concrete test beams were subjected to four-point flexural testing conducted over a test span of 9ft (2.743m) in accordance with American Society of Testing and Materials (ASTM) specifications on four-point flexure tests (C78-84). Testing consisted of an initial loading cycle up to initial cracking, in-situ CFRP repair of the specimens, and final loading until visible failure of the beam was reached. The parameters of interest were midspan deflection, strains in concrete and CFRP laminate sheets, and ultimate moment capacity. A digital data-acquisition system was used to monitor loading, midspan deflection, and deformations in the concrete and in the reinforcement.

CHAPTER 5
MATERIALS

5.1 Introduction

This chapter presents information on the mechanical properties of the three constituent materials of the test beams used in this research: concrete, reinforcing steel, and CFRP. Materials testing was conducted to verify material properties as ordered or specified by the manufacturer. All properties were determined using either uniaxial tension or compression tests. All tests were in accordance with the relevant ASTM specifications. Full knowledge of these properties provides a sound base for analytical investigation and is precautionary to ensure that the appropriate materials are being used in the full-scale tests.

5.2 Structural Concrete

The specimens were made using Type III Portland Cement which is a cement designed to develop high strength at an early stage of its curing process (Table 3-1). The modulus of elasticity of concrete varies with strength. For normal weight concrete, ACI-8.5.1 suggests that the empirical formula for modulus of elasticity, E_c, be taken as:

$$E_c = 57{,}000\,(f'_c)^{1/2} \tag{5-1}$$

The design 28-day compressive strength for the concrete in the test beams was 6000 psi (41 MPa) and this was used to calculate the modulus of elasticity used throughout this study to be $E_c = 4.415 \times 10^6$ psi. Thirty-two concrete compressive cylinders were cast on the same day as the beams were cast, from the same batch of concrete used to make the test specimens. There were four each for every test beam. These cylinders cured in the same conditions as the test beams and were tested for concrete compressive strength on the day its corresponding beam was tested. The cylinders were 4 in (100mm) in diameter and 8 in (200mm) in height. The results of the actual compressive tests on the cylinders provided compressive strengths within ±5% of the desired strength of 6000 psi (41 Mpa).

5.3 Reinforcing Steel

The internal steel rebar used was ASTM 615 Grade 60 #4 to #9 bars with the shear reinforcement being entirely #3 bars. The bars used were hot-rolled bars with a nominal yield strength of 60 ksi (414 MPa) and a minimum tensile strength of 90ksi (620 MPa).

Tensile tests were conducted on 8 in (200mm) gage length samples of each size of steel rebar at a loading rate of 0.015 in/min up to the yield load, and 0.4 in/min beyond the yield load. The average yield strain of the steel was 0.00259 micro-strains, and the average ultimate strain was found to be 0.24 micro-strains. The average yield and ultimate elongations were 0.0207 in (0.53mm) and 1.92 in (48mm) respectively. These tests were conducted in accordance with the specifications on steel tensile tests in ASTM A370 11.4.1 and 11.4.3.

5.4 Carbon Fiber Reinforced Plastics

The laminates used were pultruded carbon fiber reinforced plastic with a fiber volumetric content of 68%. Details of the FRP reinforcement as provided by the manufacturer are shown in Table 5-1.

CFRP Type	Thickness (in)	Width (in)	Cross Sectional Area (in^2)	Tensile Strength (ksi)	Modulus of Elasticity (ksi)	Fiber Content (% Vol.)	Ultimate Strain (in/in)
S512	0.047	50	0.093	348	22500	68	0.019
S812	0.047	80	0.149	348	22500	68	0.019

Table 5-1. CFRP Properties as provided by manufacturer

Tensile tests on samples of both the S512 and the S812 in accordance with ASTM D3039. The S512 test coupon was 20 in (500mm) in length, 2 in (50mm) wide with a 3 in (75mm) grip beveled at 2.5 in (63mm) providing a gage length of 9 in (225mm). The S812 test coupon was 31 in (775mm) in length, 3 in (75mm) wide with a 5 in (125mm) grip beveled at 4 in (100mm) providing a gage length of 14 in (350mm). The average ultimate strength for both specimens was found to be 435 ksi (3000 Mpa) and the

modulus of elasticity was found to be 23.8×10^6 psi. Test results are summarized in Table 5-2. Stress-strain plots confirmed the CFRP laminate to be a linear-elastic until failure.

	S512	S812
Ultimate Load (kips)	32.3	51.7
Ultimate Strain (in/in)	0.022	0.019
Ultimate Elongation (in)	0.171	0.266
Loading Rate (in/min)	0.034	0.053

Table 5-2. Experimentally Determined CFRP Properties

5.5 Structural Adhesive

Sikadur 30 was the adhesive used for bonding the laminate to the test specimens. It was developed by the Sika Corporation and it is a two-component, 100% solid, moisture-tolerant, high-modulus, high-strength, structural epoxy resin suitable for CFRP material. No tests were conducted on the adhesive, but a its mechanical properties were supplied by the manufacturer. The two components have a mixing ratio of 3:1 by volume forming a non-sag paste which when cured for 70 minutes at 73°F has a flexural strength of 6,800 psi (46.8 MPa) and a tensile strength of 3,600 psi (24.8 MPa). The modulus of elasticity is 1.7×10^6 psi in flexure and 6.5×10^5 psi in tension. The 14-day bond strength to hardened concrete is 3,100 psi (21.4 MPa).

CHAPTER 6
PRESENTATION OF DATA

6.1 Introduction

This chapter presents the results and attempts to explain the raw data. This research was designed to be as applicable to the real world civil infrastructure as possible. As a result, other studies or interested parties may attempt to verify the results of this study using the data presented here; however, before this can be achieved, a thorough understanding of the information gathered is critical.

6.2 Description of Data

The data was recorded digitally using the OPTIM software of the data acquisition system at NIST. The initial data files were captured and needed to be converted to an Excel format in order to analyze the data using readily available personal computer software. A set of data consisted of eighteen different measurements, with readings of each taken every second the beam was being loaded. The eighteen parameters correspond from left to right to the headings of the raw data tables in Table 6-1 below. As a result of recording data for every second of loading, the average file size was in excess of 5 Megabytes. It was not uncommon to record over 10,000 data sets since testing was a time consuming process with some test specimens requiring over three hours to reach failure. A description of each column is provided below.

(a) Time (sec): The time at which each row of readings was recorded. For all tests, readings were taken every second. In many cases, testing took several hours and there were data files with well over 11,000 sets of 18 readings.

(b) EAST 1 (in): The displacement of the horizontal LVDT located 2 in from the bottom of the beam on the eastern side of the test rig.

(c) EAST 2 (in): The displacement of the horizontal LVDT located 6 in from the bottom of the beam on the eastern side of the test rig.

(d) EAST 3 (in): The displacement of the horizontal LVDT located 10 in from the bottom of the beam on the eastern side of the test rig.

(e) EAST 4 (in): The displacement of the horizontal LVDT located 14 in from the bottom of the beam on the eastern side of the test rig.

(f) WEST 1 (in): The displacement of the horizontal LVDT located 2 in from the bottom of the beam on the western side of the test rig.

(g) WEST 2 (in): The displacement of the horizontal LVDT located 6 in from the bottom of the beam on the western side of the test rig.

(h) WEST 3 (in): The displacement of the horizontal LVDT located 10 in from the bottom of the beam on the western side of the test rig.

(i) WEST 4 (in): The displacement of the horizontal LVDT located 14 in from the bottom of the beam on the western side of the test rig.

(j) NORTH (in): The displacement of the vertical LVDT located under the load at the northern end of the test rig.

(k) SOUTH (in): The displacement of the vertical LVDT located under the load at the southern end of the test rig.

(l) MIDDLE (in): The displacement of the vertical LVDT located under the beam at the midspan.

(m) SGCON (e-6 in/in): The strain as measured by the strain gage located on the outermost concrete fiber in compression.

(n) SGCAR (e-6 in/in): The strain as measured by the strain gage located on the surface of the external CFRP laminate.

(o) SGSTE (e-6 in/in): The strain as measured by the strain gage located along the longitudinal axis of the internal steel reinforcement on the eastern side of the beam and rig.

(p) SGSTW (e-6 in/in): The strain as measured by the strain gage located along the longitudinal axis of the internal steel reinforcement on the western side of the beam and rig.

(q) LOADTO (lbs): The load delivered by the hydraulic ram of the Tinius Olsen machine as measured by the internal computer of the Tinius Olsen machine.

(r) DISPTO (in): The displacement of the hydraulic loading head of the Tinius Olsen as measured by the internal controls of the Tinius Olsen machine.

Time	EAST1	EAST2	EAST3	EAST4	WEST1	WEST2	WEST3	WEST4
104	-5.62E-05	-5.6E-05	-3.28E-05	-0.000312	-5.71E-05	-5.5E-05	-5.69E-05	-5.58E-05
105	-5.62E-05	-5.6E-05	-3.28E-05	-0.000312	-5.71E-05	0.0001651	0.0001706	0.0001673
106	-5.62E-05	-5.6E-05	-6.55E-05	-0.000312	-5.71E-05	-5.5E-05	-5.69E-05	0.0001673
107	-5.62E-05	-5.6E-05	-6.55E-05	-0.000312	-5.71E-05	0.0001651	-5.69E-05	-5.58E-05
108	0.0002248	-5.6E-05	-3.28E-05	-0.000624	-5.71E-05	0.0002201	-5.69E-05	-5.58E-05
109	0.0001686	-5.6E-05	-3.28E-05	-0.000312	0.0001712	-5.5E-05	0.0001706	-5.58E-05
110	0.0002248	-5.6E-05	-6.55E-05	-0.000312	-5.71E-05	-5.5E-05	-5.69E-05	-5.58E-05
111	-5.62E-05	-5.6E-05	-3.28E-05	-0.000312	-5.71E-05	-5.5E-05	0.0002275	0.0001673
112	-5.62E-05	-5.6E-05	-3.28E-05	-0.000312	-5.71E-05	-5.5E-05	-5.69E-05	-5.58E-05
113	-5.62E-05	-5.6E-05	-6.55E-05	-0.000312	-5.71E-05	-5.5E-05	-5.69E-05	0.0001673
114	-5.62E-05	-5.6E-05	-3.28E-05	-0.000312	-5.71E-05	0.0001651	0.0001706	0.0001673
115	-5.62E-05	-5.6E-05	-3.28E-05	-0.000312	-5.71E-05	0.0001651	-5.69E-05	0.0001673
116	-5.62E-05	-5.6E-05	-3.28E-05	-0.000312	-5.71E-05	-5.5E-05	-5.69E-05	-5.58E-05
117	-5.62E-05	-5.6E-05	-3.28E-05	-0.000312	-5.71E-05	-5.5E-05	-5.69E-05	-5.58E-05
118	-5.62E-05	-5.6E-05	-6.55E-05	-0.000312	-5.71E-05	-5.5E-05	0.0002275	-5.58E-05
119	-5.62E-05	-5.6E-05	-6.55E-05	-0.000312	-5.71E-05	-5.5E-05	0.0001706	-5.58E-05
120	-5.62E-05	-5.6E-05	-3.28E-05	-0.000312	-5.71E-05	-5.5E-05	0.0001706	-5.58E-05
121	-5.62E-05	-5.6E-05	-6.55E-05	-0.000624	-5.71E-05	0.0001651	-5.69E-05	-5.58E-05
122	-5.62E-05	-5.6E-05	-3.28E-05	-0.000312	-5.71E-05	-5.5E-05	-5.69E-05	-5.58E-05
123	-5.62E-05	-5.6E-05	-6.55E-05	-0.000312	-5.71E-05	0.0001651	0.0001137	0.0001673

Table 6-1(a) Excerpt from a Typical Data File Showing Columns TIME to WEST4

NORTH	SOUTH	MIDDLE	SGCON	SGCAR	SGSTW	SGSTE	LOADTO	DISPTO
0.0002742	-0.002581	-3.16E-05	-0.97488	2.9246411	3.0626521	4.0835361	97.65625	-0.000156
0.0002438	-0.002581	9.468E-05	-0.97488	-0.97488	4.0835361	-1.020884	97.65625	0.000625
0.0002742	-0.002611	-3.16E-05	-0.97488	2.9246411	5.1044202	-1.020884	-24.41406	-0.000156
0.0001828	-0.002581	-3.16E-05	-0.97488	-0.97488	-1.020884	-1.020884	73.242188	-0.000156
0.0001828	-0.00252	-3.16E-05	-0.97488	-0.97488	4.0835361	3.0626521	146.48438	0.0004687
0.0002133	-0.00255	-3.16E-05	-0.97488	2.9246411	-1.020884	3.0626521	244.14063	-0.000156
0.0002133	-0.00255	9.468E-05	-0.97488	-0.97488	-1.020884	4.0835361	73.242188	-0.000156
0.0002133	-0.002581	-3.16E-05	-0.97488	2.9246411	4.0835361	-1.020884	122.07031	0.000625
0.0002133	-0.002581	-3.16E-05	-0.97488	-0.97488	-1.020884	-1.020884	146.48438	0.0004687
0.0002133	-0.002611	-3.16E-05	-0.97488	-0.97488	-1.020884	3.0626521	170.89844	-0.000156
0.0002438	-0.002611	-3.16E-05	-0.97488	2.9246411	-1.020884	2.0417681	122.07031	-0.000156
0.0002133	-0.002581	9.468E-05	-0.97488	-0.97488	-1.020884	3.0626521	146.48438	0.0004687
0.0002133	-0.002611	0.0001262	-0.97488	-0.97488	-1.020884	-1.020884	146.48438	-0.000156
0.0001828	-0.00255	9.468E-05	-0.97488	2.9246411	-1.020884	3.0626521	170.89844	-0.000156
0.0002133	-0.002611	-3.16E-05	-0.97488	-0.97488	-1.020884	-1.020884	-24.41406	-0.000156
0.0002133	-0.002611	-3.16E-05	-0.97488	-0.97488	-1.020884	-1.020884	146.48438	0.0004687
0.0002438	-0.002581	-3.16E-05	-0.97488	-0.97488	4.0835361	2.0417681	122.07031	-0.000156
0.0001828	-0.002581	9.468E-05	-0.97488	-0.97488	-1.020884	-1.020884	122.07031	-0.000156
0.0002438	-0.002581	-3.16E-05	-0.97488	-0.97488	3.0626521	-1.020884	122.07031	-0.000156
0.0002133	-0.002581	6.312E-05	-0.97488	-0.97488	-1.020884	3.0626521	146.48438	-0.000156

Table 6-1(b) Excerpt from Typical Data File Showing Column NORTH to DISPTO

6.3 Observations

During the course of testing, it was observed that the Tinius Olsen internal computer was not reporting all of the data recorded. All of the data was checked and it was determined that five of the eight beams were unaffected by the problem. Several problems were identified in the raw data for the following test specimens. These are shown in Table 6-2.

Beam	Observation
4A	Missing the first 14,000 lbs of the load spectrum
4B	The recorded data was not affected
5	The recorded data was not affected
6	The recorded data accounts for loads up to 60,278 lbs. Hand records taken at the time of testing indicate that the peak load was slightly over 84,000 lbs
7	No data reported between approx. 30,000 and 50,000 lbs. This caused difficulty in fitting a polynomial to the load-deflection curve. Hence, the deflection ductility index reported was calculated using the unmodified method
8	No data reported between approx. 55,000 and 58,000 lbs. This did not affect the results since the yield and ultimate points did not occur within this region
9A	The recorded data was not affected
9B	The recorded data was not affected

Table 6-2 Observations of Raw Data

CHAPTER 7
DATA ANALYSIS

7.1 Introduction

This chapter presents the methods used to analyze the data. Where necessary, a brief description of the theory is provided to supplement the methodology. Numerical results obtained using these methods are presented in Chapter 8.

7.2 Strain

Strain is defined as a ratio of the change in length to the original length, i.e.

$$\varepsilon = \frac{\delta}{L_o} \tag{7-1}$$

Strain values were calculated using the displacement data from the eight horizontally mounted LVDTs using the defining equation above. The eight horizontal LVDT's each had a gage length of 10 in. This was performed using an Excel spreadsheet and strains were calculated for every second of loading time.

7.3 Deflection

Three vertical LVDT's were located directly under the outer load points and at the midspan of each specimen. They were referred to as LVDT North, South, and Middle with reference to their position along the beam length. The displacement data collected was converted to deflection via the following stages.

First, plots of the displacement data were created to identify any extreme behavior of any gage. Then this data was normalized by subtracting the initial value at zero load from every subsequent value. Plots of the normalized data were generated and checked for extreme behavior and consistency. As the beam undergoes bending, the midspan moves upward and the outer ends move downward. Hence, the plot of the midspan displacement, Δ_{middle}, should be negative and the plots of both North and South displacements, Δ_{north} and Δ_{south}, should be positive. The final midspan deflection was calculated using Equation (7-2), which sums the midspan displacement to the average of

the outer displacements. This gives the total relative midspan deflection, $\Delta_{midspan}$.

$$\Delta_{midspan} = \left(\frac{\Delta_{north} + \Delta_{south}}{2} \right) - \Delta_{middle} \tag{7-2}$$

7.4 Ultimate Load Capacities

There are two measures of ultimate load capacities for reinforced concrete beams, namely, ultimate loads and ultimate moments. However, typically moments are referenced when discussing flexural strength. In this study, ultimate load capacity will be evaluated in terms of ultimate moments. Moment prediction calculations were performed for each specimen using standard ACI design equations given by

$$M_n = A_s f_y \left(d - \frac{a}{2} \right) \tag{7-3}$$

$$M_n = 0.85 f_c' ab \left(d - \frac{a}{2} \right) \tag{7-4}$$

Equation (7-3) determines the nominal strength in the case of a tension failure while Equation (7-4) determines the nominal strength for compression failure cases. Both the compression and tension failure values were calculated in order to provide an indication of the actual mode of failure. The entire moment-curvature response also was predicted using the Sika program and a secondary check for consistency was performed using the COMCURVE program which will be described subsequently. Finally, after the experimental moment was determined as theoretically possible, it was compared to the results of the Sika program to determine the percent of ultimate stress that was developed in the laminate. This was used to determine a numerical factor that would account for insufficient or inadequate action of the laminate. This was called the compositeness reduction factor, α.

The applied moment was calculated directly from the recorded load data. The four- point-bending configuration used is identical to a simply supported beam with two equal symmetrical point loads. From the laws of statics, the midspan moment in this

configuration is the product of the applied load, P, and the distance from the end support to the point of application of that load, L. In this case, the load supplied by the loading ram was evenly spread to two point loads. Thus, the applied moment is calculated as

$$M_a = \left(\frac{P}{2}\right)L \tag{7-5}$$

7.5 Curvature

Mechanics of materials dictates that for a straight member undergoing symmetric bending deformation, the curvature of the elastic arc, ϕ, located at a distance y from the neutral axis, is determined below from Equation (7-6). The bending curvature was calculated using the strains, ε, recorded on the concrete surface, the carbon laminate, and along the longitudinal axis of the internal steel reinforcement.

$$\phi = -\frac{\varepsilon}{y} \tag{7-6}$$

A graphical comparison of these three different curvature calculations was performed. It was found that the steel strain readings deviated greatly after the steel yielded, and the possibility of CFRP delamination or debonding reduced the reliability of the curvature calculated using the carbon strain data. The curvature calculated using the concrete strain was found to be the most consistent and was adopted for use in the research.

7.6 Unified Serviceability Approach

Energy absorption in concrete beams can be estimated by considering the area under load-deflection or moment-curvature diagrams. This approach is based on satisfying the serviceability criteria of deflection and crack width. It considers the deflection and serviceability criteria in accordance with ACI 318-95, applied moments corresponding to maximum allowable crack width of 0.016 in (ACI 318R-95 10.6.4), and a deflection of 0.6 in (based on a span/180 limit, Table 9.5 (b), ACI 318-95). Past test results identified curvatures based on the two serviceability criteria to be approximately 0.0005 1/in (Vijay and GangaRao 1996). In this research, this value was adopted for

energy-based determinations of curvature and deflection ductility indices. Consideration of serviceability-based energy level with respect to total energy in a moment-curvature plot provides a basis for addressing ductility in the design of CFRP reinforced concrete systems. If more stringent serviceability criteria are implemented, the curvature limit will be lower than 0.0005. This will lead to increased safety of the structure.

7.7 Deflection and Curvature Ductility

To guarantee a minimum level of ductility before failure, the ACI Building Code recommends that the steel reinforcement ratio of a flexural member, ρ, be less than a maximum value equal to 75 percent of the balanced reinforcement ratio. The balanced reinforcement ratio in a flexural member is defined as the ratio for which failure occurs in the concrete at the same time as the onset of yielding of the steel ($\varepsilon_y = 1500 \times 10^{-6}$ in/in). This perfectly balanced condition is described as over-reinforced because the ACI code considers under-reinforced design cases to be 75% or less of steel area corresponding to balanced steel area. For flexural members, structural ductility is defined as the ratio of deflection at ultimate or at failure to the deflection at yielding of the reinforcement. Hence, for balanced conditions, a theoretical structural ductility index of 1 is obtained.

The analytical models used to interpret the ductility of the experimental beams were modified from models developed previously by Spadea, Bencardino, and Swamy (1998). In this paper, ductility indices are evaluated in terms of the structural characteristics of midspan deflection and curvature at yielding of the tension steel and at ultimate failure. The deflection ductility index, $\mu_{\Delta,}$ calculated from the load-deflection curve gives Equation (7-7) and the curvature ductility index, $\mu_{\phi,}$ calculated from the moment-curvature curve gives Equation (7-8).

$$\mu_{\Delta} = \frac{\Delta_{ultimate}}{\Delta_{yield}} \tag{7-7}$$

$$\mu_{\phi} = \frac{\phi_{ultimate}}{\phi_{yield}} \tag{7-8}$$

Two modifications to this method were made for the purposes of this study. The

first was to evaluate the ductility in terms of the energy at these two points. The energy is the area under the curves at these points. The second modification was to choose the yield and ultimate points based on the unified serviceability based approach (Vijay and GangaRao, 1996). This approach satisfies the ACI crack width and deflection criteria simultaneously and hence this increases the direct usefulness of this research. The ultimate value was evaluated at the assumed concrete limiting strain of 0.0025, and the yield value was taken at the moment corresponding to the serviceability curvature limit of 0.005/d.

7.8 Energy-Based Approach

Ductility of reinforced concrete beams is a measure of the energy absorption capacity. Ductility definitions of steel reinforced concrete beams depend mainly upon the plastic deformation of the steel reinforcement. The area under a load-deflection or moment- curvature curve is a measure of plastic deformation. A ductility index presented in the literature (Spadea et al. 1996) depended mainly upon the distinct yielding level and post-yielding plateau of steel rebars. The ductility in this model was determined simply as the ratio of deflection or curvature at the ultimate limit to the deflection or curvature at the yield point. This model was modified to an energy-based approach. Instead of merely considering the ultimate and yield values of deflection and curvature, the areas under the respective curves at these points would be compared. These areas were evaluated from the moment-curvature curves by integrating trendlines fitted to the curves. Each trendline was a fifth or sixth-order polynomial and had a correlation coefficient to the plotted curves of 0.99 or higher with the exception of Beam 7. Beam 7 did not show acceptable correlation at the sixth order and as a result no ductility index was calculated. Instead, the ductility index was determined as the ratio of the deflections at ultimate to that at yield as suggested by the unmodified ductility index definition (Spadea et al. 1998).

Two areas were evaluated from each load-deflection and moment-curvature curve. The first was calculated at the ultimate limit and was identified by that curvature resulting from the ultimate moment. The ultimate load and moment for each beam was determined from the concrete strain curves. It was taken as that moment corresponding to

the assumed ultimate concrete strain, $\varepsilon_u = 0.0025$. For cases where the strain in the concrete did not reach this limiting value, the maximum recorded concrete strain measured was used. The second area was calculated at the yield limit. The unified serviceability approach provided values for the yield limit. Based on limiting the deflection and crack width, the yield curvature was determined to be 3.03×10^{-4} per inch and the yield deflection was evaluated to be 0.317 in (8mm).

7.9 Reinforcing Ratio

The reinforcement ratio was calculated for the beams under investigation according to Equation (7-9) (ACI 318-95 10.2.7.3).

$$\rho = \frac{A_s}{bd} \tag{7-9}$$

This method is inadequate for reinforced concrete beams with an externally bonded CFRP sheet. The researcher proposes that for design with CFRP laminates an adjusted ρ called ρ^* be used which would account for the difference between the ultimate strength of CFRP and the yield strength of steel by adjusting the area of steel used in the calculation of the reinforcement ratio. The adjusted area of steel, A_s^*, should be calculated as follows:

$$A_s^* = A_s + n\alpha A_{composite} \tag{7-10}$$

where

$$n = \frac{f_{ult\ composite}}{f_{y\ steel}} \tag{7-11}$$

Interviews with prominent researchers suggest that the compositeness reduction factor, α, should vary from 0.5 to 0.7. In this study, it was chosen as 0.7 because the closely monitored conditions of research would eliminate inadequate loss of compositeness. This value was evaluated later in the research by using the Sika program and the experimental results of nominal strength. It was shown that 0.66 was the actual compositeness reduction factor based on the experimental study. The adjusted steel area depends also on a composite-to-steel weighting factor. The weighting factor, n, is the

ratio of the equivalent area of composite in terms of steel, to the area of steel reinforcement. For this research, it was determined that a given area of composite had a strength equivalent to 5.8 times that given area in terms of steel area, $A_s = 5.8 * A_{composite}$, so 5.8 in^2 of steel is equivalent to 1 in^2 of composite.

Replacing the area of steel with the adjusted area of steel gives ρ* as

$$\rho^* = \frac{A_s^*}{bd} \tag{7-12}$$

7.10 Ultimate Strength

The ACI method for determining ultimate strength is based on the plastic deformation of the reinforcement. This is incompatible with fiber reinforced plastics due to the linear stress-strain relation of CFRP until failure. Alternative analysis techniques are necessary to deal with this condition. The technique chosen from the literature to predict the strength of the specimens was a simultaneous equation technique developed by Sika, the manufacturer of the CFRP used. This analytical model is based on the Swiss Code (SIA 162, 1989) and uses a flexural analysis method for CFRP-strengthened members which is very similar to the ACI flexural analysis principles for conventional reinforced concrete. Both methods are based on the equilibrium of the cross-section and the constitutive properties of concrete, steel reinforcement, and CFRP, and rely on certain common assumptions:

1. Bernoulli's hypothesis (plane sections remain plane)
2. No slip between any longitudinal reinforcement and concrete
3. Tensile strength of concrete is zero
4. Steel is bilinear elastohardening, and FRP and adhesive are perfectly linearly elastic

The ultimate or nominal strength was calculated by adding a term to the standard ACI equation to account for the reinforcement contribution of the composite area, $A_{composite}$, giving

$$M_n = A_s f_y\left(d - \frac{a}{2}\right) + A_{composite} f_{ult}\left(h - \frac{a}{2}\right) \qquad (7\text{-}13)$$

7.11 Sika Program

The Sika program served two purposes. The first was to provide a check of the predictions of ultimate moment performed using adjusted ACI guidelines. The second was to establish a compositeness reduction factor for this study using the experimental data. The recorded ultimate moments were compared to the SIKA program to establish the percentile range of ultimate laminate stress which had developed in each specimen. For each percentile range reported by the Sika program, the lower limit was used. This was to incorporate a factor of safety in the calculations. These values were averaged and the average percent of ultimate stress developed was taken as the compositeness reduction factor, α. Table 7-1 shows the percent range of ultimate laminate stress developed given by the Sika program and the average developed stress for the specimens.

Beam	Ultimate Moment (Experimental) (kip-ft)	Percentile Range of Ultimate Laminate Stress (Sika) (%)
4A	75.41	90-100
4B	125.55	100-110
5	97.05	100-110
6	90.42	50-60
7	119.86	60-70
8	107.29	0-10
9A	184.28	--
9B	172.41	60-70
		Mean of the Lower Percentile 65.7%

Table 7-1 Results of Compositeness Reduction Factor Evaluation

7.12 COMCURVE Program

The overall objective of this study as previously stated is to provide information on the ductility of CFRP retrofitted reinforced concrete beams to aid in the development of design guidelines. To achieve this, a computer-based method to predict the moment-curvature response of any tension reinforced rectangular beam was developed using Matlab 5.2 software. The program was titled COMCURVE, and was designed and written to analyze any singly reinforced rectangular beam repaired with any existing type of FRP. While this program was not the prime focus of the research itself, it represents a major achievement of this study and should be mentioned in this report.

This study suggests that one approach to the development of design guidelines governing the use of CFRP to repair damaged concrete infrastructure be the simple modification of existing guidelines. The proposal is to model the CFRP as additional steel reinforcement but with two differences. The tensile strength of the CFRP is much higher than that of steel. The model accounts for this by regarding the CFRP as an extremely high strength steel. The second difference is that CFRP is completely linearly elastic. Steel behaves in a similar fashion up to its yield point. Due to the fact that ACI design is driven primarily by the behavior of steel up to and including this point, the model proposed treats the CFRP ultimate value as if it were the yield value of a much stronger steel.

In order to verify the accuracy of the suggested modifications of existing ACI guidelines, a parametric analysis of the underlying theory had to be performed. The program combines strain compatibility and force equilibrium criteria independent of applied load in an iterative process to predict the moment-curvature relationship of a beam. These principles are the same principles used by ACI 318-95 in the design of beams to fail in tension. Typical results of the COMCURVE analysis are provided in Chapter 8 and Appendix A10.

CHAPTER 8
RESULTS AND DISCUSSION

8.1 Introduction

This chapter presents the results of the tests performed on the eight beams. A discussion of the important points and trends associated with each result is also provided. The graphical and computer-based results are presented in Appendices A3 - A11.

8.2 Reinforcement Ratio and Predicted Failure Modes

Table 8-1 shows the results of the reinforcement ratio calculations and denotes the predicted modes of failure for the specimens. These predictions were made based on a comparison of the adjusted reinforcement ratio, ρ^*, to the maximum design reinforcement ratio as specified by ACI Code. Columns 2 and 3 show the tension steel area and the area of CFRP added. Column 4 shows n, the weighting factor used in the determination of the adjusted area of steel. Column 5 shows the compositeness reduction factor, α. Column 6 lists the adjusted areas of steel for each beam. Column 7 shows the initial reinforcement ratio, ρ, calculated according to ACI guidelines. Columns 8 and 9 show the adjusted reinforcement ratio and the ACI limiting design reinforcement ratio, respectively. Finally, column 10 predicts the mode of failure based on whether the values of ρ^*, the adjusted reinforcement ratio, exceed the ACI recommended limit of ρ_{max}.

Beam	A_s (in^2)	A_{com} (in^2)	n	α	A_s^* (in^2)	$\rho_{initial}$	ρ^*	ρ_{max}	Predicted Failure
4A	0.40	0.093	5.8	0.7	0.778	0.0040	0.0078	0.0283	Tension
4B	0.40	0.149	5.8	0.7	1.005	0.0040	0.0102	0.0283	Tension
5	0.62	0.093	5.8	0.7	0.998	0.0063	0.0101	0.0283	Tension
6	0.88	0.093	5.8	0.7	1.258	0.0089	0.0127	0.0283	Tension
7	1.20	0.093	5.8	0.7	1.578	0.0121	0.0159	0.0283	Tension
8	1.58	0.093	5.8	0.7	1.958	0.0159	0.0198	0.0283	Tension
9A	2.0	0	5.8	0.7	2.000	0.0202	0.0202	0.0283	Tension
9B	2.0	0.093	5.8	0.7	2.378	0.0202	0.0240	0.0283	Tension

Table 8-1 Reinforcement Ratios and Mode of Failure Predictions

A typical tension failure was predicted for all eight of the beams based on a comparison of the proposed adjusted reinforcement ratio, ρ^*, with the ACI design limit, ρ_{max}. The adjusted reinforcement ratio, ρ^*, did not exceed the value of ρ_{max}. A compositeness reduction factor of 0.7 indicates the degree of composite action predicted for the externally applied CFRP laminate. This factor is a combined reduction factor which attempts to account numerically for any circumstances which may adversely affect the CFRP from being fully effective. Such factors are weaknesses in the epoxy adhesive, voids in the glue line, weaknesses in the CFRP laminate, and inadequate surface preparation.

8.3 Graphical Results

Figures 8-1 to 8-5 show recorded and computed results for Beam 4A. They are load vs. steel strain (Figure 8-1), load vs. carbon strain (Figure 8-2), load vs. concrete strain (Figure 8-3), load-deflection (Figure 8-4), and moment-curvature (Figure 8-5).

For the internal steel rebar (Figure 8-1), strain gages recorded steel strain on each bar. The resulting plots are labeled Steel East and Steel West. These gages recorded identical strains below 30 kips and deviate just slightly as load approaches 50 kips. Here, note that the maximum recorded load is about 53 kips. The maximum strains were approximately 0.018 in/in for Steel West and 0.023 in/in for Steel East.

Figure 8-2 shows the load-strain relationship recorded for the CFRP laminate. Notice the maximum strain was 0.00994 in/in or approximately 0.01 in/in, which is 53% of the manufacturer's ultimate strain of 0.019 in/in. In addition, notice that the overall response is not linear elastic but bi-linearly elastic with the tangent modulus of elasticity decreasing after ε_{carbon}= 0.008 approximately. This is because, after yield of the steel, the CFRP carries a greater portion of the tensile load.

Figure 8-3 provides the load-strain behavior for the concrete. Here, the maximum concrete strain is approximately 0.018 in/in. In this case, concrete crushing occurred well before the assumed crushing strain of 0.0025 in/in. This is because the CFRP was able to carry an increased tensile load after the steel had yielded. The corresponding, equilibrium compressive force in the concrete caused the concrete to crush before this theoretical limiting strain had been reached.

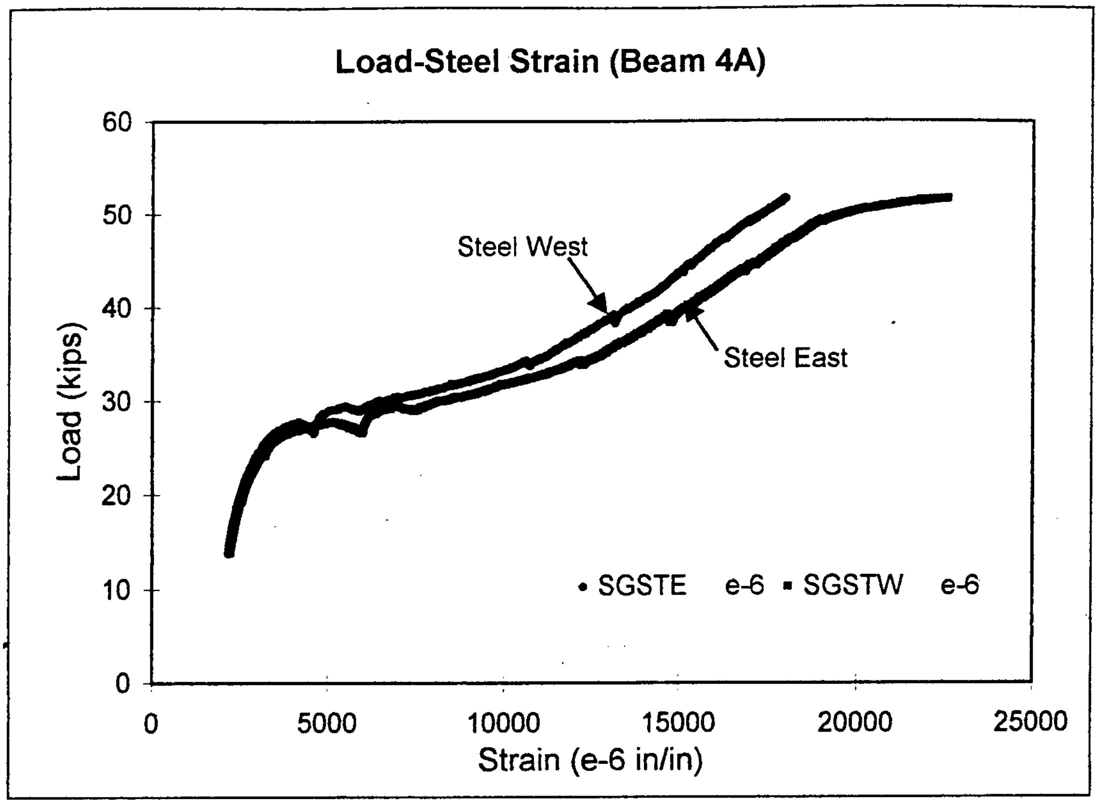

Figure 8-1 Load-Strain Curve (Beam 4A)

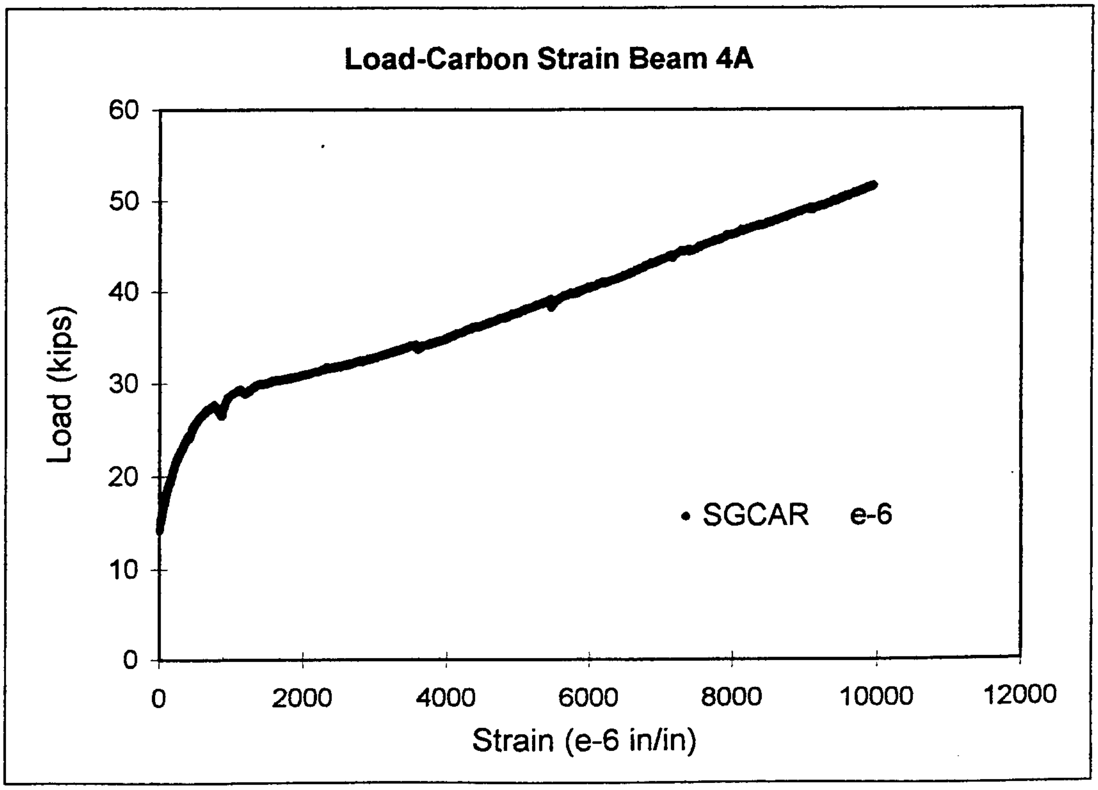

Figure 8-2 Load-Strain Curve (Beam 4A)

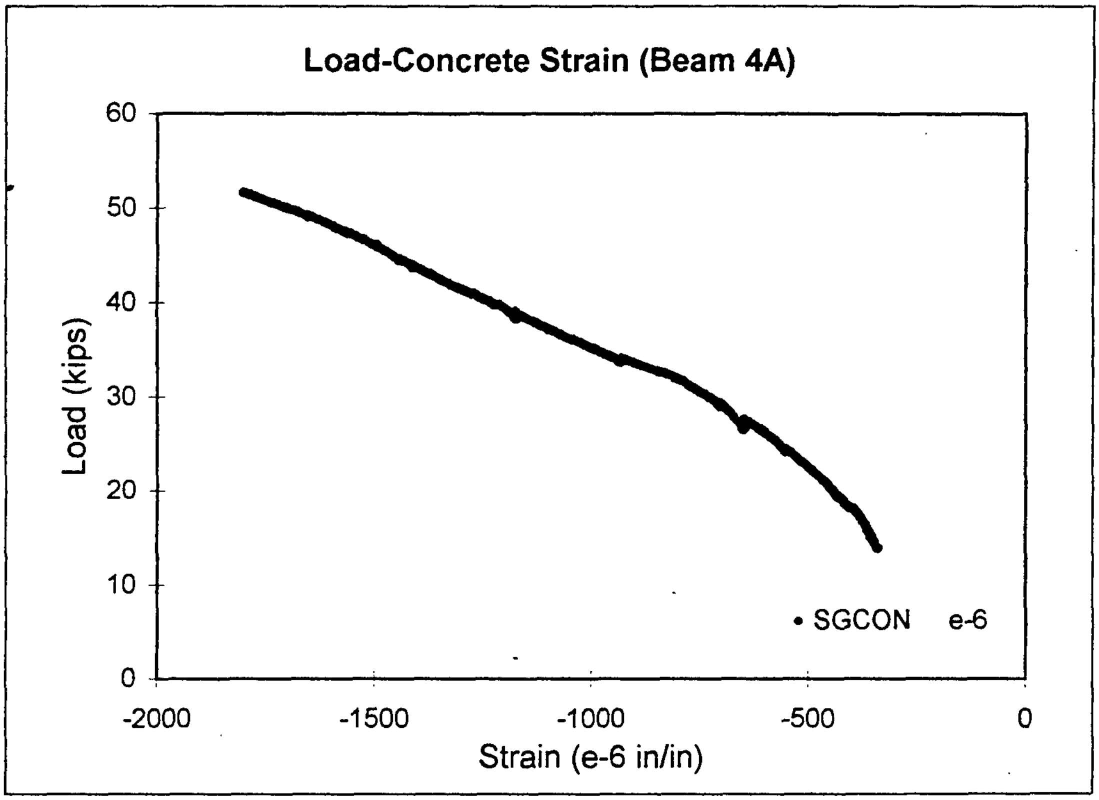

Figure 8-3 Load-Strain Curve (Beam 4A)

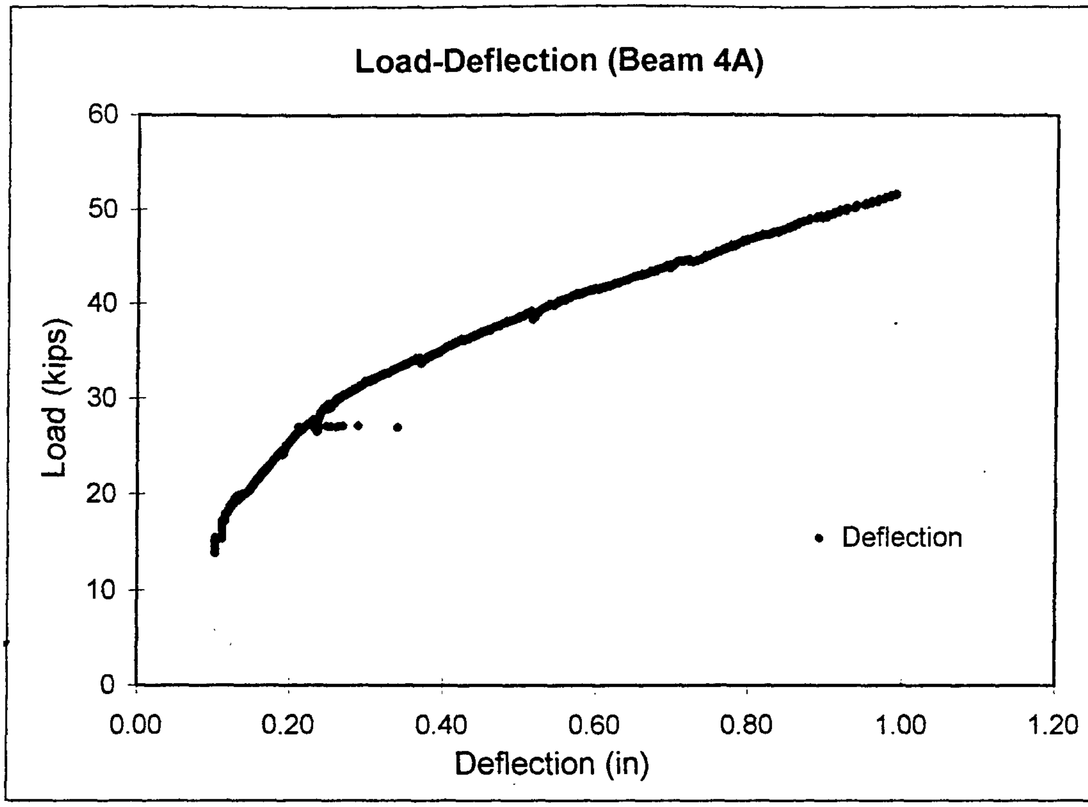

Figure 8-4 Load-Deflection Curve (Beam 4A)

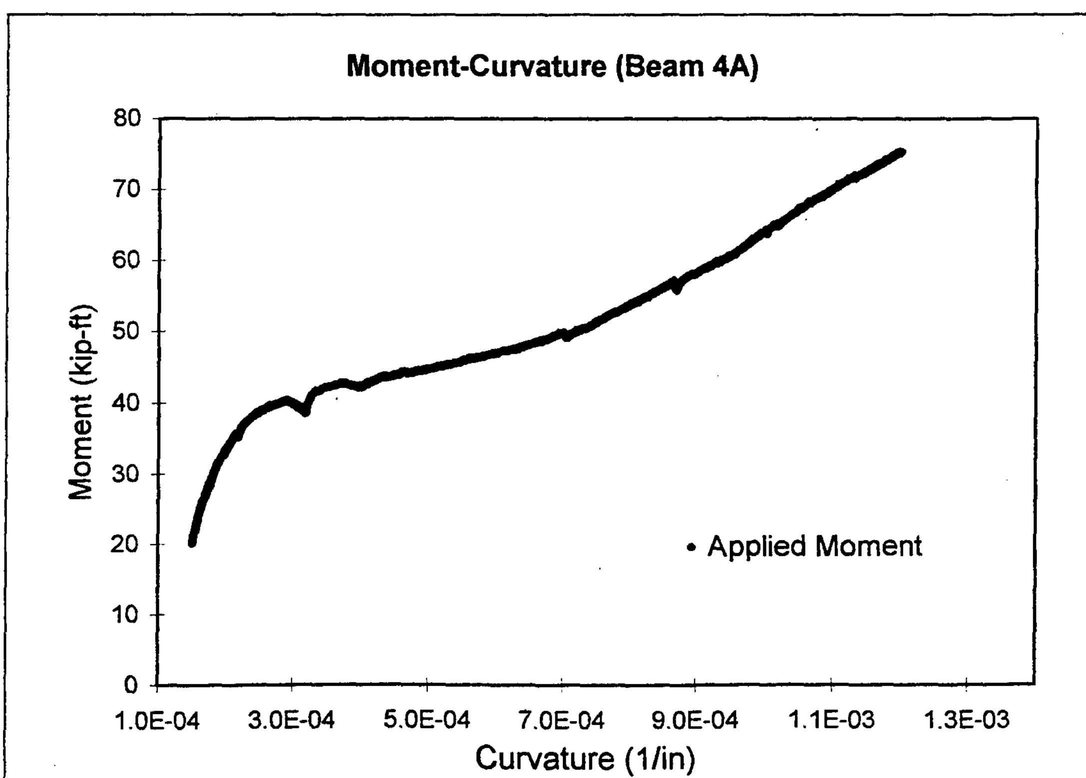

Figure 8-5 Moment-Curvature Curve (Beam 4A)

Figures 8-4 and 8-5 represent the computed structural response for the recorded data. The midspan deflection in Figure 8-4 reaches a maximum deflection of approximately 1 inch at failure. Notice that the stiffness changes as the load is increased beyond 30 kips. This corresponds to the yield point of the steel.

In Figure 8-5, the moment-curvature relationship of the beam is shown. The maximum curvature is approximately 0.0012 per inch. The trend of this curve closely mirrors classical moment-curvature plots in the literature. Again, the distinct yielding point of the internal steel reinforcement is visible as a 'bend' on the curve.

Similar plots for the remaining seven beams are shown in Appendices A3-A9. Figures A3.1, A4.1, A5.1, A6.1, A7.1, A8.1, and A9.1 show the load-strain relationship of the internal steel reinforcement for each remaining beam. In Figures A8.1 and A9.1 corresponding to Beams 8 and 9, respectively, only one curve is shown. This is because the strain data for the other beam was discarded due to faulty or damaged gages.

Figures A3.2, A4.2, A5.2, A6.2, and A7.2 show the load-strain relationship for the CFRP. There are no figures corresponding to Beams 9A and 9B. Beam 9A was the control un-laminated specimen and hence no carbon strain data was collected; Beam 9B carbon data was discarded due to a faulty gage.

Figures A3.3, A4.3, A5.3, A6.3, A7.3, A8.3, and A9.3 show the load-strain relationship for the concrete. These plots were used to determine the ultimate limit for the beams. The load corresponding to the assumed ultimate concrete strain of 0.0025, was identified as the ultimate load. The corresponding ultimate moment was then determined.

Figures A3.4, A4.4, A5.4, A6.4, A7.4, A8.4, and A9.4 show the load-deflection behavior of Beams 4B through 9B. The yield and ultimate deflection values were taken from these plots and used to determine the deflection ductility index. For each curve, a fifth or sixth order polynomial was fitted to the curve and the equation of the curve was integrated twice to provide a measure of the energy beneath the curve. The first integration provided the energy up to the yield value and the second integration provided the total energy at the ultimate value.

Figures A3.5, A4.5, A5.5, A6.5, A7.5, A8.5, and A9.5 show the moment-curvature relationship for each of the remaining eight beams. The yield and ultimate curvatures were taken from these plots and used to determine the curvature ductility index. For each

curve, a fifth or sixth-order polynomial was fitted to the curve and the equation of the curve was integrated twice to provide a measure of the energy beneath the curve. The first integration provided the energy up to the yield value and the second integration provided the total energy at the ultimate value.

8.4 Load-Strain

The structural behavior of the eight beams is represented by their load-strain behavior of the constituent components. Parameters of specific interest are maximum concrete strain, steel and laminate strain trends for both pre- and post cracking stages, as well as strains at yield and ultimate.

Analysis of the load-strain behavior of each beam reveals that the internal steel yielded on all of the beams before failure. This could occur because the yield strain of the internal steel was much lower than the ultimate strain of the external sheet. This had an effect of decreasing the stiffness of the system after it occurred. The marked stiffness decrease could be observed when this occurred from the concrete and carbon load-strain curves. In the carbon case, this is visible as a 'bend' or change in slope (Figures A3.2, A4.2, A5.2, A6.2, and A7.2). This indicates the change in the load environment after steel yield. The more gentle gradient indicates that the carbon experienced more strain per unit load after the steel had yielded than before.

The load-strain relationships for the concrete in the specimens reveals that in the beams with more internal reinforcing (Beam 7, 8, 9A and 9B), the strain in the concrete developed to a much greater extent than in beams with less reinforcement. In each case, concrete strain developed to 2000 microstrains or greater. A similar occurrence was noted in Beam 4B and Beam 5, where high concrete strains in excess of 2000 microstrains were observed. The adjusted reinforcement ratio of Beam 4B as seen in Table 8-1, was almost identical to that of Beam 5. This is because Beam 4B was reinforced with more CFRP than Beam 5. The close agreement in their structural response, as evidenced by the maximum concrete strain, indicates that CFRP and steel behave similarly. This validates the use of our proposed model in which CFRP is modeled as an extremely strong steel. This emphasizes the suitability of CFRP as a replacement or repair material for steel reinforced concrete systems.

In addition, distinct cracking trends can be observed from analysis of the load-strain behavior for concrete. All specimens tested showed at first a linear-elastic behavior followed by a first crack within the constant moment region of the beam. This can be seen as a discontinuity or change in slope on each of the load-concrete strain plots (Figures A3.3, A4.3, A5.3, A6.3, A7.3, A8.3, and A9.3). Thereafter a large nonlinear phase was recorded corresponding to the development of numerous flexural cracks.

8.5 Load-Deflection

The load-deflection curves for Beams 4A, 4B, 5 and 6 show clear tri-linear phases. This means that there are three distinct linear trends in behavior. Each linear segment corresponds to significant events in the loading.

The first linear segment is very steep and corresponds to the stage up to initial cracking. The beam is being loaded without significant deflection. In this pre-cracking stage, the beam is able to support the most load per unit deflection that it will be able to support for the remainder of the loading. This is seen by the steepest line gradient.

The second segment corresponds to the elastic region of the internal steel reinforcement after cracking has occurred and is represented by a line of gentler slope. After the concrete has cracked, the cross section of concrete available for compression is reduced and the concrete carries a smaller compressive load. Consequently, the internal steel which carries the equivalent tension load can now carry a smaller load per unit deflection.

The third line segment corresponds to the post-yielding region of the internal steel reinforcement. In this region, the load carrying capacity of the steel is again reduced but this time, it is due to the steel yielding and not the concrete cracking. After the steel yields, it is not able to support significant increases in load without being significantly strained. The carbon laminate is now the primary tension reinforcement in the system. This segment continues until failure of either the CFRP or the concrete.

The tri-linear behavior was not as noticeable in Beams 7, 8, 9A and 9B. This is because these beams can carry significantly more load before yielding occurs due to more internal steel reinforcement. The load-deflection curves were used to determine the ductility deflection indices by evaluating the energy ratio at ultimate deflection to that at

yield. In the case of Beams 6 and Beams 7, where small gaps in the raw data existed, indices were calculated based on extrapolated values predicted from the linear load-deflection curves.

8.6 Moment-Curvature

In evaluating structural behavior, the moment-curvature curve is more critical and provides better evidence of ductility than the load deflection behavior. The ductility indices evaluated from the moment-curvature plots were more spread than the deflection values and matched more closely the results of similar studies (Spadea et al. 1998).

There is a close relationship between both load and moment and deflection and curvature. Moment and curvature are the first derivative products of load and deflection, respectively. Consequently, there should be a discernible relationship between load-deflection curves and moment-curvature curves. This was definitely true of this study. The tri-linear behavior discussed in the section above was also noticeable in the moment-curvature curves and in the cases where it was not so apparent in the load-deflection plots; the moment-curvature plots displayed it clearly (Figures A3.5, A4.5, A5.5, A6.5, A7.5, A8.5, and A9.5). The tri-linear stages correspond exactly to the stages previously discussed.

In the case of Beam 7 (Figure A6.5), the moment-curvature curve showed the degree of plastic deformation which had taken place. This was not evident after preliminary analysis of the load-deflection curves. As a result, the deflection ductility index for Beam 7 was noted to be possibly inaccurate.

The moment-curvature curves for the test specimens almost exactly mirror traditional theoretical curves. It was established from analysis of each curve that all of the specimens displayed trends and shapes similar to those that occur for beam members in civil infrastructure, particularly those members in four-point bending. This suggests that the results of the tests are viable representations of actual results and indicate that the experimental program of the study was successful.

8.7 Ultimate Load Capacities

All beams tested generally showed large increases in load capacity accompanied by the development of very small cracks. The ultimate loads and moments of the beams and their modes of failure are summarized in Table 8-2. As the concrete strength and the reinforcement ratio increases, the ultimate moment capacity increases, but this increase is limited by the concrete compressive failure strain. Similar remarks have been made by Nanni (1995) and Masmoudi, Theriault and Benmokrane (1996), who documented that the maximum moment capacity is highly variable, because it depends on the concrete maximum strain. This is verified by Beam 6, which, contrary to theoretical predictions, had a significantly lower moment than Beam 5. Analysis of the peak concrete strain for Beam 6 shows it to be appreciably lower than that of Beam 5.

The control beam, 9A, failed at an ultimate load of 123 kips (547 kN) in the predicted tension failure mode. As expected during loading, deflections at midspan were clearly visible and large cracks developed in the tensile zone. By contrast, Beam 9B failed at an ultimate load of 119 kips (529 kN) in brittle balanced failure with crushing of the concrete in the compression zone almost simultaneously as the steel had yielded. The presence of the CFRP caused the reinforcement ratio to approach the maximum recommended reinforcing ratio. This resulted in a change of failure mode from desirable tensile failure to undesirable brittle balanced failure.

Beams 4A, 4B, 5 and 6 displayed large increases in ultimate load capacity over their design values as well as controlled tension failures. This compares well with analytical predictions of failure mode and increased load capacity. Thus, it is shown that modifications to existing design guidelines can accurately model experimental data and it is possible to use CFRP to strengthen damaged systems without changing their design failure mode.

All load capacities were evaluated and presented in terms of nominal strengths, M_n. Table 8-2 shows the nominal strength capacities for the beams. Column 2 provides the ACI theoretical design prediction of nominal strength. Columns 3 and 4 show the semi-experimental calculations of nominal strength for a compression as well as a tension failure. These were calculated according to ACI guidelines. The mode of failure is determined by comparing the experimental moment in column 5 with the theoretical

moments in columns 3 and 4. In cases where the experimental nominal strength exceeds the nominal strength for the tension case, the failure is said to be a tension failure. In cases where, experimental nominal strength exceeds the nominal strength for the compression case, the failure is said to be a compression failure. Exact agreement of tension and compression values would indicate a balanced failure.

Beam	Theoretical M_n (kip-ft)	Semi-Experimental M_n (Compression) (kip-ft)	Semi-Experimental M_n (Tension) (kip-ft)	Experimental M_n (kip-ft)	Observed Failure Mode
4A	39.40	81.81	30.93	75.41	Tension
4B	39.40	126.20	29.86	125.55	Tension
5	59.79	125.26	46.02	97.05	Tension
6	82.76	97.63	67.07	90.42	Tension
7	109.42	157.88	86.05	119.86	Tension
8	138.88	143.47	115.10	107.29	Tension
9A	168.61	190.22	137.97	184.28	Tension
9B	168.61	144.62	145.51	172.41	Tension

Table 8-2 Nominal Strengths and Determination of Failure Mode

There were two methods used in this research to predict nominal strength for the repaired beams. Table 8-3 shows the results of both methods and compares them to the experimentally determined nominal strengths (Column 4). The first was the method proposed in this study. Standard ACI equations and theory were slightly modified to model CFRP as a type of steel reinforcement. To account for the CFRP, an additional term was superimposed on to the standard equations. Thus, Equation (8-1) below was modified to form Equation (8-2). Column 2 lists the modified ACI predictions of nominal strength.

$$M_n = A_s f_y \left(d - \frac{a}{2} \right) \tag{8-1}$$

$$M_n = A_s f_y \left(d - \frac{a}{2} \right) + A_{composite} f_{ult} \left(h - \frac{a}{2} \right) \tag{8-2}$$

The second method of predicting nominal strength was using the Swiss Code based computer program provided by Sika. The Sika program predicts nominal strengths for different percentages of laminate effectiveness. In this study, a compositeness reduction factor was determined from discussion with Dr. Hota V.S. GangaRao of the Constructed Facilities Center at West Virginia University. The value of α chosen was 0.70. This was taken to correspond to the Sika case where only 70% of the laminate's ultimate stress was developed. The values quoted in column 3 represent the Sika predictions at 70% of the ultimate stress.

Beam	Modified ACI M_n (kip-ft)	Sika M_n (kip-ft)	Experimental M_n (kip-ft)
4A	83.87	63.00	75.41
4B	110.5	82.00	125.55
5	105.00	80.00	97.05
6	119.60	99.00	90.42
7	138.30	121.00	119.86
8	161.40	147.00	107.29
9A	168.61	147.00	184.28
9B	180.00	178.00	172.41

Table 8-3 Nominal Strengths of Repaired Specimens

The modified ACI and Sika methods both followed similar trends with similar notable points. The ultimate load capacities were higher than the design load capacities. This emphasizes the strengthening properties of CFRP retrofit techniques. In addition, their predictions were verified by experimental nominal strengths. They both predicted that Beam 4B would have a higher ultimate strength than Beam 5. Experimental results showed these predictions to be accurate. In all cases, the modified ACI method predicted strengths significantly higher than those predicted by the Sika method. This is because the ACI method does not account for inadequate composite behavior, whereas the Sika method takes into account insufficient compositeness. Notice also that the percent

difference between the two methods decreases as the internal steel area increases. This is because the larger size rebar dominates the bending behavior of the beam for the majority of the load spectrum. The contribution of the composite is by comparison, relatively less in these cases. Thus, it can be seen that the modified ACI method provided reasonable predictions of the nominal strength. This supports the proposal in this study.

8.8 Reinforcement Ratios and Observed Failure Modes

Table 8-4 shows the adjusted reinforcement ratio and the balanced reinforcement ratio as well as the observed failure mode

Beam	Reinforcement Ratio, ρ		Observed Mode of Failure
	ρ^*	ρ_{max}	
4A	0.00785	0.028275	Tension
4B	0.01015	0.028275	Tension
5	0.01008	0.028275	Tension
6	0.01270	0.028275	Tension
7	0.01594	0.028275	Tension
8	0.01977	0.028275	Tension
9A	0.02020	0.028275	Tension
9B	0.02402	0.028275	Tension (almost Balanced)

Table 8-4 Comparison of Reinforcement Ratios and Mode of Failure

Test results were identical to predicted failure modes. This data supports the proposal that modified ACI guidelines can accurately model FRP retrofitted systems. In theory, since CFRP laminates have high failure strains (1.5-2.5%) as compared to 0.2% yield strain of Grade-60 steel reinforcement, loading CFRP sheets to their maximum value limits the depth of the concrete compression zone in a reinforced concrete beam if the full strain in the carbon can be induced. This is due to an almost linear variation of strains along the beam depth (plane sections remain plane). However, this linearity does not practically occur due to slip between the reinforced concrete beam and the composite laminate. Increased carbon strains are the result of inadequate or insufficient

compositeness between the beam and the CFRP, while reductions in strain result from bond failure at the glue-line. Similarly, if the same beam is provided with additional CFRP reinforcement, then a larger resisting moment is obtained due to larger compressive area satisfying the force equilibrium criteria. This was the cause of the difference in moments between 4A and 4B, which had the same undamaged configuration but 4B was repaired with more CFRP than was 4A.

Beams 5, 6, 7, 8 and 9A both reached failure by crushing of the concrete long after yielding of the steel reinforcement. Beam 9B displayed a semi-brittle collapse that can be termed as a tension almost brittle failure. This data, more than any other, shows the possible dangers associated with CFRP retrofit. As a result of adding CFRP, Beam 9B experienced a change in failure mode from tension to balanced. This is an undesirable sudden concrete compressive failure. The SIKA results show that only 60% of the laminate ultimate stress was developed. This suggests that the carbon laminate did not bond well with the concrete beam. In situations where 100% compositeness of the CFRP is achieved, beams with initial reinforcement ratios near to the maximum design reinforcement ratio, may possibly exceed that limit. Changes in failure mode from ductile to brittle could be expected. Based on our determined 66% mean compositeness development, it can be shown that additional caution should be exercised in retrofit cases where the initial internal steel reinforcement is greater than 85% of the maximum design reinforcement ratio.

Thus, it has been shown that addition of FRP laminate can result in failure modes other than flexural failure and that these shifts in failure modes can alter the strength and ductility of the system. This leads to the big question as to how to delineate the failure modes in such systems. Prevention of brittle failure is an important criterion for safe and effective retrofit engineering; thus, all particulars of the performance must be established including the failure behavior before recommending a retrofit procedure.

8.9 Ductility Indices

Table 8-5 shows the computed ductility indices for the deflection (column 3) and curvature cases (column 4) as well as the adjusted reinforcement ratio (column 2).

Beam	ρ^*_{adj} (%)	μ_Δ	μ_ϕ
4A	0.785	5.67	10.2
4B	1.015	5.63	7.63
5	1.008	3.50	8.94
6	1.270	3.77	8.24
7	1.594	N/A	7.81
8	1.977	2.55	2.82
9A	2.020	1.93	2.05
9B	2.402	1.60	1.59

Table 8-5 Ductility Indices

Ductility of reinforced concrete beams is essentially a measure of energy absorption capacity through plastic deformation. The ductility index of a concrete beam has been defined as the ratio of deflection (or as curvature) at ultimate to yield. Thus, when a system is non-ductile, as in the balanced case for example, the yield and ultimate values correspond. This would result in a ductility index of 1 since there would be no difference in the yield and ultimate values.

As expected, the control beam, 9A, which displayed a typical tension failure, had a ductility index greater than 1. Beam 9B experienced an almost balanced failure and correspondingly had a lower ductility index. Beams 4A and 4B, which had the lowest laminated reinforcing ratios, still satisfy the ACI criteria for 75% of balanced reinforcing ratio, displayed the most ductile behavior. This is the optimum combination for a repaired beam. These beams showed increases in flexural capacity while retaining significant ductile qualities. Such beams can therefore be considered safe for design on considerations of strength and ductility.

As reinforcement ratio increases, the ductility indices decrease. This is because

the beam is becoming stiffer as more steel or carbon is added and after the steel has yielded, this stiffness limits the amount of deflection and curvature possible. The reinforcement ratio, ρ, is approaching the balanced condition when no deflection after yield occurs.

Another observation shows that as the laminate percentage of total reinforcement increases, the ductility index decreases. The CFRP laminate accounted for 23.3% and 37.3% of the total tensile reinforcement in Beams 4A and 4B, respectively, while for Beams 9A and 9B, the CFRP contribution was 0% and 4.7%, respectively. In both cases, the increases in CFRP contribution corresponded to a decrease in ductility. This means that externally bonding CFRP to reinforced concrete beams results in reduced ductility. Thus, it can be seen that increased load capacities of the repaired beams are accompanied by losses in ductility.

Deflection and curvature ductility indices appear to follow similar trends. The curvature ductility index is greater than the deflection ductility index for all beams except Beam 9B, where the values are essentially the same. The differences in these two ductility indices range from as low as 10.85% for Beam 9A to a high of 60.85% for Beam 5. This shows the unpredictable behavior of retrofitted beams and reinforces the need for an increased understanding of reinforced concrete mechanics with FRP composites.

8.10 COMCURVE Results

As previously discussed, a computer-based method to predict the moment-curvature response of any tension reinforced rectangular beam was developed using Matlab 5.2 software. While this program was designed and written to be applied to any tension reinforced rectangular beam repaired with any existing type of FRP, there was a specific purpose of this program for this research. In order to verify the accuracy of the suggested modifications of changing existing ACI guidelines, a parametric analysis of the underlying theory had to be performed. As discussed in Chapter 6, COMCURVE was developed specifically to test certain modifications of existing ACI guidelines. Results of this study are shown as printouts in Appendix A10.

8.11 Sika Results

This study was conducted using existing ACI sanctioned theory and guidelines with the objective being to assist in the development of guidelines for the United States similar to those already in existence in Europe and Japan. The Sika program is based on existing Swiss Code (SIA 162, 1989) which does cater to FRP usage. The program was run after completion of testing and data analysis in order to provide a check of overall behavior, specifically ultimate moments, initial moment capacity and percentage of ultimate laminate stress developed at particular loads. Printouts of the Sika program spreadsheet for each beam are in Appendix A11. Results from the program were used to first check and second propose a value for α, the compositeness reduction factor suggested for use in the determination of the adjusted reinforcement ratio.

8.12 Summary

In summary, these results have great significance in the design of CFRP reinforced concrete systems, and emphasize that engineers should be fully aware of the structural as well as the safety implications resulting from the use of advanced composites as externally bonded reinforcement.

CHAPTER 9
CONCLUSIONS AND RECOMMENDATIONS

9.1 Introduction

Based on the analytical and experimental results obtained in this study some general and specific conclusions can be drawn. These are reported in the following sections. In addition, no research is complete without a follow up. Recommendations for future work also are included.

9.2 General Conclusions

1. The bonding of CFRP composites to damaged reinforced concrete beams is a viable technology for repair.
2. The strengthening technology consisting of externally bonded CFRP sheets is easy to perform and results in significant improvements in ultimate load capacity.
3. Prediction of load-deflection and moment-curvature behavior is possible using computer-based methods.
4. Existing ACI guidelines do not accurately model the experimental behavior of CFRP retrofitted concrete beams; however, minor modifications to account for the strength and constitutive behavior of CFRP enables reasonably accurate predictions to be made.
5. The use of CFRP as external reinforcement reduces the ductility of an under-reinforced concrete beam, but it is possible to design beams with FRP that still exhibit ductile failure by ensuring that the reinforcement ratio of the retrofitted beam does not exceed the balanced reinforcement ratio.

9.3 Specific Conclusions

1. The adjusted reinforcement ratio, ρ^*, proposed in this study is a better indicator of the combined reinforcing effect of steel and CFRP, hence possible adoption by the American Concrete Institute (ACI) is recommended.
2. The compositeness reduction factor, α, proposed in this study is a suitable model from which to asses the loss of composite action due to defects of external CFRP

composites.

3. The energy-based definition of ductility better assesses the ductile behavior of reinforced concrete beams than traditional discrete-based definitions.
4. The unified serviceability approach provides more appropriate methods for design engineers to define the yield and ultimate limit states.

9.3 Recommendations for Future Work

1. Additional testing of a companion set of beams to validate experimental results.
2. Investigate the fatigue and long-term response of CFRP retrofitted reinforced concrete beams.
3. Investigate the effect of varying the CFRP geometric and mechanical properties.
4. Investigate the environmental effects of moisture, temperature and corrosive salts on the epoxy bond and the CFRP laminate.

REFERENCES

1. American Concrete Institute (1995). "Building Code Requirements for Reinforced Concrete." *ACI 318-95, Am. Concrete Inst.*, Detroit, Michigan.

2. ACI 318-95. (1995). "Building Code Requirements for Structural Concrete and Commentary." *Am. Concrete Inst.*, Farmington Hills, Michigan.

3. An, W., Saadatmanesh, H., and Ehsani, M. (1991). "RC Beams Strengthened with FRP Plates. II: Analysis and Parametric Study." *J. Struct. Engrg.*, 117(11), 3434-3455.

4. Arduini, M., and Nanni, N. (1997). "Behavior of Precracked RC Beams Strengthened with Carbon FRP Sheets." *J. Comp. Constr.* 1(2), 63-70.

5. Baaza, I., M., Missihoun, M., and Labossiere, P. (1996). "Strengthening of Reinforced Concrete Beams with CFRP Sheets." *Proc., 1st Int. Conf. on Compos. in Infrastruct. ICCI 96*, Dept of Civ. Engrg. And Engrs. Mech., Univ. of Arizona, Tuscon, Arizona., 746-759.

6. Bakeri, P.A., (1989). "Analysis and Design of Polymer Composite Bridge Decks," MS thesis, Dept. of Civ. Engrg., Massachusetts Inst. of Technol., Cambridge, Massachusetts.

7. Bencardino, F., Spadea, G., and Swamy, R. N. (1996). "Use of Non-metallic Reinforcements for Rehabilitating New and Deteriorating Structures." *Proc., Int. Conf. on Mat. Engrg.*, XXV AIAS Nat. Conf., Gallipoli, Lecce, L'Editrice Salentina, Lecce, 1185-1192.

8. Buyukozturk, O., and Hearing, B., (1998). "Failure Behavior of Precracked Concrete Beams Retrofitted with FRP." *J. Comp. Constr.*, 2(3), 138-144.

9. Chajes, M., Thomson T., Januszka, T., and Finch, W. (1994). "Flexural Strengthening of Concrete Beams using Externally Bonded Composite Materials." *Constr. and Build. Mat.*, 8(3), 1991-201.

10. Childs, P. J. (1999). "Glass Rebar's Growing Pains". *Civil Engrg,*. Feb. 1999, 65-67

11. Deskovic, N., and Triantafillou, T.C., (1995). "Innovative Design on FRP Combined with Concrete: Short-term behavior." J. Struct. Engrg., ASCE, 127(7), 1069-1078.

12. Diab, J. M., Cook, J. P., and Morsi, A. (1984). "The Strength of FRP Reinforced Concrete Beams." *Proceedings of the Spring Meeting of the American Society of Civil Engineers*, Atlanta, Georgia, pp. 4-17.

13. Faza, S., and GangaRao, H. V. S. (1992). "Pre- and Post-cracking Deflection Behavior of Concrete Beams Reinforced with Fiber-Reinforced Plastic Rebars." *Proc., 1st Int. Conf. Adv. Composite Mat. In Bridges and Struct.*, K. W. Neale and P. Labossiere, eds., Can. Soc. for Civ. Engrg., Montreal, Canada, 151-160.

14. GangaRao, H. V. S., and Faza, S. (1991). "Bending and Bond Behavior and Design of Concrete Beams Reinforced with Fiber Reinforced Plastic Rebars." *Final Report to Federal Highway Administration*, West Virginia Univ.

15. GangaRao, H.V.S., and Vijay , P. V. (1998). "Bending Behavior of Concrete Beams Wrapped with Carbon Fabric." *J. Struct. Engrg.* 124(1), 3-10.

16. Hull, D. (1981). *"An introduction to composite materials."* Cambridge University Press, Cambridge, England.

17. ICCI '96. (1996). "Fiber Composites in Infrastructure,". *1st Int. Conf. on Composites in Infrastructure, ICCI '96*, Department of Civil Engineering and Engineering Mechanics, Univ. of Arizona, Tuscon, Arizona.

18. Jones, R. M. (1999). "Mechanics of Composite Materials". *Taylor & Francis*, Philadelphia, Pennsylvannia.

19. Kaiser, H.P. (1989). "Strengthening of Reinforced Concrete with Epoxy-Bonded Carbon Fibre Plastics", Doctoral Thesis, Diss. ETH Nr. 8918, 1989 ETH Zurich, CH-8092 Zuricj/Switzerland.

20. MacGregor, G.J. (1997). "Reinforced Concrete Mechanics and Design, 3rd Edition". Prentice-Hall, Englewood Cliffs, N.J.

21. Masmoudi, R., Theriault, M., and Benmokrane, B. (1996). "Flexural Behavior of Concrete Beams Reinforced with FRP C-BAR Reinforcing Rods." *Tech. Rep. 2 submitted to Marshall Industries Company, Inc.*, Dept. of Civ. Engrg., Univ. of Sherbrooke, Sherbrooke, Canada.

22. Matthys, S. and Taerwe, L. (1995). "Loading Tests on Concrete Slabs Reinforced with FRP Grids." *Second International Symposium on Non-Metallic (FRP) Reinforcement for Concrete Structures* (FRPRCS-2), E & FN Spon, London.

23. McCormick, F.C. (1978). "Laboratory and Field Studies of a Pedestrian Bridge Composed of Glass Reinforcement Plastic." *Transp. Res. Rec. 665*, Transp. Res. Board, Washington, D.C., 99-107.

24. Meier, U. (1995). "Strengthening of Structures Using Carbon Fiber/Epoxy Composites." *Constr. And Build. Mat.*, 9(6), 341-351.

25. Meier, U., and Deuring, M., Meier, H., and Schuregler, G. (1992). "Strengthening of Structures with CFRP laminates: Research and Applications in Switzerland." Proc., 1st Int. Conf. on Advanced Composite Mat. In Bridges and Struct., The Canadian Soc. for Civ. Engrg., Montreal, Canada, 243-251.

26. Meier, U., and Kaiser, H., (1991). "Strengthening of Structures with CFRP Laminates." Proc., Adv. Comp. Mat. In Bridges and Struct., The Canadian Soc. for Civ. Engrg., Montreal, Canada, 407-417.

27. Nanni, A. (1995). "Concrete Repair with Externally Bonded FRP Reinforcement: Examples from Japan", *Concrete Int.*, 17(6), 22-26.

28. Norris, T., Saadatmanesh, H., and Ehsani, M. (1997). "Shear and flexural strengthening of R/C beams with carbon fiber sheets". *J. Struct. Engrg.* 123(6), 903-911

29. Notes on ACI 318-95. (1996). "Building Code Requirements for Structural Concrete." *Portland Cement Assoc.*, Skokie, Illinois.

30. Plevris, N., Triantafillou, T. C., and Veneziano, D. (1995). "Reliability of R/C Members Strengthened with CFRP laminates." *J. Struct. Engrg.*, ASCE, 121(7), 1037-1044.

31. Ritchie, P., Thomas, D., Lu, L., and Connelly, M., (1991). External Reinforcement of Concrete Beams using Fiber Reinforced Plastics." *ACI Struct. J.*, 88(4), 490-500.

32. Rostasy, F., Hankers, C., and Ranisch, E. (1992). "Strengthening of R/C and P/C-Structures with Bonded FRP Plates." *Advanced composite materials in bridges and structures*, Canadian Soc. for Civ. Engrg., 253-263.

33. Saadatmanesh, H., and Ehsani, M.R. (1989). "Application of Fiber-Composites in Civil Engineering." Structural materials, J. Orifino, ed.

34. Saadatmanesh, H., and Ehsani, M. R. (1990). "Fiber Composite Plates Can Strengthen Beams." *Concrete Int.*, 12(30), 65-71.

35. Saadatmanesh, H., and Ehsani, M.R. (1991). "Analytical Study of Concrete Girders Retrofitted with Epoxy-Bonded Composite Laminates". *J. Struct. Engrg.*, ASCE 117(11), 3434-3455.

36. Saadatmanesh, H., and Ehsani, M. R. (1991a). "Fiber Composite Bars for Reinforced Concrete Construction." *J. Comp. Mat.*, 188-203.

37. Saadatmanesh, H., and Ehsani, M. (1991b). "RC Beam Strengthening with GFRP Plates: Experimental Study." *J. Struct. Engrg.*, ASCE, 117(11), 3417-3433.

38. Saadatmanesh, H., and Ehsani, M. (1991c). "RC Beam Strengthening with GFRP Plates: Analytical and Parametric Studies". *J. Struct. Engrg.*, ASCE, 117(11), 3432-3455.

39. Sen, R. and Liby, L. (1994). "Repair of Steel Composite Bridge Sections using CFRP Laminates." Department of Civil Engineering and Mechanics, Univ. of South Florida, Tampa, Florida.

40. Sika Design Manual, "4.1 Design Procedures (Swiss Code SIA 162)" (1989).

41. Sims, G. D., Johnson, A. F., and Hill, R. D. (1987). "Mechanical and Structural Properties of a GFRP Pultruded Section." Composite Struct., 8: 173-187.

42. Spadea, G., Bencardino, F., and Swamy, R. N. (1998). "Structural Behavior of Composite RC Beams with Externally Bonded CFRP" *J. Compos. Constr.,* 2(3), 132-137.

43. Starr, T. F. (1983). "Structural Applications for Pultruded Profiles." *Composite Struct. 2: Proc., 2nd Int. Conf. on Composite Struct.*, 193-213.

44. Swamy R. N., Lynsdale, C. J., and Mukhopadhyaya, P. (1996). "Effective Strengthening with Ductility: Use of Externally Bonded Plates Made of Non-metallic Composite Materials." *Proc., 2nd Int. Conf. on Adv Comp Mat. in Bridges and Struct.*, The Canadian Soc. for Civ. Engrg., Montreal, Canada, 481-488.

45. Triantafillou, T., and Deskovic, N. (1991) "Innovative Prestressing with FRP sheets: Mechanics of Short-term Behavior." J. Engrg. Mech., 117(7), 1652-1672.

46. Triantafillou, T., Deskovic, N., and Deuring, N. (1992). "Strengthening of Concrete Structures with Prestressed Fiber Reinforced Plastic Sheets." *ACI Struct. J.*, 89(3), 235-244.

47. Triantafillou, T.C., and Plevris, N. (1992). "Strengthening of RC beams with Epoxy-Bonded Fiber-Composite Materials," *Mat. And Struct.,* Paris, France, 25, 201-211.

48. Uy, B., and Bradford, M.A. (1995). "Dutcility of Profiled Composite Beams. Part II: Analytical Study." *J. Struct. Engrg.,* ASCE, 121(5). 883-889.

49. Vijay, P.V. and GangaRao, H.V.S. (1996). "A Unified Limit State Approach using Deformability Factors in Concrete Beams Reinforced with GFRP Bars." *Proc., Mat. for the New Millenium*, 4th Mat. Conf., ASCE, Wash. D.C., 657-665.

APPENDIX A1
BEAM DESIGN CALCULATIONS

A1.1 Introduction

Below is a summary of the critical points in the design of the test specimens. The beams to be tested needed to satisfy two criteria. First, they needed to be designed to ensure they would fail in flexure only. Secondly, they needed to be designed primarily with materials already available in the Structures Laboratory at NIST in order to reduce project costs. NIST inventory available for this project at the start was an 11 ft long box beam section and standard Grade 60 #3 thru #9 steel reinforcement. It was decided to utilize the box beam as the spreader beam of the test rig. The design was done by hand using the #9 bar case.

OBJECTIVE: To design and construct a rectangular reinforced concrete beam using 1 layer of tension steel reinforcement (#3 to #9 steel rebar) with a maximum span less than or equal to the 11 ft spreader beam that would fail in flexure under four-point loading.

Step 1: Determine Beam Dimensions

Width

For a rectangular beam with 2 #9 bars, to satisfy ACI Code for minimum beam width, minimum clear distance between reinforcing bars and minimum cover, width, b, must be greater than or equal to 6.38 in. Table 14.5 of the Civil Engineering Reference Manual (CERM) states that minimum width, b_{min} is 6.1 in. The smaller of the two controls the design, thus:

$$b_{min} \geq 6.1 \text{ in}$$

Take b = 6 in, since for short term unexposed research beam, clear cover of 1.5 in is not essential. Choosing the lower value of 6 in will reduce costs while satisfying research goals.

<u>Depth</u>

The reinforcement ratio, ρ is calculated:

$$\rho = \frac{A_{st}}{bd} \qquad \text{(A1.1)}$$

where d = effective beam depth (depth to the tension reinforcement).

ACI 10.3.2 governs the usable limits for ρ:

$$\frac{200}{f_y} \le \rho \le 0.75\rho_{balanced} \qquad \text{(A1.2)}$$

The balanced reinforcing ratio, $\rho_{balanced}$ is dependent on the concrete compressive strength. The design concrete strength desired is 6,000 psi. The yield strength, f_y, is 60,000 psi for Grade 60 steel. We have

$$\rho_{balanced} = \frac{0.85\beta_1 f'_c}{f_y} * \left(\frac{87{,}000}{87{,}000 + f_y}\right)$$

where β_1 = 0.75 for concrete with strength of 6000 psi. β_1 is an empirical constant.

$$\rho_{balanced} = 0.0377$$

$$\rho_{\max} = 0.75\rho_{bakanced}$$

$$\rho_{\max} = 0.0283$$

$$0.0283 \ge \frac{A_{st}}{bd}_{\min}$$

For 2 #9 bars, $A_{st} = 2.00$ in^2, giving

$$d \ge \frac{2.00}{0.0283 * 6}$$

$$d \ge 11.78 \text{ in}$$

Introduce CFRP laminate which has an ultimate strength approximately 6 times the yield

strength of steel. Account for the laminate by equating it to an area of steel six times larger. This results in the total area of tensile reinforcement to be 2.5760 in^2.

$$\rho_{\max} \geq \frac{A_{total}}{b*d}$$

$$d \geq \frac{A_{total}}{b*\rho_{\max}}$$

$$d \geq 15.476$$

Let d = 16 in for ease of construction. ACI 7.7.1 specifies that the nominal depth, h, for a beam should be h = d + 1.5. This gives h = 17.5 in but let h = 18 in for ease of construction.

Step 2: Determine Span Length

The span length was limited to less than that of the spreader beam identified for use in the test rig. The span would need to be less than 11 ft. In order to perform a four-point flexural test, it was desired to have three equal length regions. This determined that a span of 9 ft was ideal. It was the longest span that could be divided in three equal sections easily. This was refined to 9 ½ ft after the load plates were made. They were 6 in x 6 in x 1in plates. The load would be applied to the center of each plate, leaving two 3 in sections to the outside of the load points. The addition of 6 in accounted for this while still allowing the four-point flexure to be performed over a 9 ft span.

Step 3: Design Shear Reinforcement

The shear reinforcement was designed to reduce or eliminate as much as possible the probability of a shear failure occurring in the specimens. The purpose of shear reinforcement is not to prevent crack formation but to limit the length of cracks. V_c = nominal shear strength provided by concrete, V_s = nominal shear strength provided by steel shear reinforcement, V_n = nominal shear strength overall, and V_u = required shear strength of the member.

$$V_C = 2\sqrt{f'_c}bd$$

Calculate with b = 6 in, d = 16 in and f'_c = 6000 psi

$$V_C = 15{,}274 \text{ lbs}$$

$$V_U \geq \phi V_C$$

ϕ = 0.85 for shear (Strength Reduction Factor, ACI 9.3)

$$V_U \geq 12{,}983 \text{ lbs}$$

$$V_{st} = \frac{V_u}{\phi} - V_c$$

$$V_{st\ max} = 8\sqrt{f'_c}bd \quad \text{(ACI 11.5.6.8)}$$

$$V_{st\ max} = 61{,}094 \text{ lbs}$$

Use maximum shear strength provided by steel to find the required minimum factored shear strength

$$\frac{V_u}{\phi} = V_{st} + V_c$$

$$V_u = 64{,}912 > \phi V_c$$

So we need more than the minimum reinforcement ACI 11.5.4 specifies that the spacing of shear reinforcement, s, shall be the minimumof 24 in or $h/2$, which in this case equals 9 ft. Therefore let s = 9 ft. To calculate the minimum area of shear reinforcement, ACI 11.5.5.3 defines A_v as:

$$A_{v\ min} = 50\frac{b*s}{f_y} \geq 0.0675$$

$$A_{v\ max} = \frac{sV_{st}}{f_y d} = 0.7637$$

Try 7 #3 bars, $A_v = 0.77$ in^2

$$s = \frac{A_v f_y}{50*b}$$

$$s_{max} = 4.5 \text{ in} \quad \text{(ACI 11.5.4.3)}$$

$$\text{Since } V_{st} \geq 2V_c$$

$$A_{v\ min} = 0.0338 \text{ in}^2, \text{ Try } s = 4 \text{ in}$$

$$A_v = 0.3818 \text{ in}^2$$

$$\text{Take 4 \#3 bars, } A_v = 0.44 \text{ in}^2$$

To over - reinforce for shear use more than 4 #3 bars, for this study use 7.

APPENDIX A2
COMCURVE CODE

A2.1 Introduction

This program served two purposes. First, it was developed to predict moment-curvature behavior of CFRP retrofitted reinforced concrete beams. Second, it was used to test the suggestion that present ACI guidelines can be easily and adequately modified to design for FRP-reinforced concrete beam systems. Described here is the COMCURVE program code with accompanying explanations *italicised.* This program uses an iterative simultaneous method solution method to determine moment-curvature pairs of values. Only the COMCURVE code is presented here. Results of the COMCURVE analysis are presented in Appendix A10.

COMCURVE Code

```
clear
format long
%Program for Moment-Curvature Graph%
%
As = input ('What is the area of steel?');
Al =  0;
Epyield = .002;
Epult = .0154;
Es = 2.9e7;
El = 2.25e7;
error = 1000;
b = input ('What is the width of the beam?');
d = input ('What is the depth to the centroid of steel?');
h = input ('What is the nominal depth of the beam?');
%
```

The above lines establish the material properties and beam dimensions. In addition, an accuracy to within 1 kip (1000 lbs) is set.

```
Fy = As*Es*Epyield;
Fu = Al*El*Epult ;
%
```

The above lines set up the force calculations according to existing ACI practice.

```
fprimec = 6000;
Eprimeconc = 0.0035;
```

COMCURVE ensures that the full spectrum of loading is predicted by over-estimating ϵ_{cu}. For ϵ_{cu} , ACI uses 0.003 for the maximum possible concrete strain, COMCURVE uses 0.0035 in order to be conservative.

```
ii=1:35;
deltac = 5*d/60;
for j = 1:10;
c(j) = d - deltac*(j-1)
end;
Epc = 0.001*ii;
 n = 0;
 for l = 1:length(c);
 for k = 1:length(Epc);
```

The above lines generate the iterative solution. There are two beam characteristics which are highly dependent on other parameters and cannot be known with certainty from a design perspective. They are c, the depth to the neutral axis, and ϵ_{cu}, the ultimate concrete strain. Above, limiting values for each are assumed and the range over which they can possibly exist is discretised. Thus, two variables are established: Depth to the neutral axis, which varies between 0 and the nominal depth of any beam, and ultimate concrete strain which varies between 0 and an assumed limiting value 0.0035.

```
 Eps = (Epc(k)/c(l))*(d - c(l));
% Epl = (Epc(k)/c(l))*(h - c(l));
```

Strain compatibility is checked. This is first of the two underlying criteria for ACI code.

```
 Fsteel = As*Es*Eps;
% Flam = Al*El*Epl;
  if Fsteel>Fy;
  Fs = Fy;
  else
  Fs = Fsteel;
  End
%   Fl = Flam;
%   if Flam > Fu;
%   Fl = Fu;
```

```
% end
```

Force values in the steel are established for both pre- and post steel yielding.

```
fcon = fprimec*(2*(Epc(k)/Eprimeconc) - (Epc(k)/Eprimeconc)^2);
 Fc = b*c(l)*fcon;
```

The above lines are a parabolic approximation to the concrete compressive stress block. Fc is the sum of many small horizontal compressive forces in the concrete modeled to follow a parabolic distribution.

```
%fprintf('\n\t\r %e %e %e %e',Fs,Fc,Fsteel,Fy)
% if(Fc - Fs - Fl) < error;                                        (*)
```

*Force equilibrium is checked (see *). This line is of critical importance. It details that the difference between Fc, the compressive force in the concrete and (Fs + Fl), the tensile force must be less than the allowable limit. Essentially, they must be equal and opposite and hence in equilibrium. COMCURVE will not continue to the end until force equilibrium is established. The values at which equilibrium is established are printed.*

```
   deltaf = abs(Fc - Fs);
  while deltaf <error;
   n = n + 1;
   i = 1:20;
   y = (c(l)*i)/20;
   Epconc = (Epc(k)/c(l))*y;
   fconk = fprimec*(2*(Epconc/Eprimeconc) - (Epconc.^2)/(Eprimeconc^2));
   Fc1 = (fconk*b*c(l))/20;
% FCtotal = sum (Fc1(:));
 M(n) = sum (Fc1.*y);
```

At this stage, both Force Equilibrium and Strain Compatibility have been checked and passed. COMCURVE uses the forces at equilibrium to calculate the corresponding moment at that instant.

```
 Curvature(n) = Epc(k)/c(l);
```

The curvature is calculated based on the concrete strain that satisfied the ACI assumptions. This is paired to the moment calculated above. This forms one pair of

moment-curvature values. COMCURVE logs these values in a matrix and returns to the loop to repeat the procedure for every discretized value of c and ϵ_{cu}.

```
 fprintf('\r')
   fprintf('\n Data does  satisfy equilibrium')
   fprintf('\n %f %f %f %f %f',l,k,n,Fc,Fs)
  fprintf('\n Data does not satisfy equilibrium')
%   fprintf('\n\t\r %8.2e %8.2e',M(n),Curvature(n))
   end;
end;
end;
   plot(Curvature,M,'-+')
```

These commands print the full range of corresponding moment-curvature pairs and plots them against each other.

APPENDIX A3–A9

GRAPHICAL RESULTS OF BEAM TESTS

The following are the plots of the load-strain relationships for the steel, carbon laminate and concrete, as well as the load-deflection and moment curvature responses for Beams 4B, 5, 6, 7, 8, 9A, and 9B. Please note that Figures A8.2 and A9.2 corresponding to the load-strain response in the CFRP for Beams 9A and 9B have been intentionally omitted for the reasons given in Chapter 8.

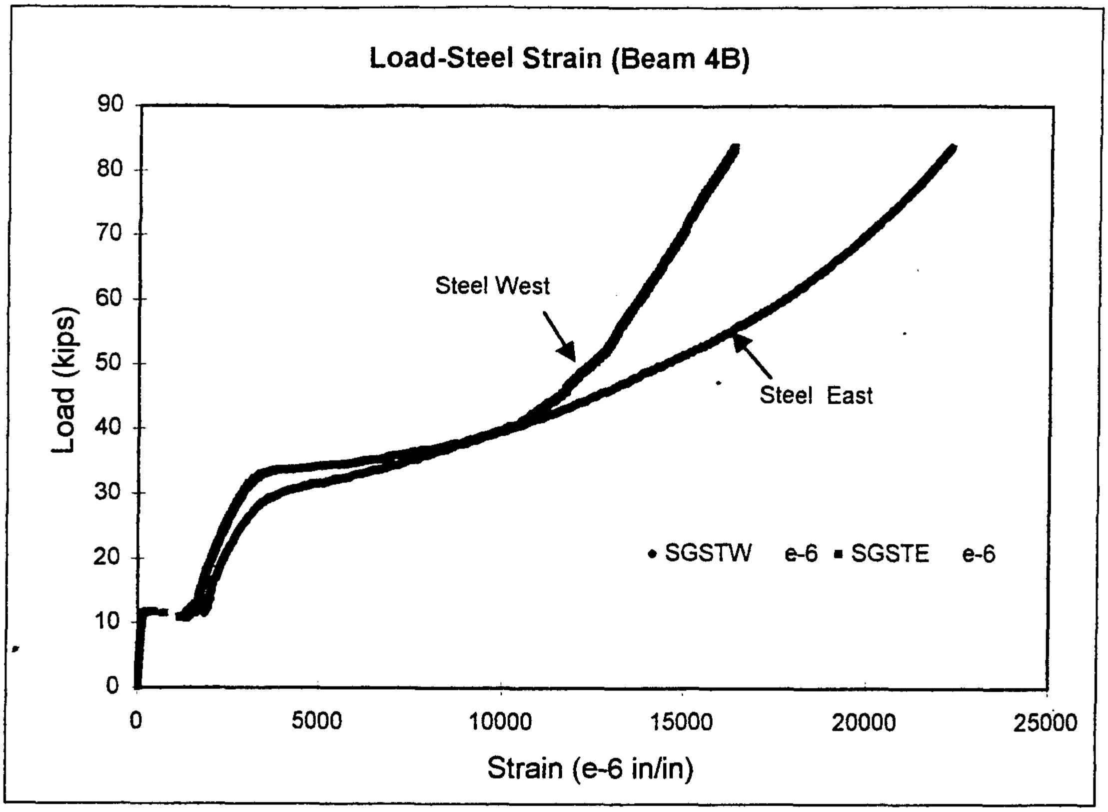

Figure A3.1 Load-Strain Curve (Beam 4B)

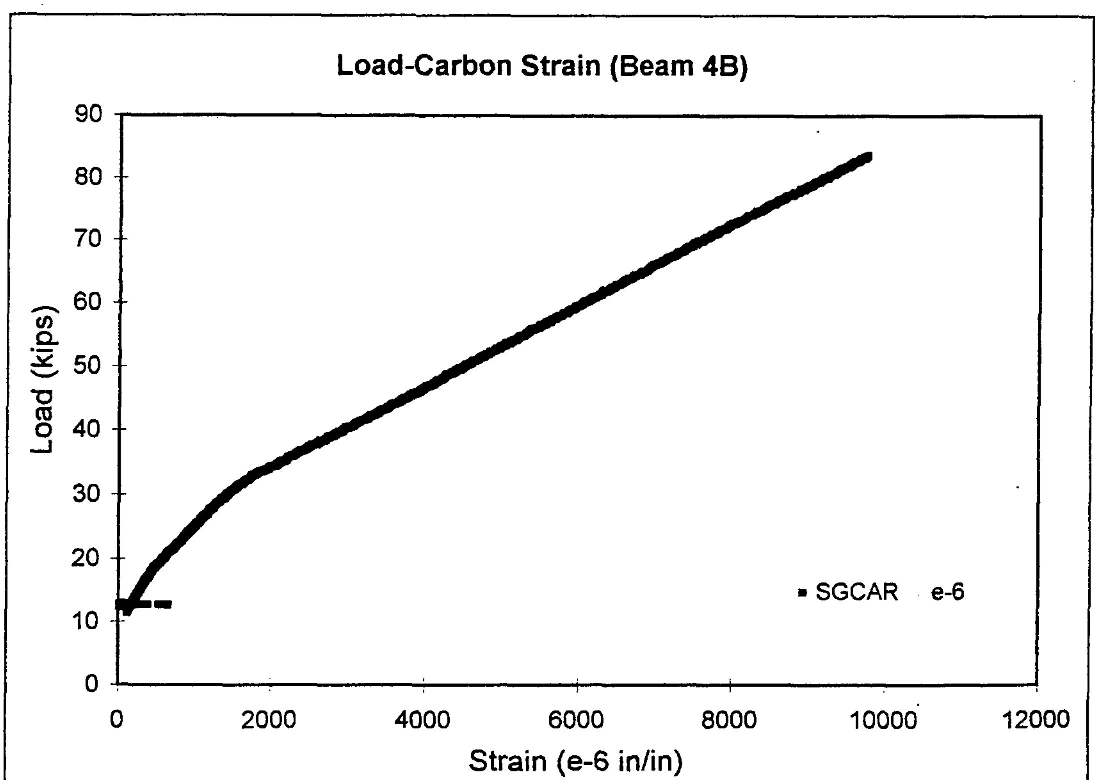

Figure A3.2 Load-Strain Curve (Beam 4B)

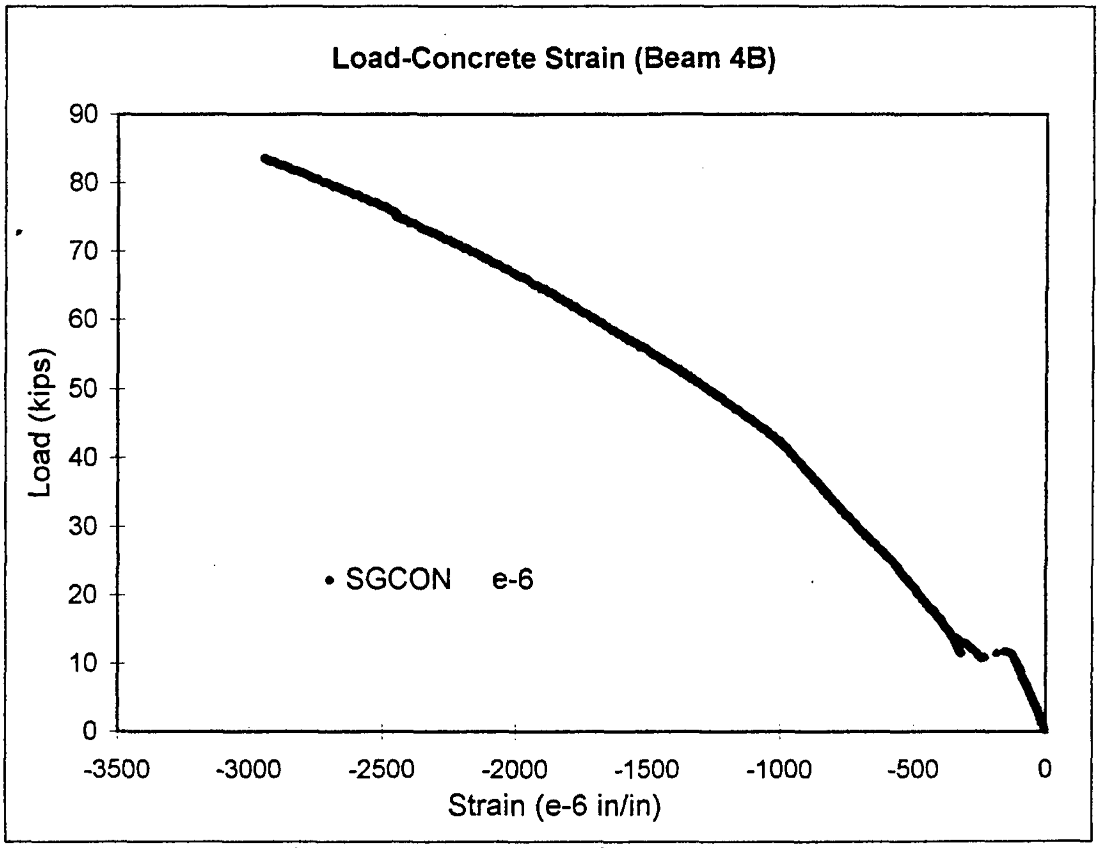

Figure A3.3 Load-Strain Curve (Beam 4B)

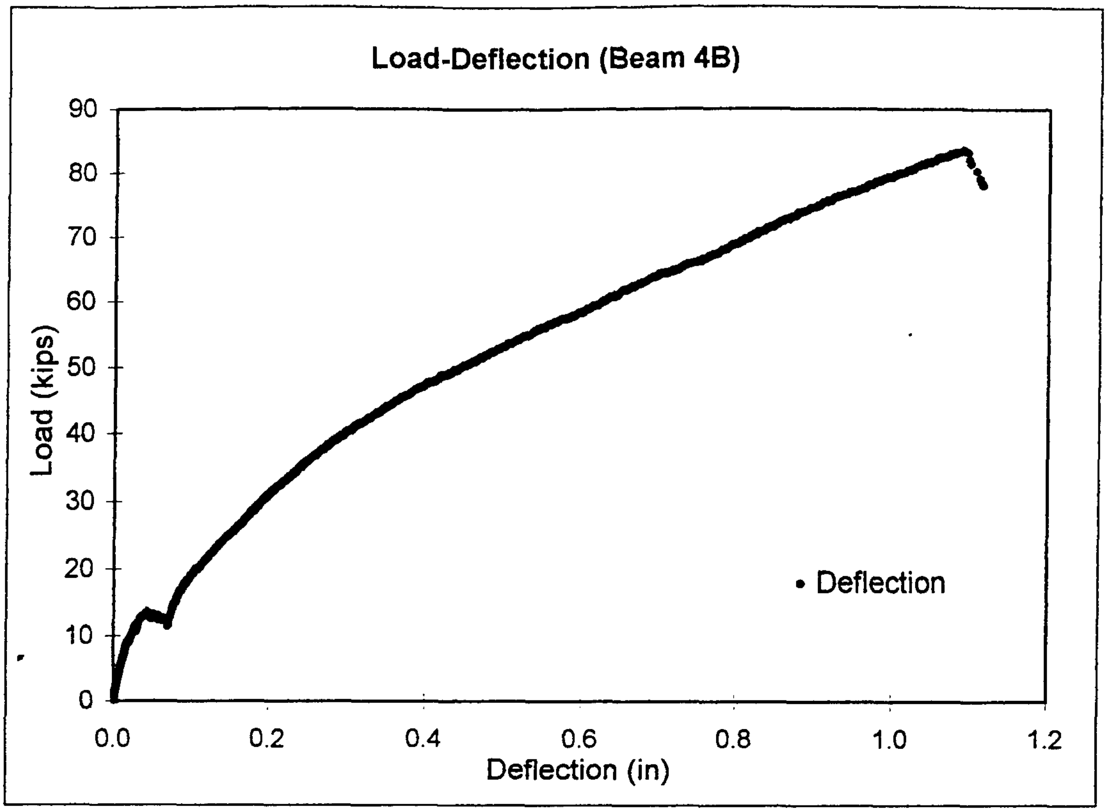

Figure A3.4 Load-Deflection Curve (Beam 4B)

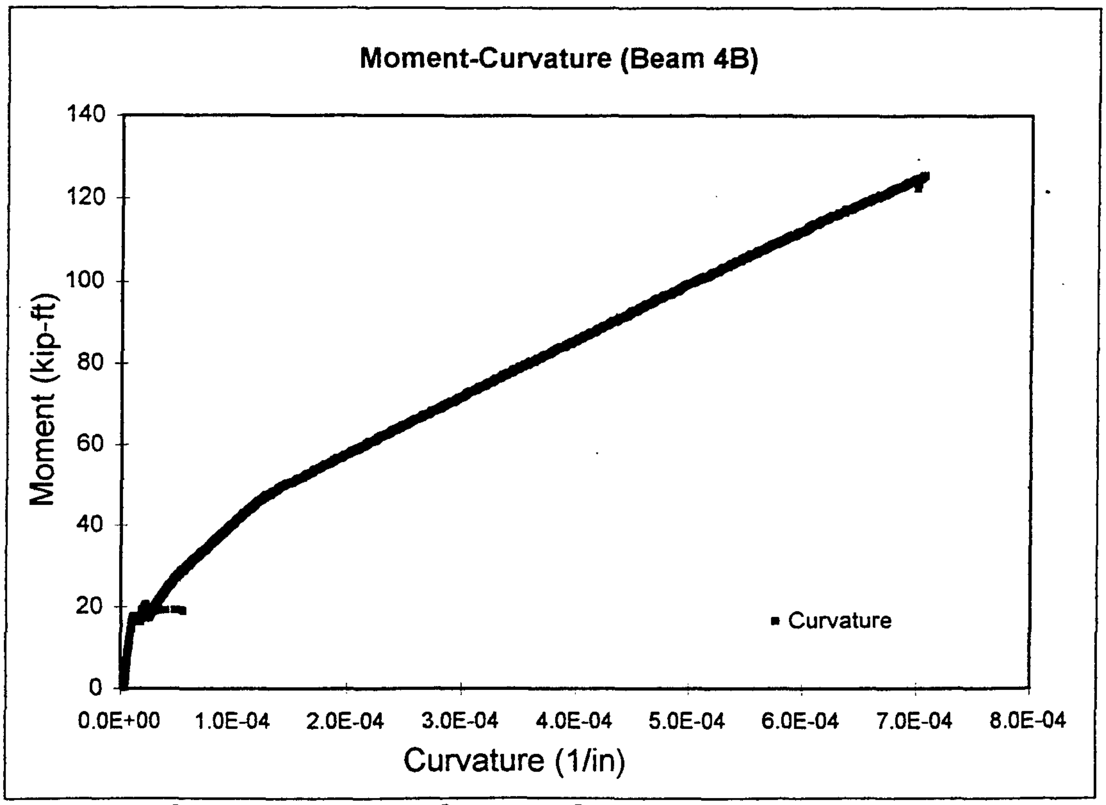

Figure A3.5 Moment-Curvature Curve (Beam 4B)

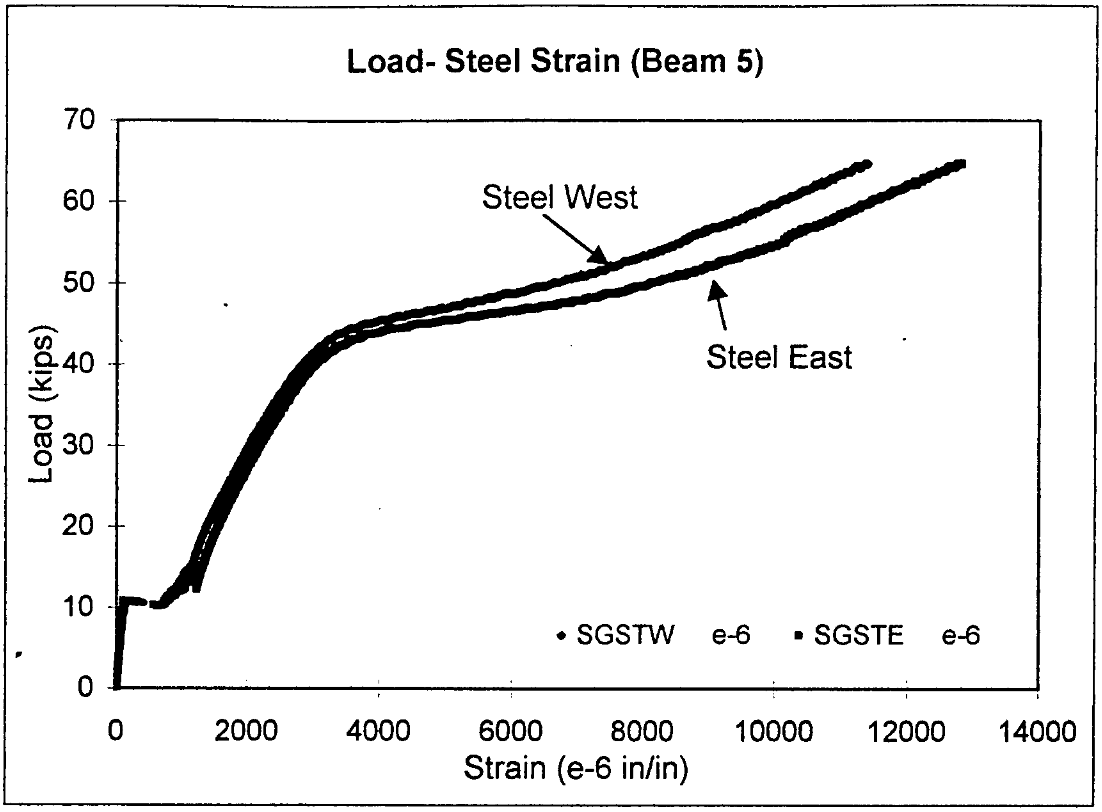

Figure A4.1 Load-Strain Curve (Beam 5)

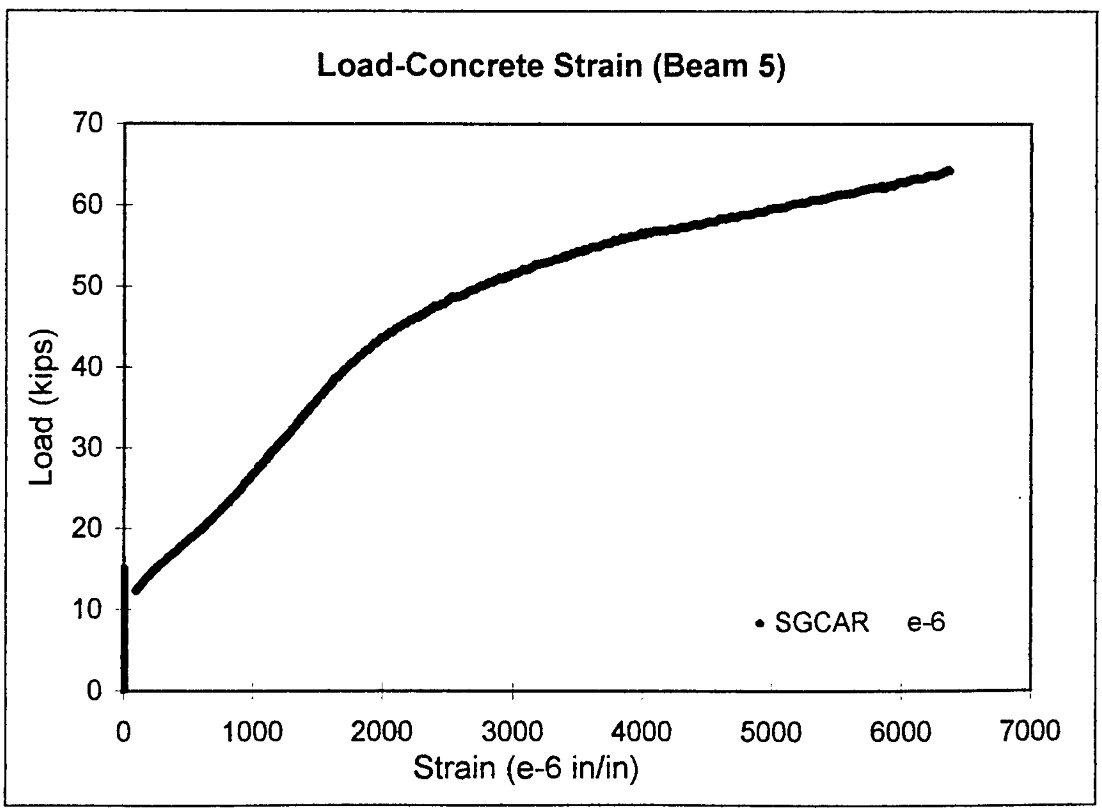

Figure A4.2 Load-Strain Curve (Beam 5)

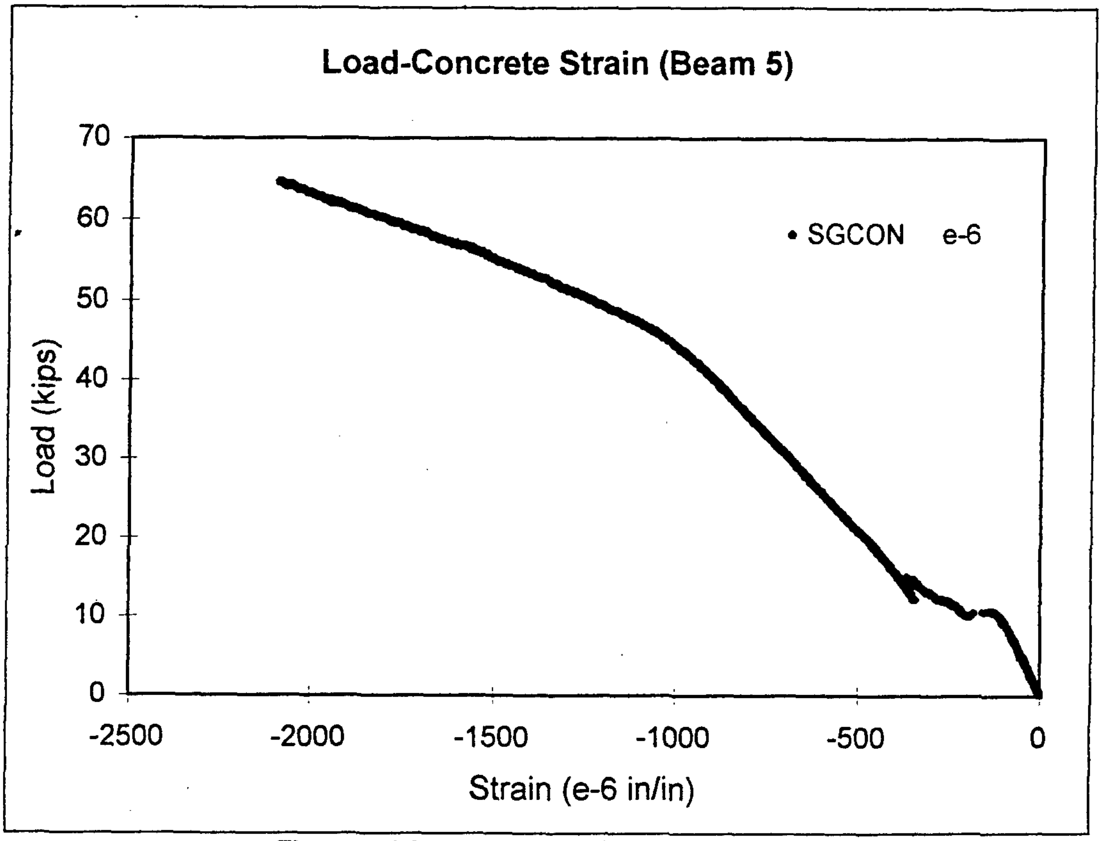

Figure A4.3 Load-Strain Curve (Beam 5)

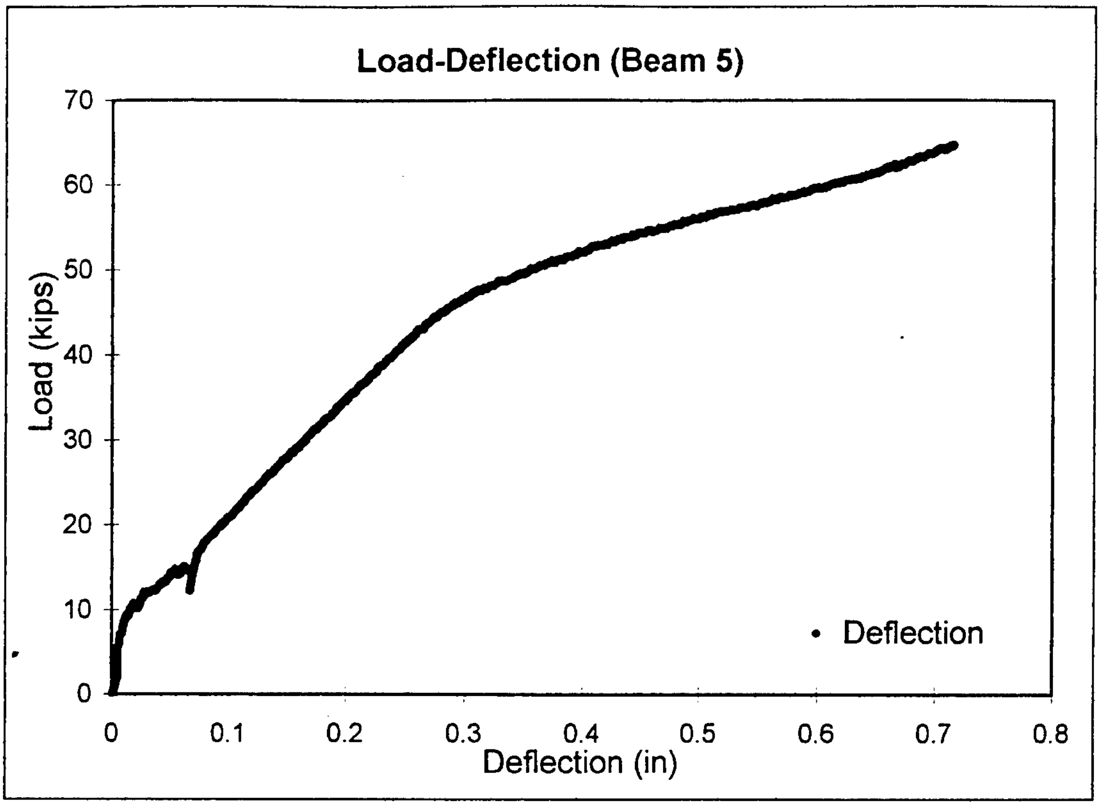

Figure A4.4 Load-Deflection Curve (Beam 5)

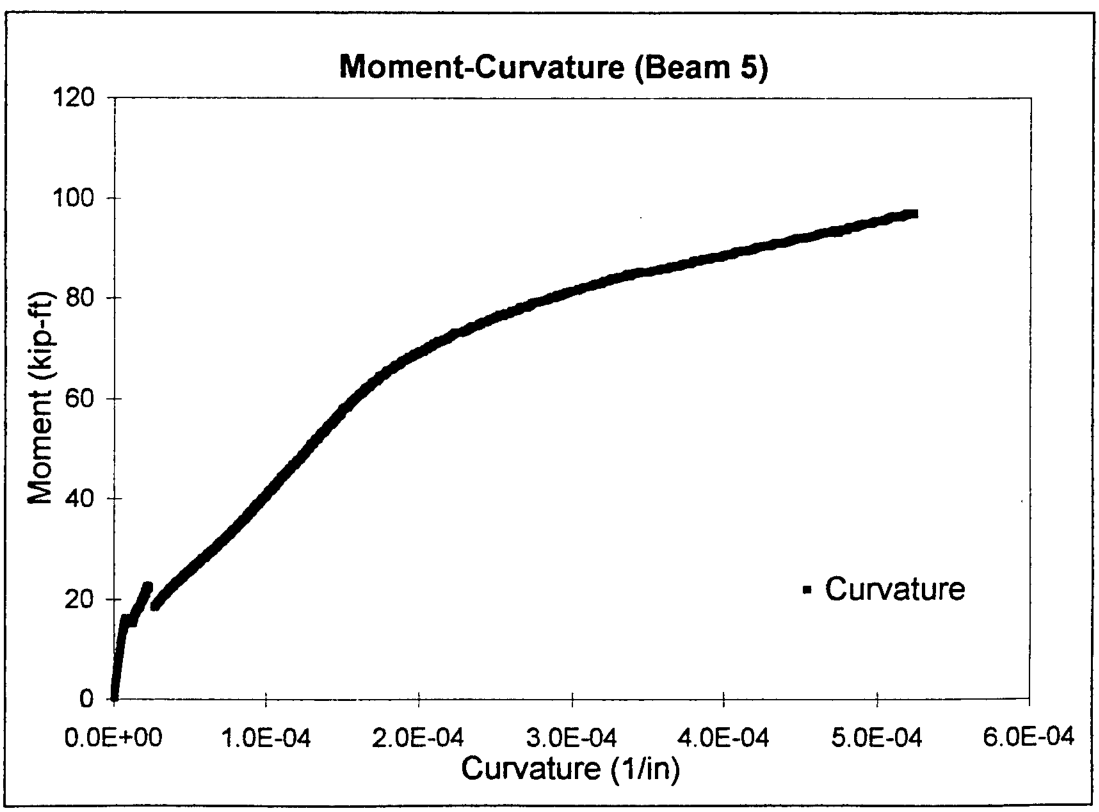

Figure A4.5 Moment-Curvature Curve (Beam 5)

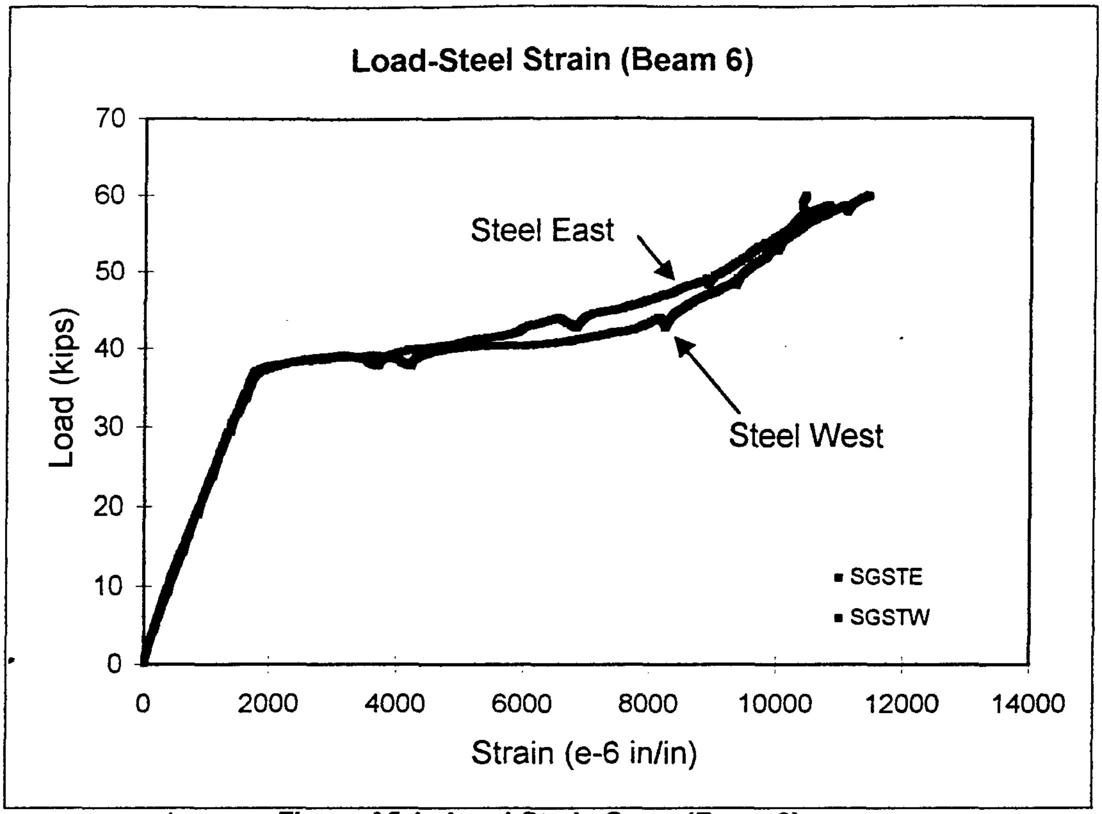

Figure A5.1 Load-Strain Curve (Beam 6)

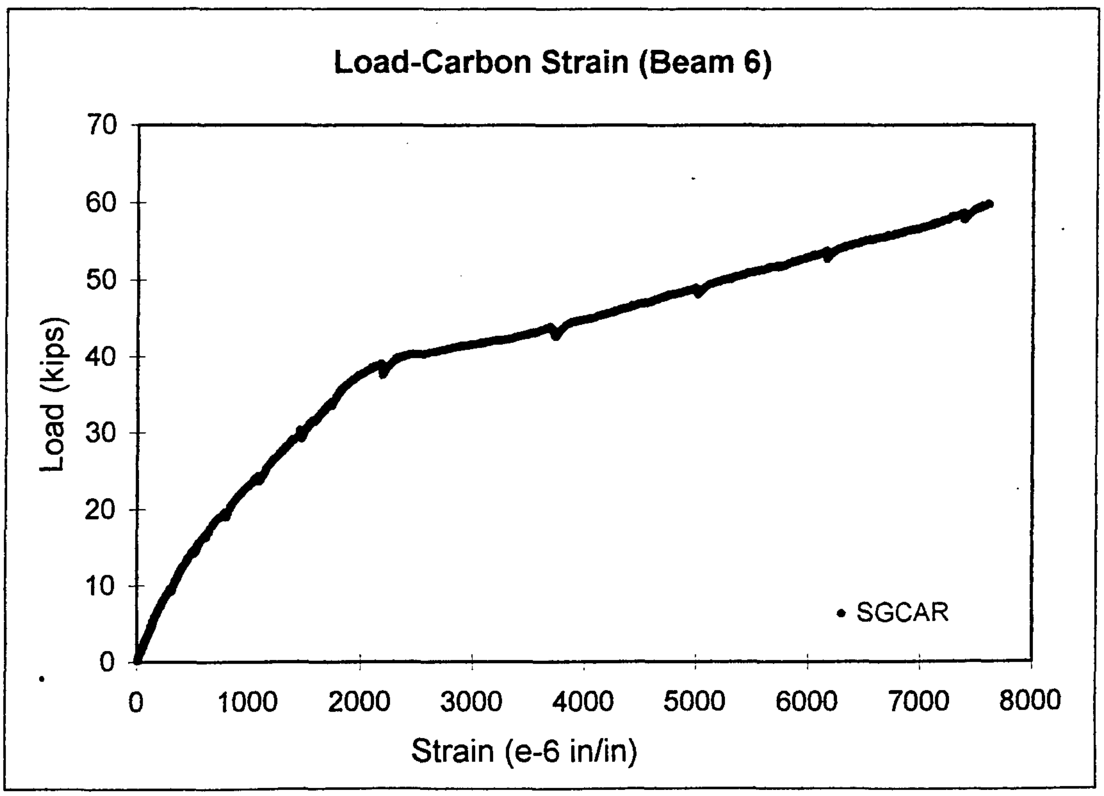

Figure A5.2 Load-Strain Curve (Beam 6)

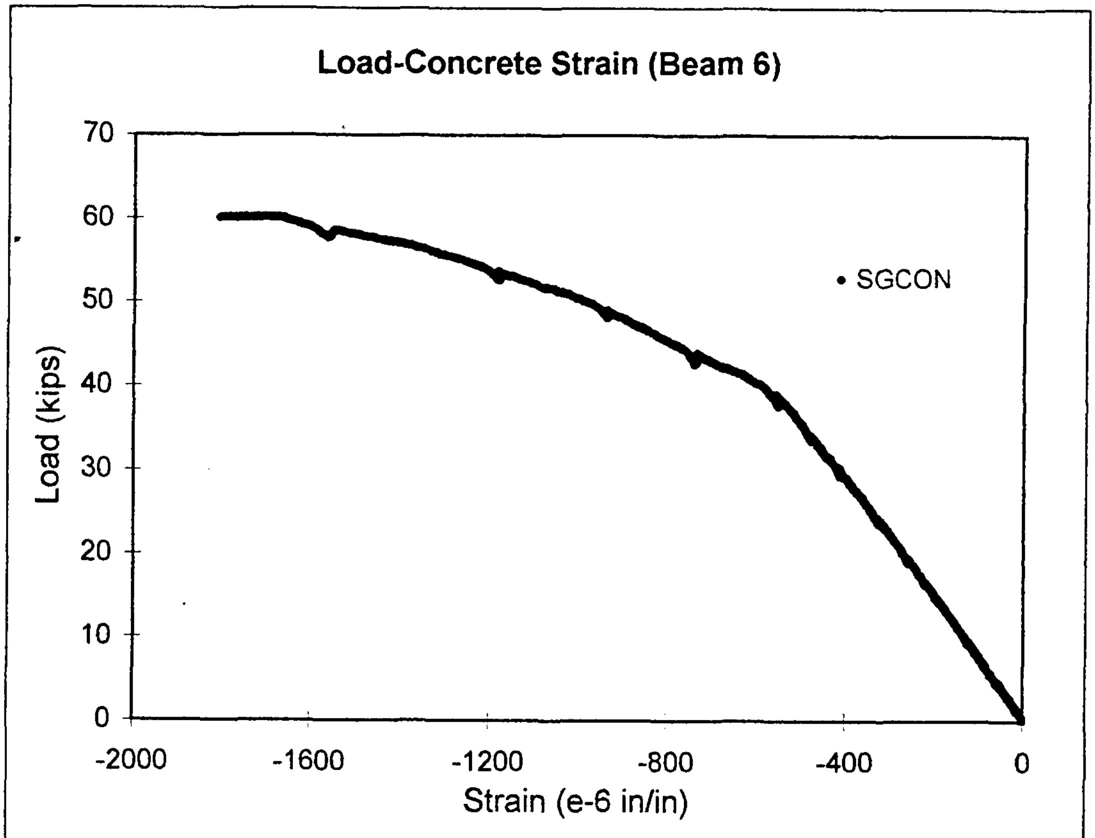

Figure A5.3 Load-Strain Curve (Beam 6)

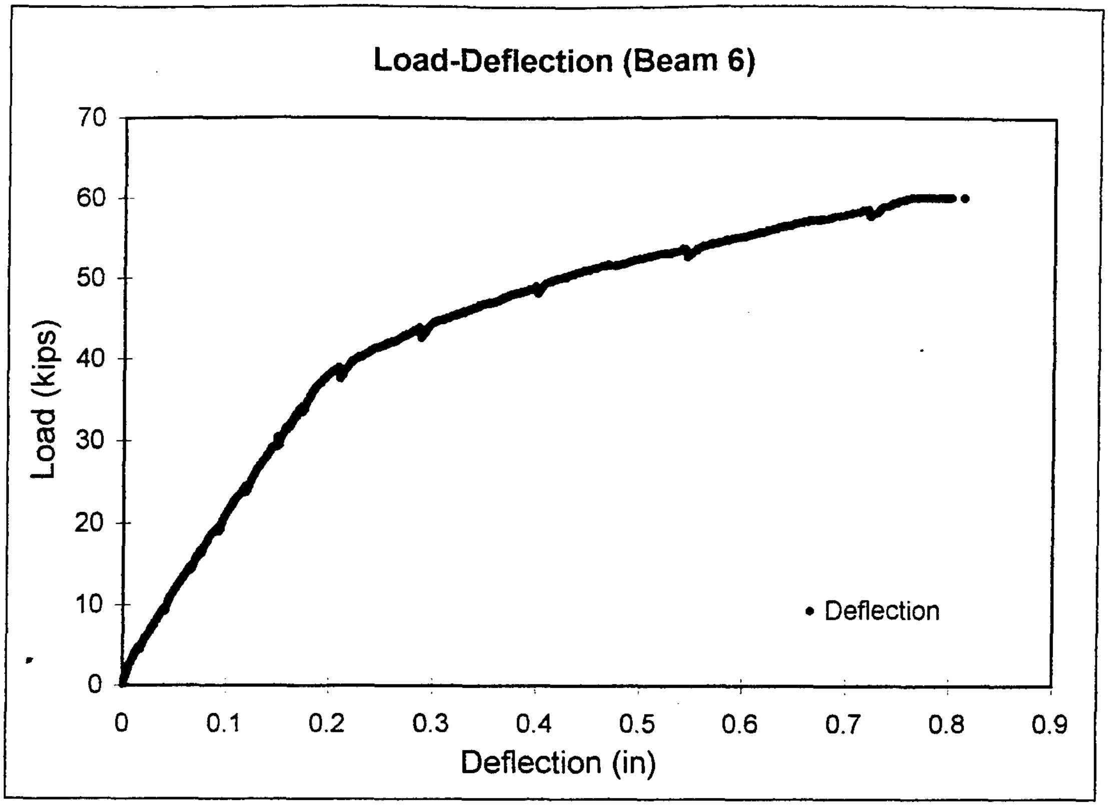

Figure A5.4 Load-Deflection Curve (Beam 6)

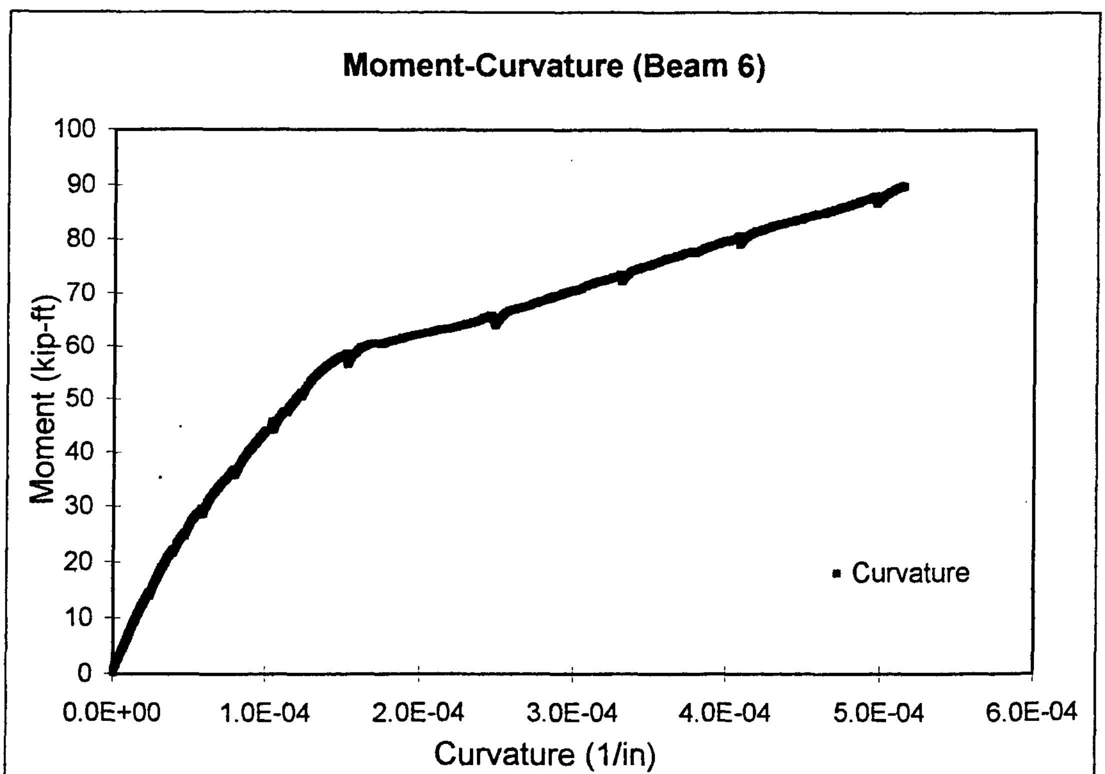

Figure A5.5 Moment-Curvature Curve (Beam 6)

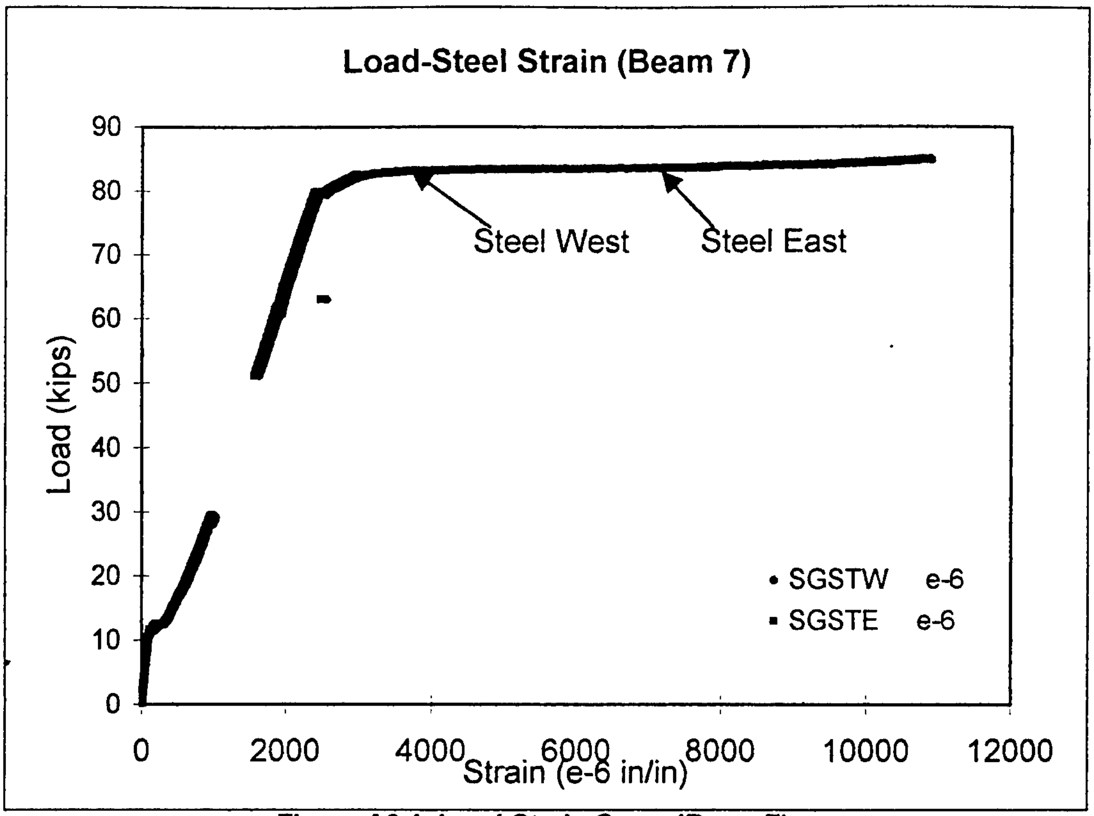

Figure A6.1 Load-Strain Curve (Beam 7)

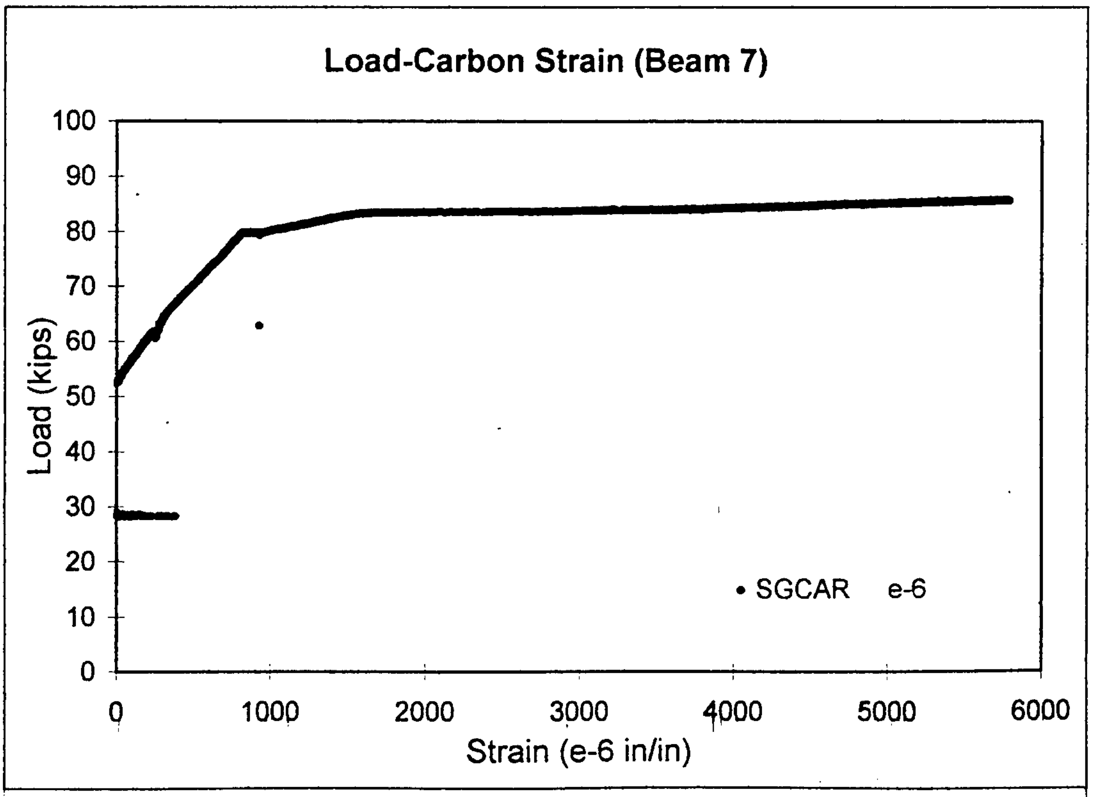

Figure A6.2 Load-Strain Curve (Beam 7)

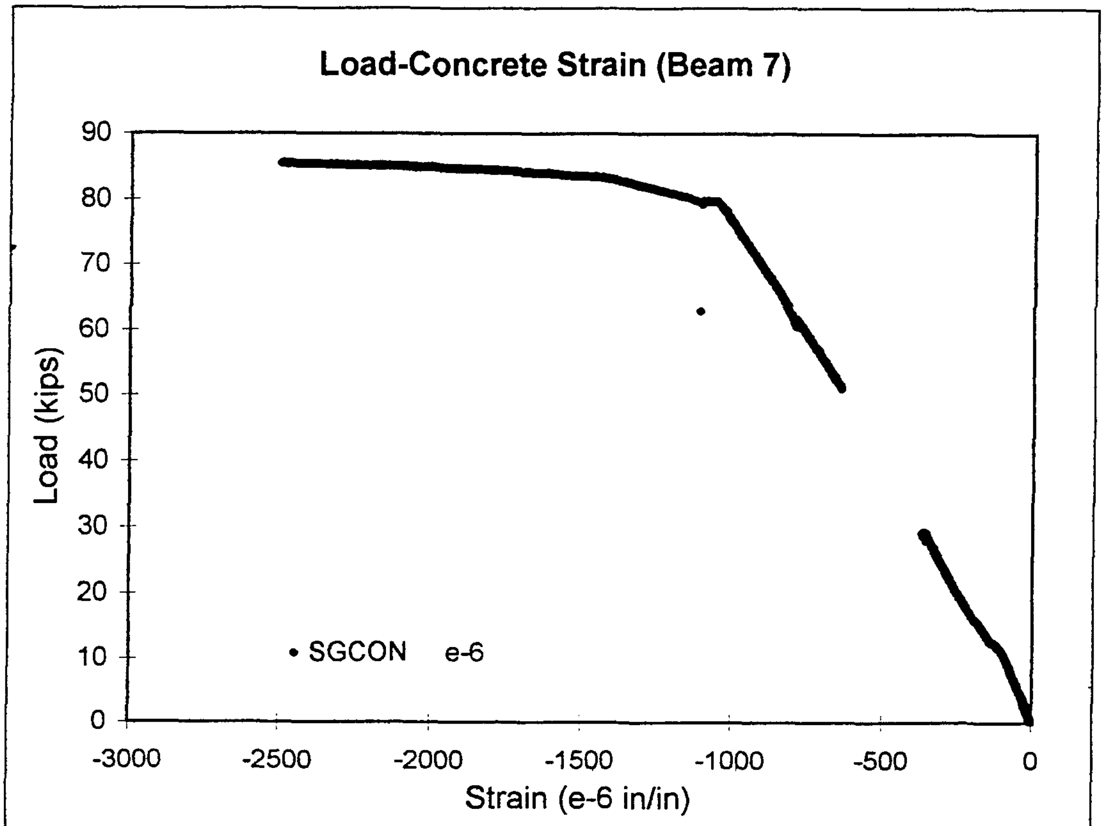

Figure A6.3 Load-Strain Curve (Beam 7)

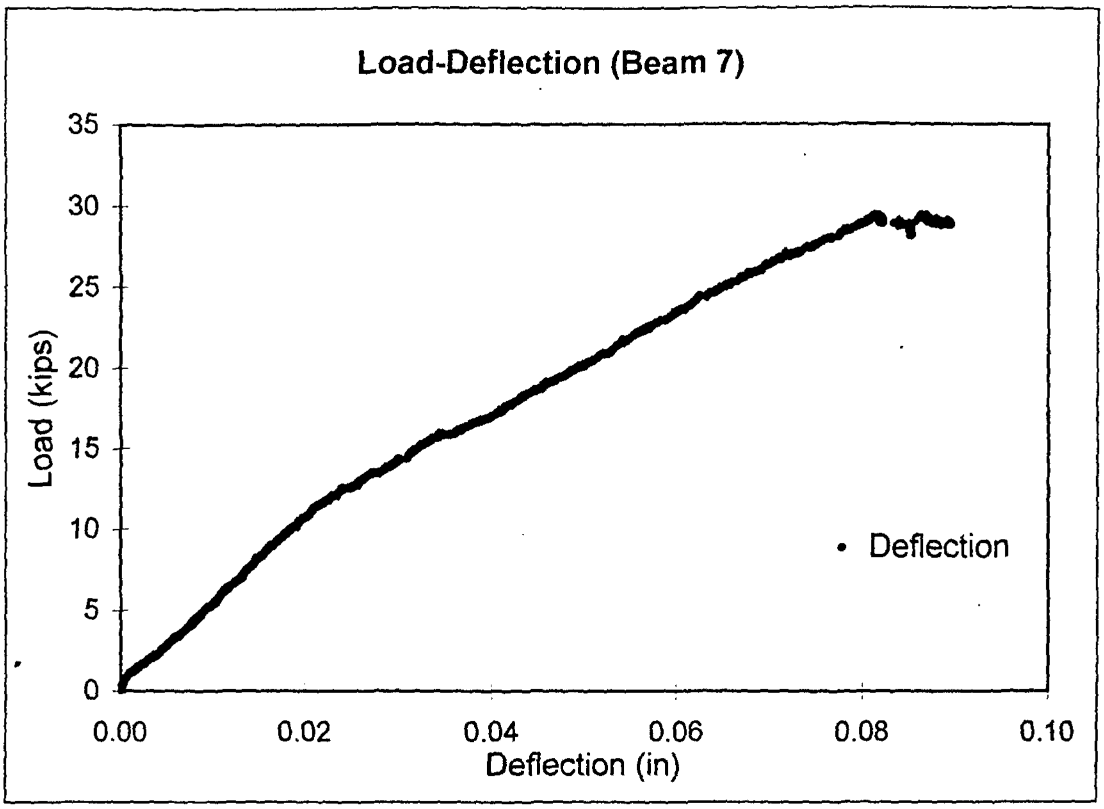

Figure A6.4 Load-Deflection Curve (Beam 7)

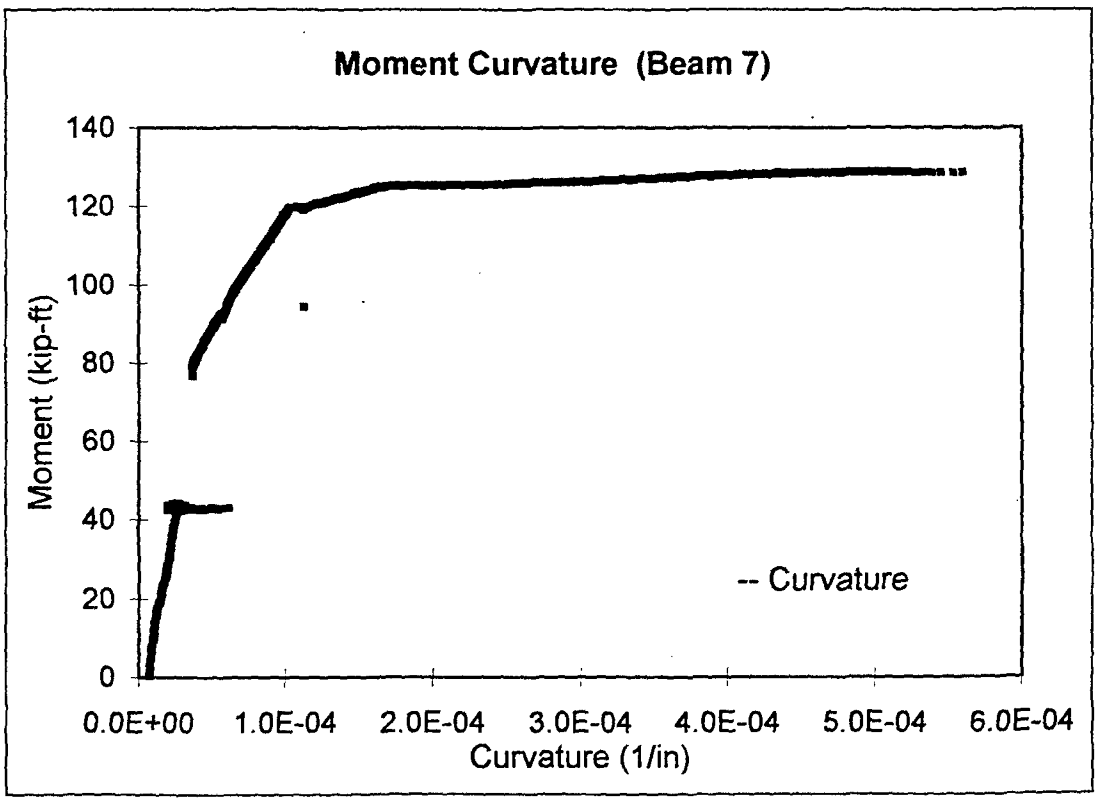

Figure A6.5 Moment-Curvature Curve (Beam 7)

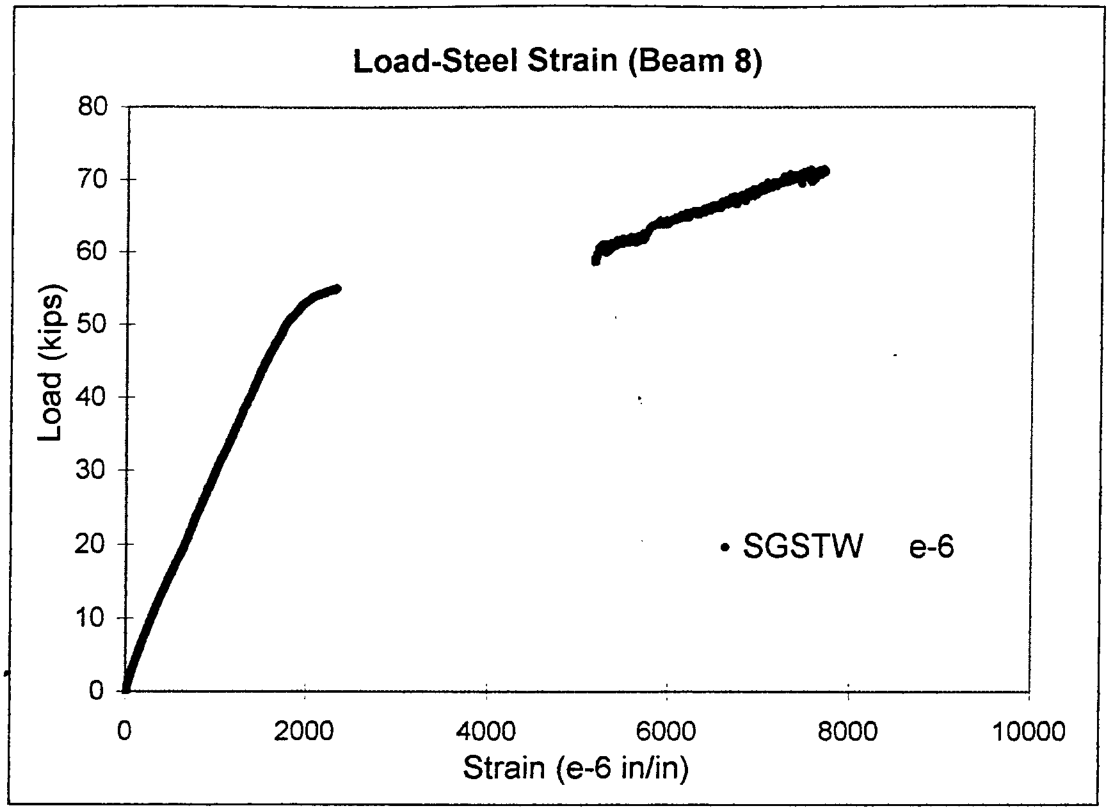

Figure A7.1 Load-Strain Curve (Beam 8)

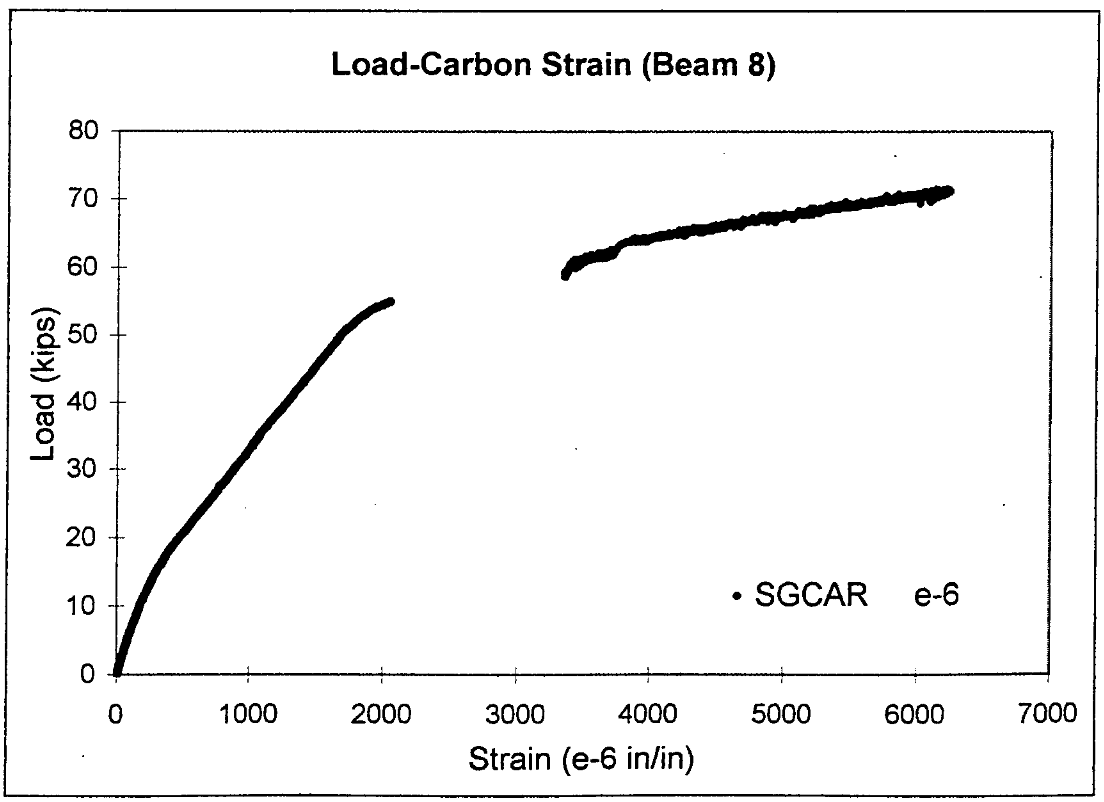

Figure A7.2 Load-Strain Curve (Beam 8)

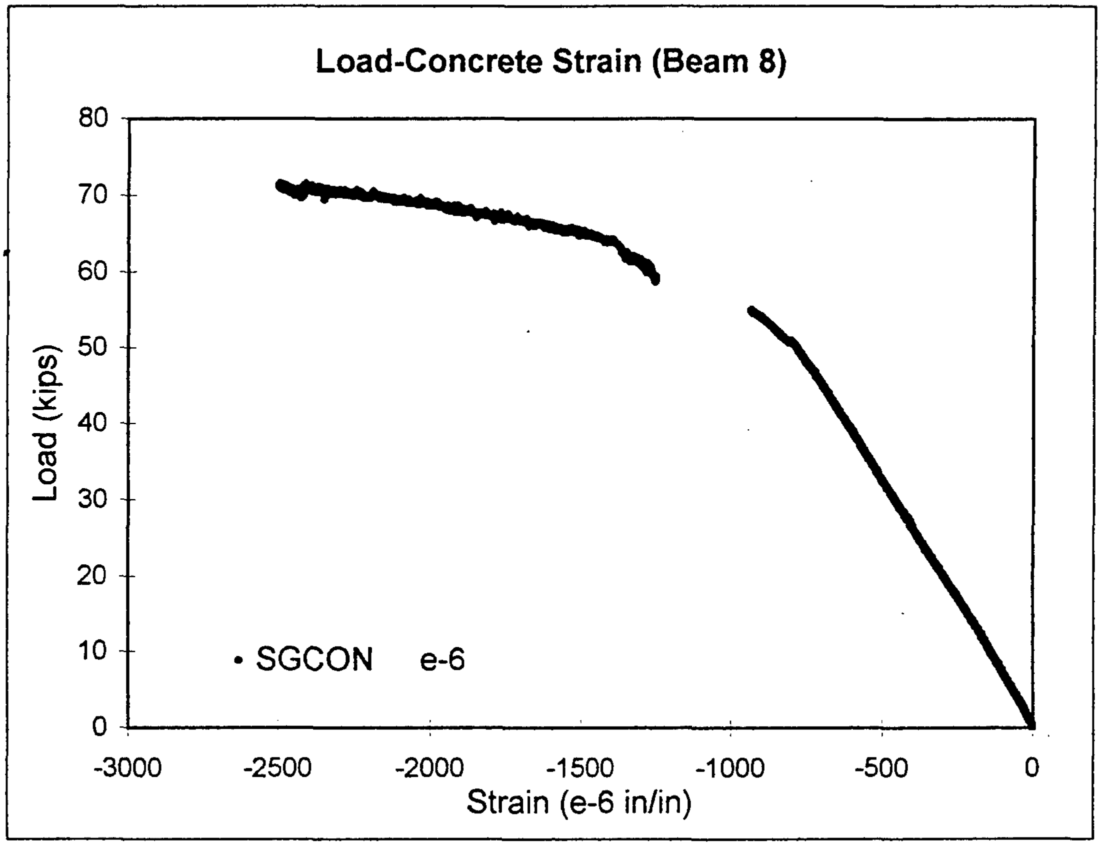

Figure A7.3 Load-Strain Curve (Beam 8)

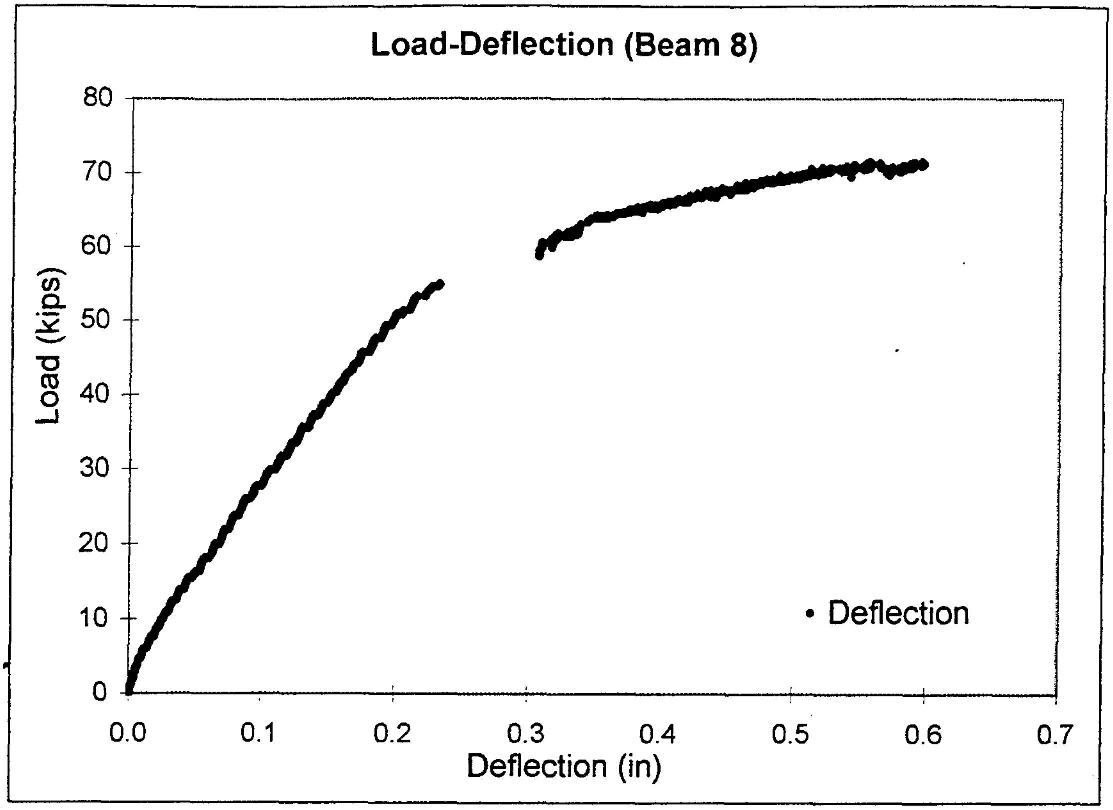

Figure A7.4 Load-Deflection Curve (Beam 8)

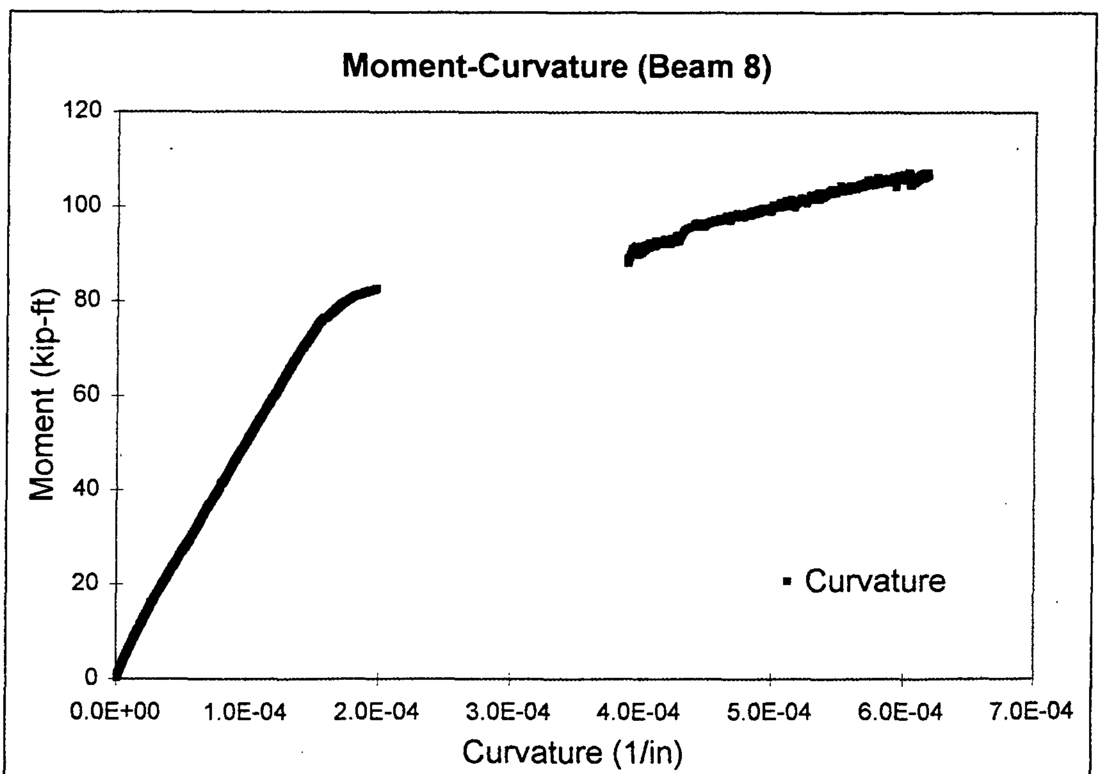

Figure A7.5 Moment-Curvature Curve (Beam 8)

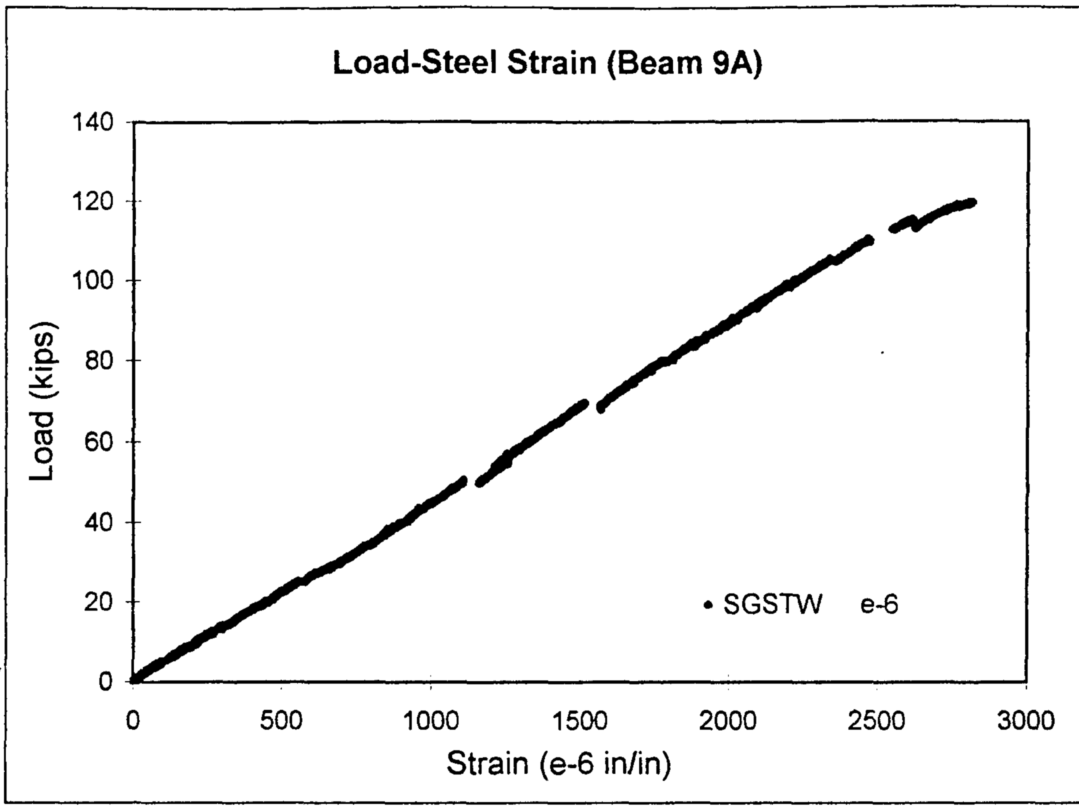

Figure A8.1 Load-Strain Curve (Beam 9A)

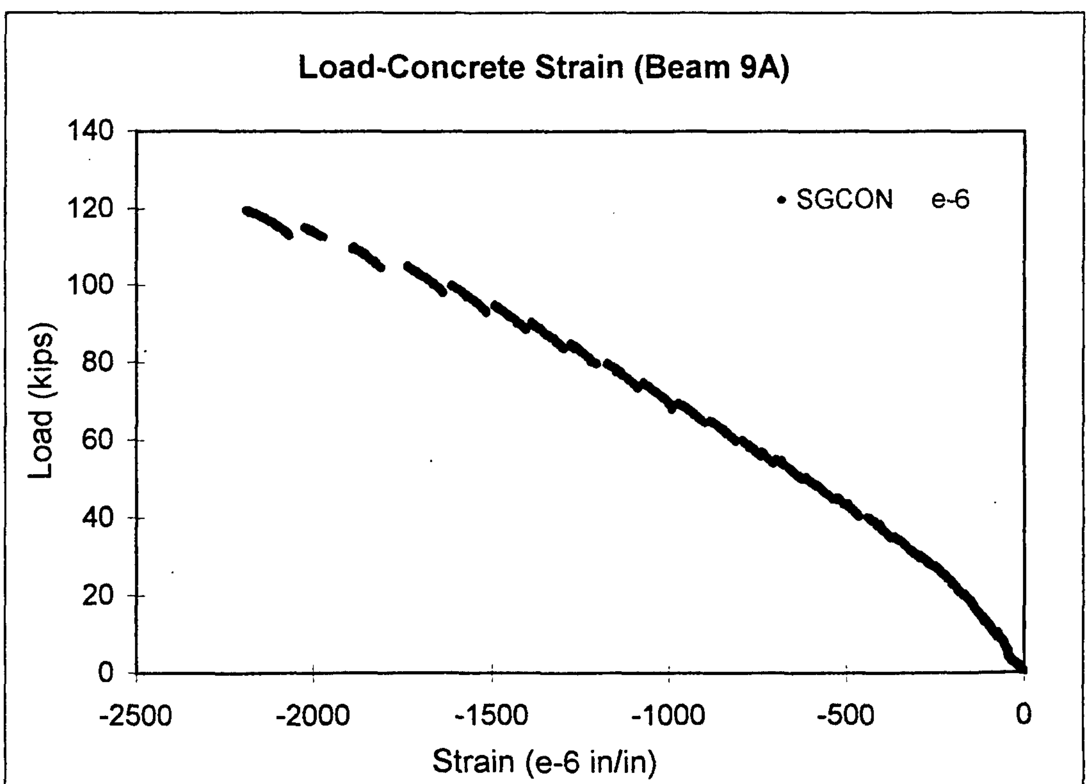

Figure A8.3 Load-Strain Curve (Beam 9A)

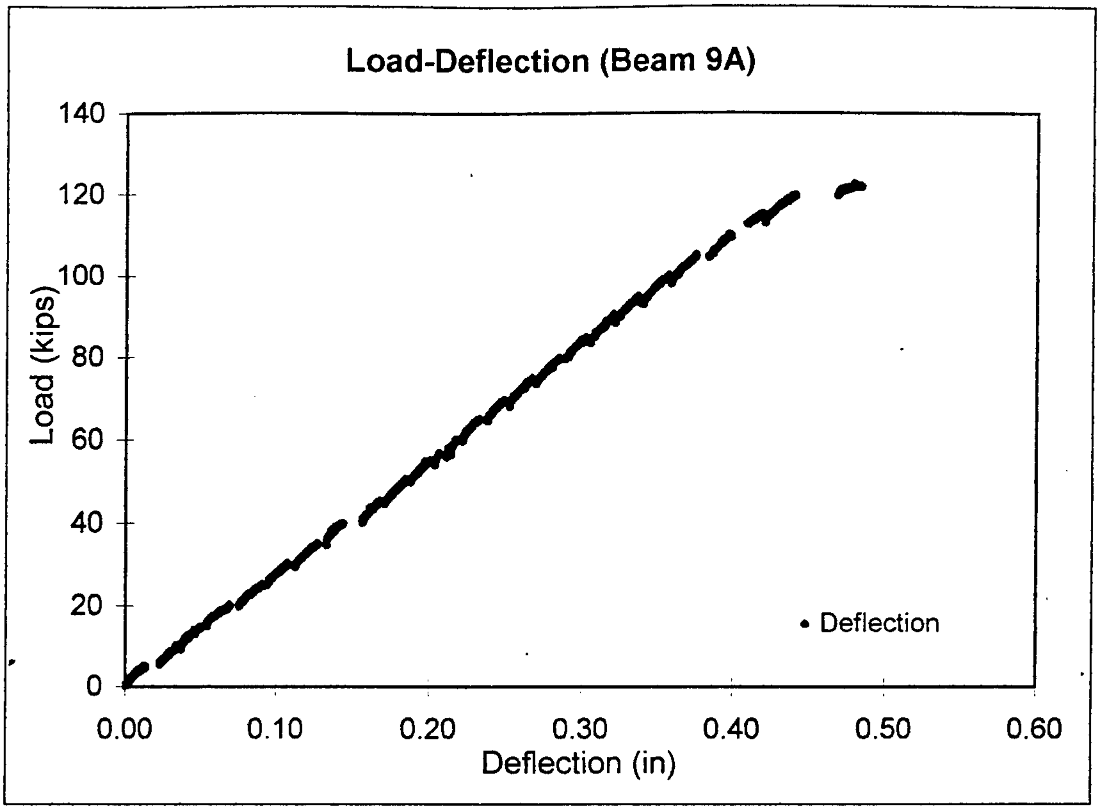

Figure A8.4 Load-Deflection Curve (Beam 9A)

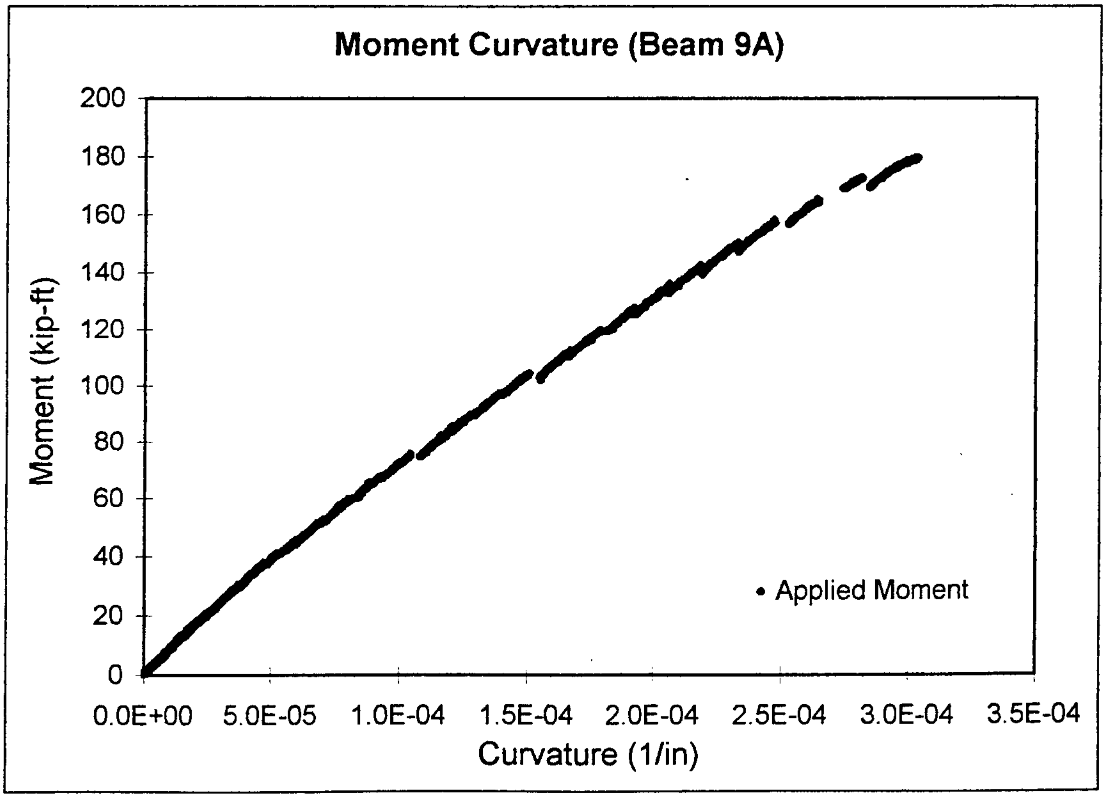

Figure A8.5 Moment-Curvature Curve (Beam 9A)

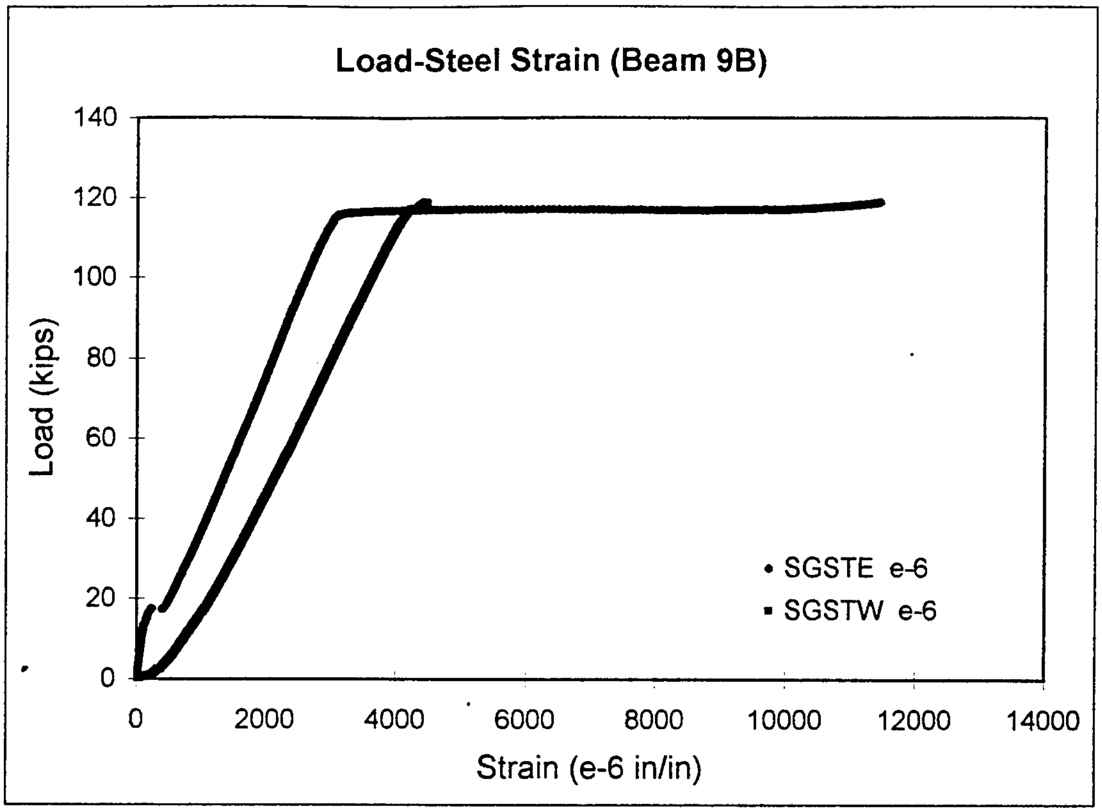

Figure A9.1 Load-Strain Curve (Beam 9B)

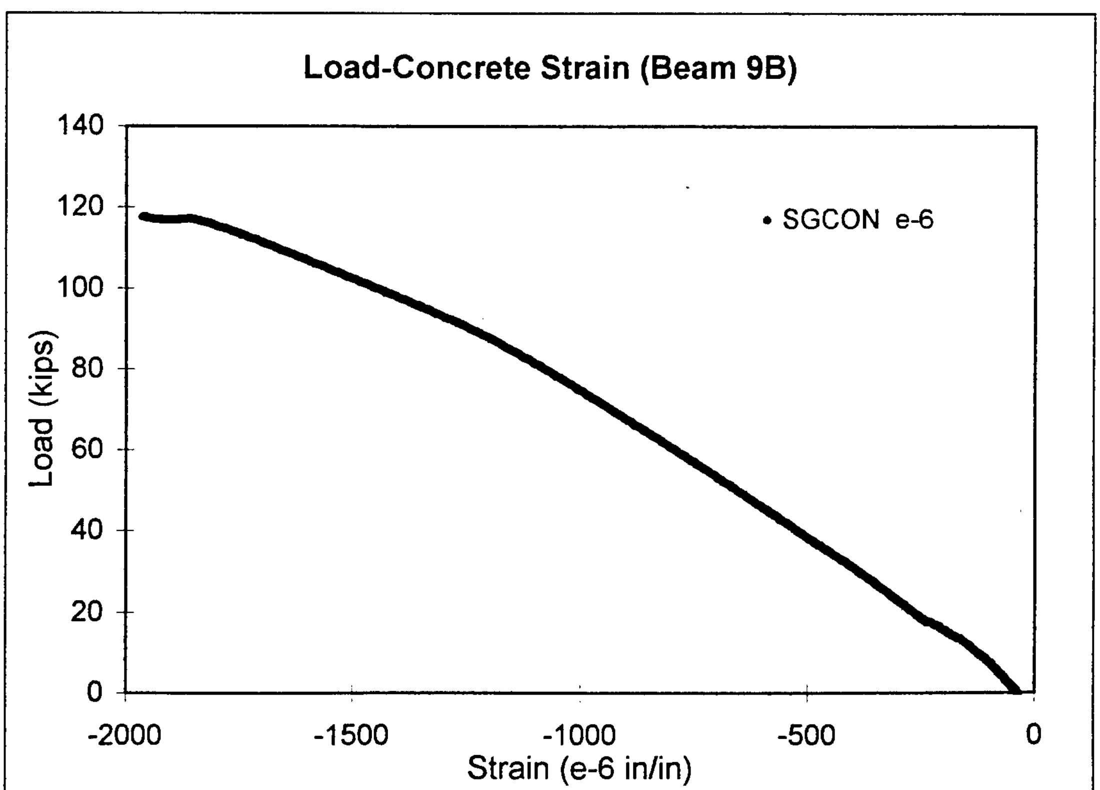

Figure A9.3 Load-Strain Curve (Beam 9B)

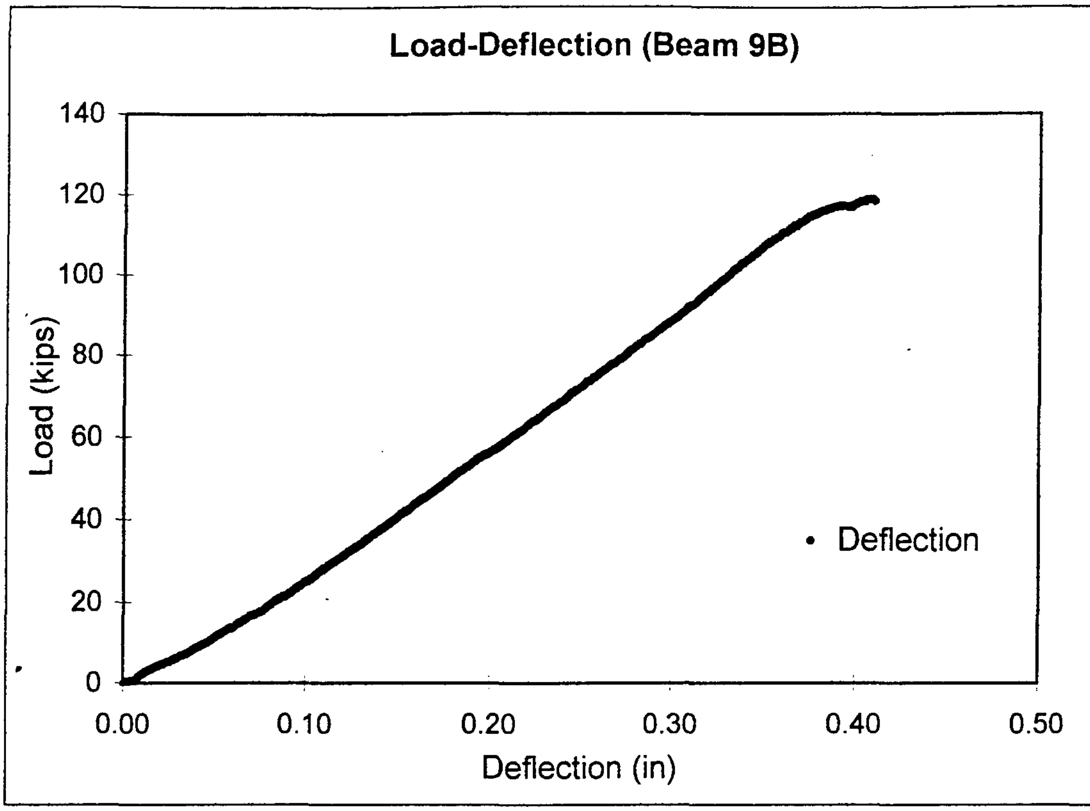

Figure A9.4 Load-Deflection Curve (Beam 9B)

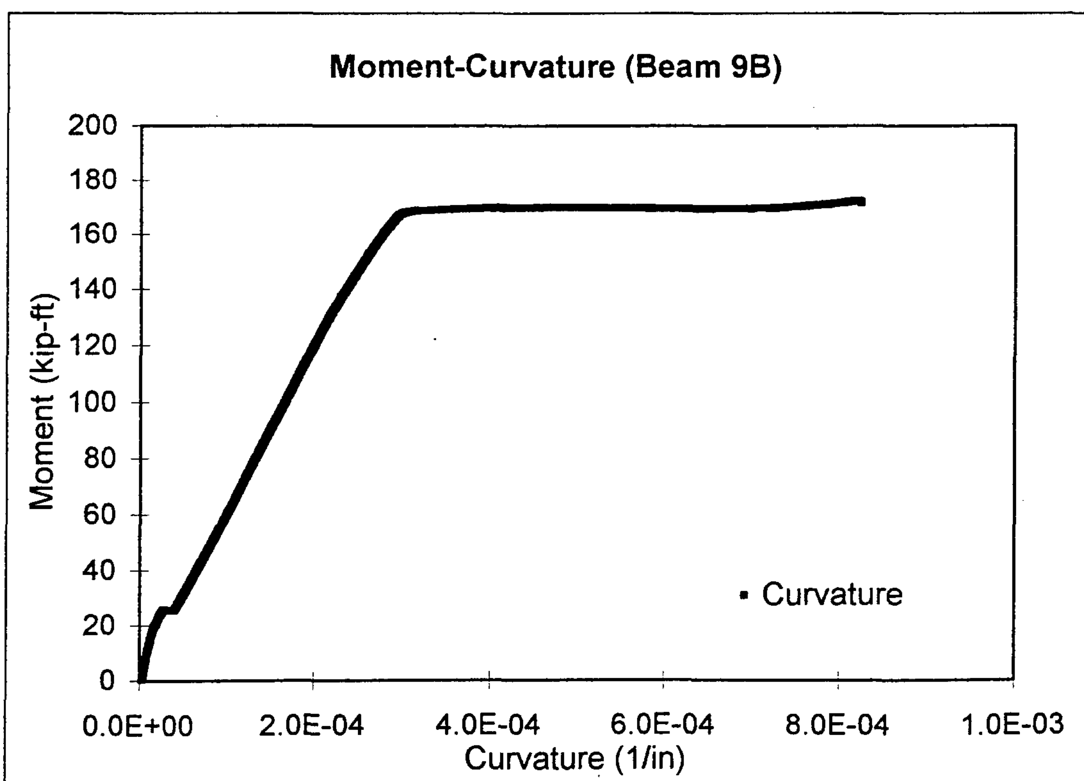

Figure A9.5 Moment-Curvature Curve (Beam 9B)

APPENDIX A10
TYPICAL COMCURVE OUTPUT

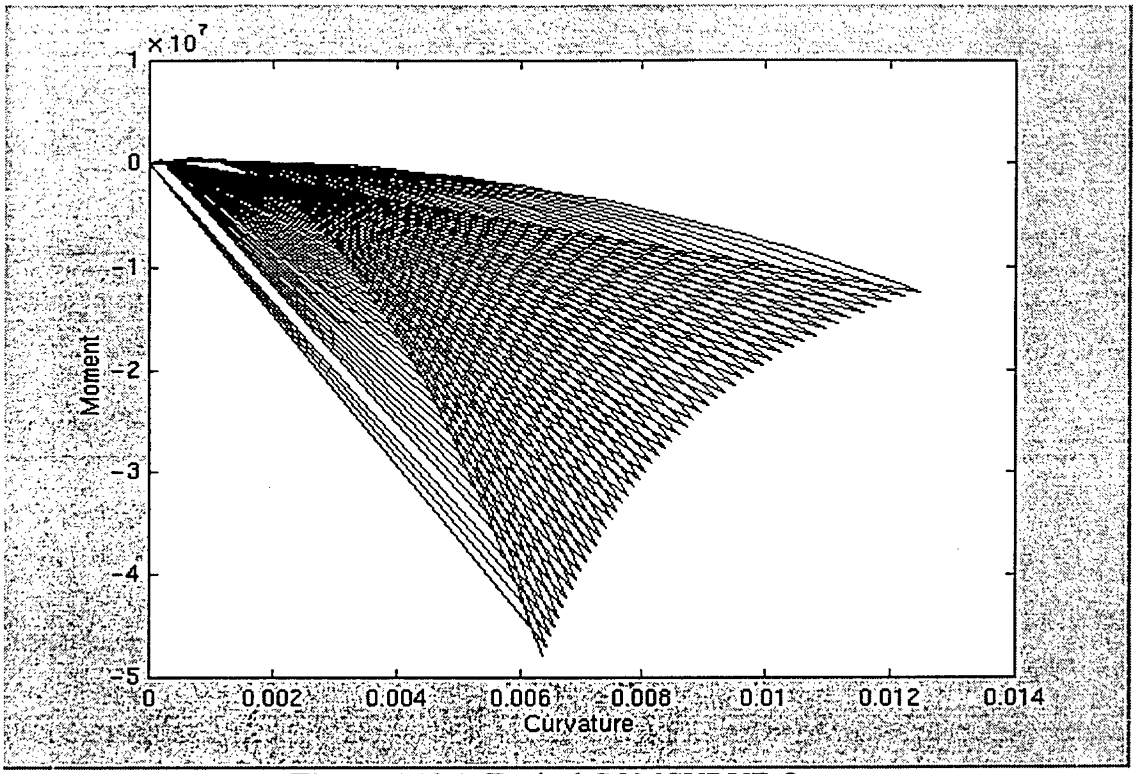

Figure A10.1 Typical COMCURVE Output

A10.1 Introduction

The Matlab plot shown above is a typical output for the COMCURVE program. It shows the total envelope of moment-curvature pairs possible for specimens of the size tested. The program was written based on modified ACI guidelines for the purpose investigating whether modifications could accurately predict experimental behavior. In each case tested, the experimental moment-curvature curves lay at approximately the same location inside the COMCURVE envelope. This suggests that there is some defining relationship based on existing ACI guidelines which can be used to predict moment-curvature beam response. This relationship requires further investigation.

APPENDIX A11
SIKA SPREADHSEET OUTPUT

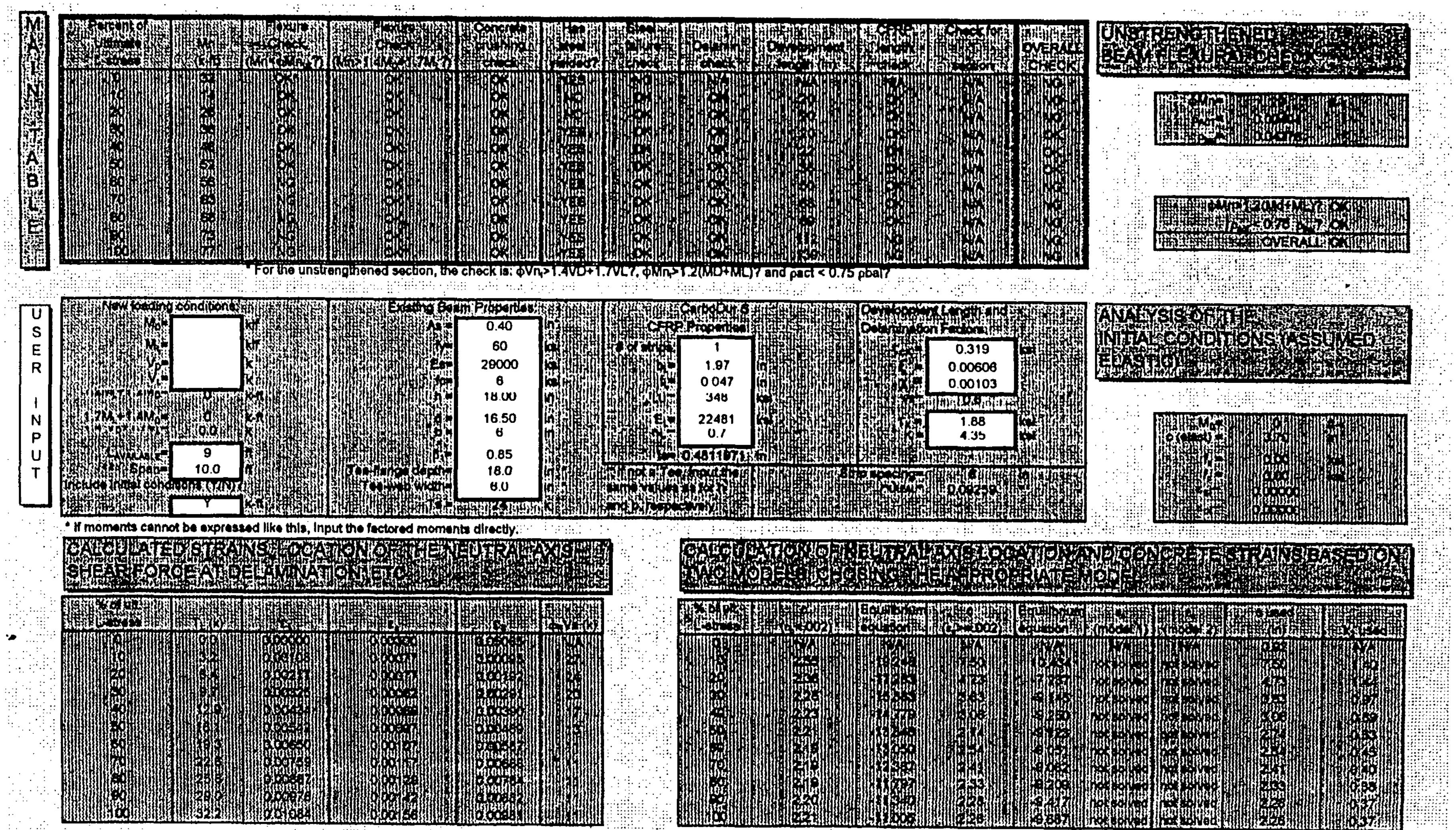

Fig. A11.1 Sika Results for Beam 4A

MAIN TABLE

Percent of Ultimate L-stress	Mn (k-ft)	Flexure Check (Mn<φMn?)	Flexure Check (Mn>1.4Mn+1.7M?)	Concrete crushing check	Has steel yielded?	Steel failure check	Delamin check	Development length (in)	CFRP length check	Check for section	OVERALL CHECK
0	[illegible]	OK	OK	OK	YES	NG	N/A	N/A	N/A	N/A	NG
10	[illegible]	OK	OK	OK	[illegible]	OK	OK	[illegible]	OK	N/A	[illegible]
20	[illegible]	OK	OK	OK	[illegible]	OK	OK	[illegible]	OK	N/A	[illegible]
30	[illegible]	OK	OK	OK	[illegible]	OK	OK	[illegible]	OK	N/A	[illegible]
40	[illegible]	OK	OK	OK	[illegible]	OK	OK	[illegible]	OK	N/A	[illegible]
50	[illegible]	OK	OK	OK	[illegible]	OK	OK	[illegible]	OK	N/A	[illegible]
60	[illegible]	NG	OK	OK	[illegible]	OK	OK	[illegible]	OK	N/A	NG
70	[illegible]	NG	OK	OK	[illegible]	OK	OK	[illegible]	OK	N/A	NG
80	[illegible]	NG	OK	OK	[illegible]	OK	OK	[illegible]	OK	N/A	NG
90	[illegible]	NG	OK	OK	[illegible]	OK	OK	[illegible]	NG	N/A	NG
100	[illegible]	NG	OK	OK	YES	OK	OK	[illegible]	NG	N/A	NG

* For the unstrengthened section, the check is: φVn>1.4VD+1.7VL?, φMn>1.2(MD+ML)? and ρact < 0.75 ρbal?

UNSTRENGTHENED BEAM FLEXURAL CHECK

φMn>1.2(MD+ML)? OK

OVERALL OK

USER INPUT

New loading conditions:

Span = 9 ft

10.0 ft

Include initial conditions (Y/N)? Y

Existing Beam Properties:

As =	0.40	in²
fy =	60	ksi
Es =	29000	ksi
f'c =	6	ksi
h =	18.00	in
d =	16.50	in
b =	8	in
β1 =	0.85	
The flange depth =	18.0	in
The web width =	8.0	in

CarboDur ® CFRP Properties:

# of strips =	1	
b =	3.15	in
t =	0.047	in
f =	348	ksi
E =	22481	ksi
	0.7	
	0.481197	in

Development Length and Delamination Factors:

	0.319	ksi
	0.00606	
	0.00103	
	1.88	ksi
	4.35	ksi

* If moments cannot be expressed like this, input the factored moments directly.

ANALYSIS OF THE INITIAL CONDITIONS (ASSUMED ELASTIC)

c (elast) =

CALCULATED STRAINS, LOCATION OF THE NEUTRAL AXIS, SHEAR FORCE AT DELAMINATION, ETC.

% of ult L-stress	T (k)	ε_s	ε_f	ε_c	ϕV_s (k)
0	0.0	0.00000	0.00000	[illegible]	N/A
10	5.2	0.00108	[illegible]	[illegible]	[illegible]
20	10.3	0.00217	[illegible]	[illegible]	[illegible]
30	15.5	0.00325	[illegible]	[illegible]	[illegible]
40	20.6	0.00434	[illegible]	[illegible]	[illegible]
50	25.8	0.00542	[illegible]	[illegible]	[illegible]
60	30.9	0.00650	[illegible]	[illegible]	[illegible]
70	[illegible]	0.00759	[illegible]	[illegible]	[illegible]
80	41.2	0.00867	0.00129	[illegible]	2
90	46.4	0.00976	0.00142	[illegible]	2
100	[illegible]	0.01084	0.00156	[illegible]	2

CALCULATION OF NEUTRAL AXIS LOCATION AND CONCRETE STRAINS BASED ON TWO MODELS, CHOOSING THE APPROPRIATE MODEL

% of ult L-stress	c (ε_c<.002)	Equilibrium equation	c (ε_c>=.002)	Equilibrium equation	c (model 1)	c (model 2)	c used (in)	ε_c used
0	N/A	N/A	N/A	N/A	N/A	N/A	[illegible]	N/A
10	[illegible]	[illegible]	[illegible]	[illegible]	not solved	not solved	[illegible]	[illegible]
20	[illegible]	[illegible]	[illegible]	[illegible]	not solved	not solved	[illegible]	[illegible]
30	[illegible]	[illegible]	[illegible]	[illegible]	not solved	not solved	[illegible]	[illegible]
40	[illegible]	[illegible]	[illegible]	[illegible]	not solved	not solved	[illegible]	[illegible]
50	[illegible]	[illegible]	[illegible]	[illegible]	not solved	not solved	[illegible]	[illegible]
60	[illegible]	[illegible]	[illegible]	[illegible]	not solved	not solved	[illegible]	[illegible]
70	[illegible]	[illegible]	[illegible]	[illegible]	not solved	not solved	[illegible]	[illegible]
80	[illegible]	[illegible]	[illegible]	[illegible]	not solved	not solved	[illegible]	[illegible]
90	2.20	[illegible]	2.26	[illegible]	not solved	not solved	2.26	[illegible]
100	[illegible]	[illegible]	2.25	[illegible]	not solved	not solved	2.26	[illegible]

VERSION 1.0

Fig. A11.2 Sika Results for Beam 4B

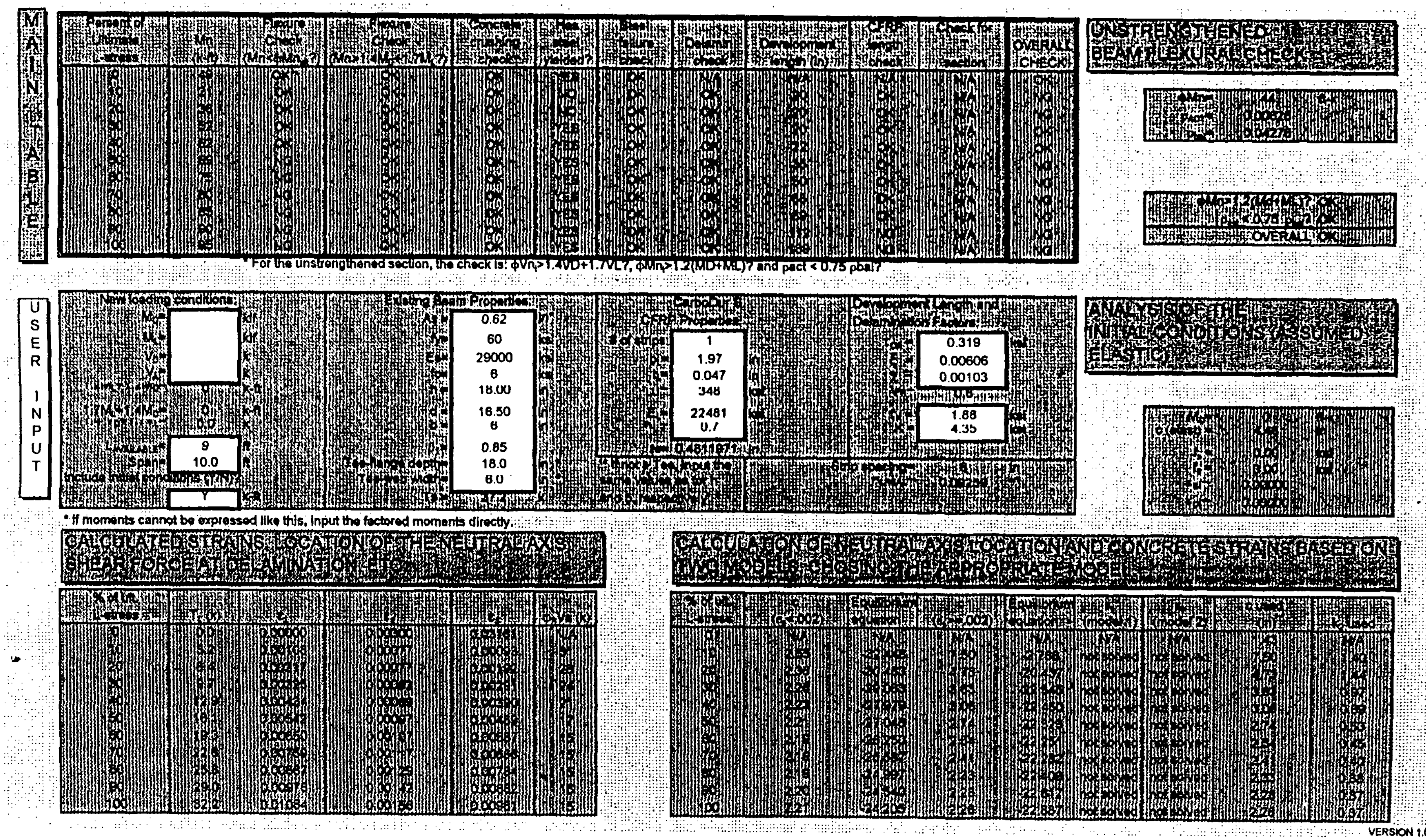

Fig. A11.3 Sika Results for Beam 5

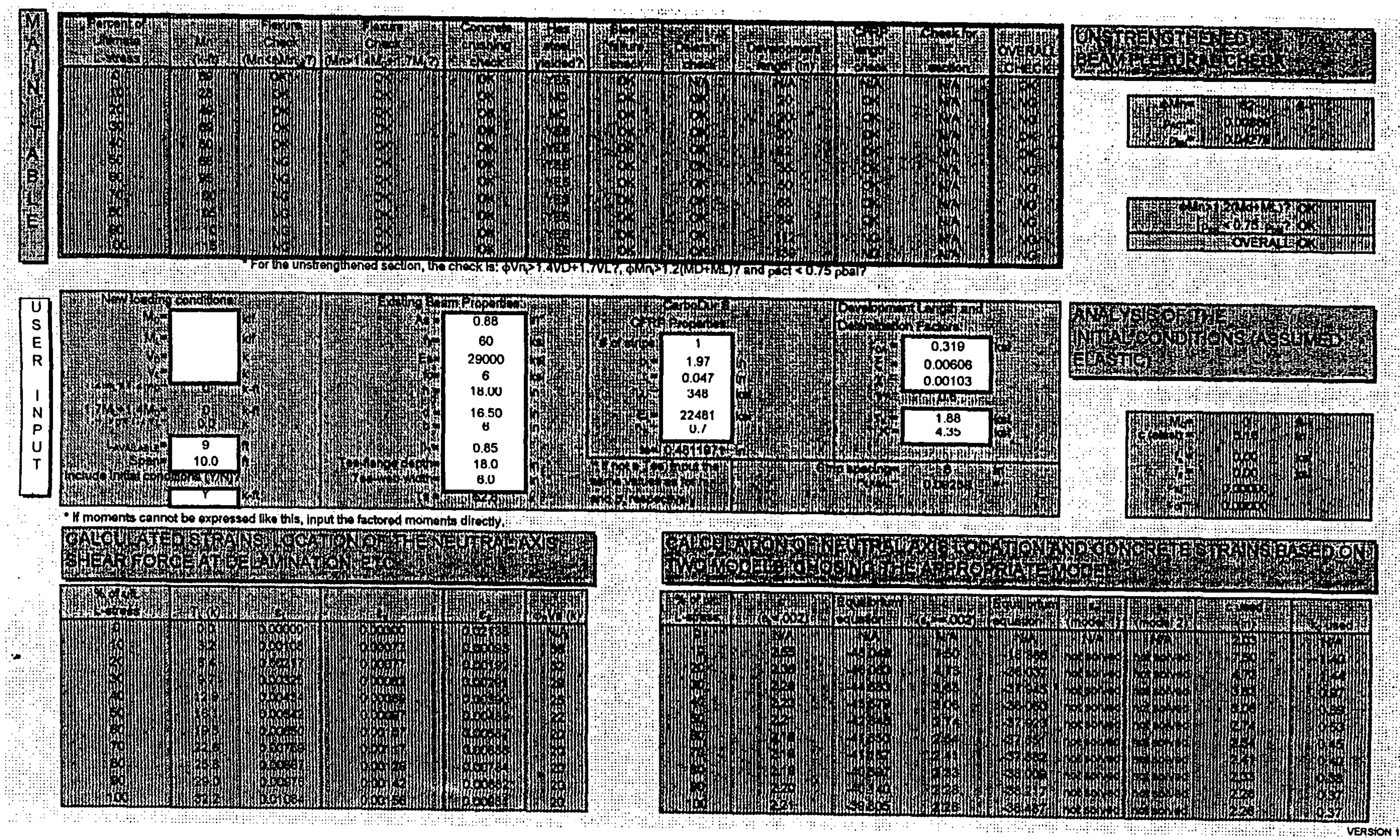

Fig. A11.4 Sika Results for Beam 6

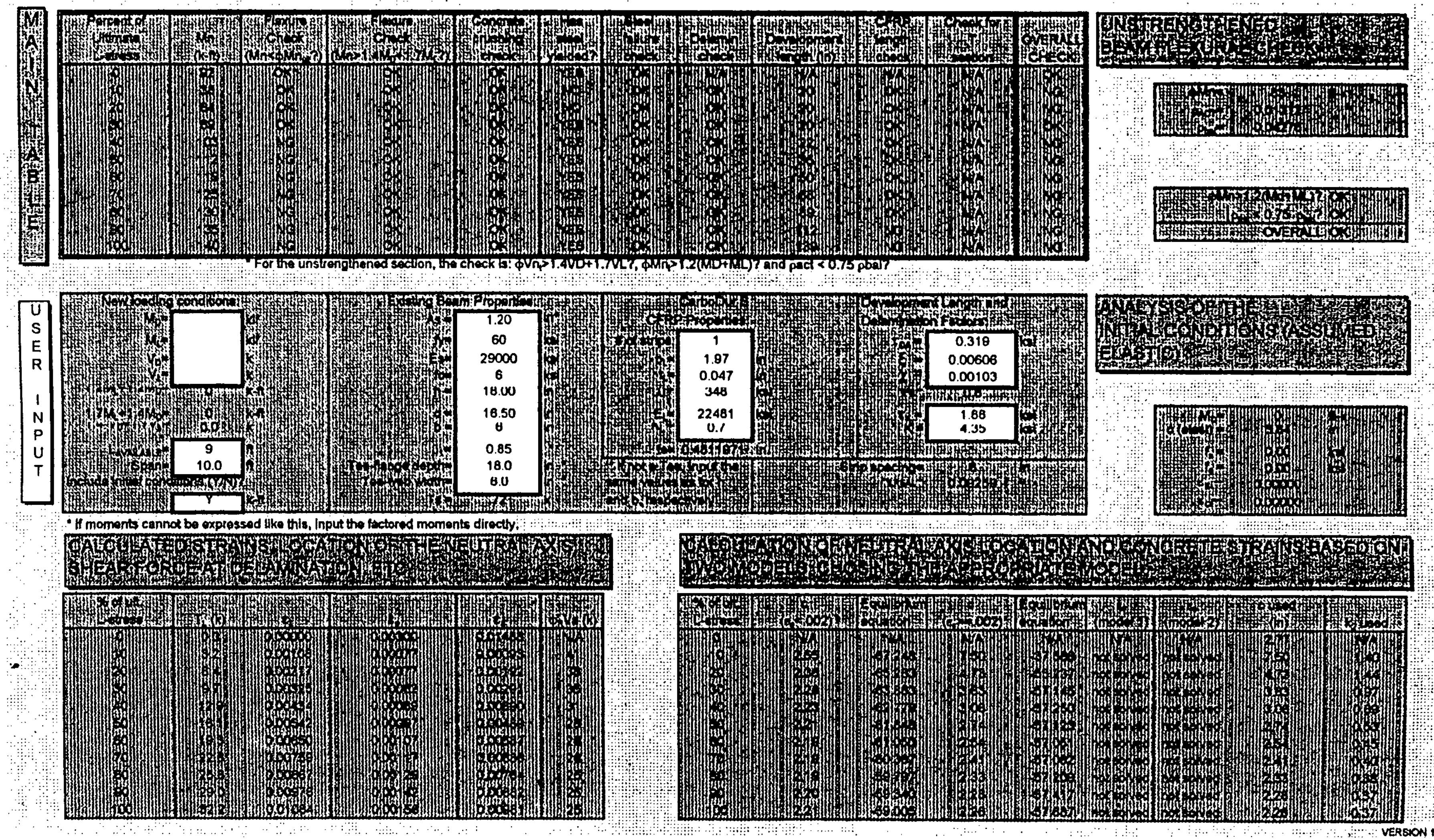

Fig. A11.5 Sika Results for Beam 7

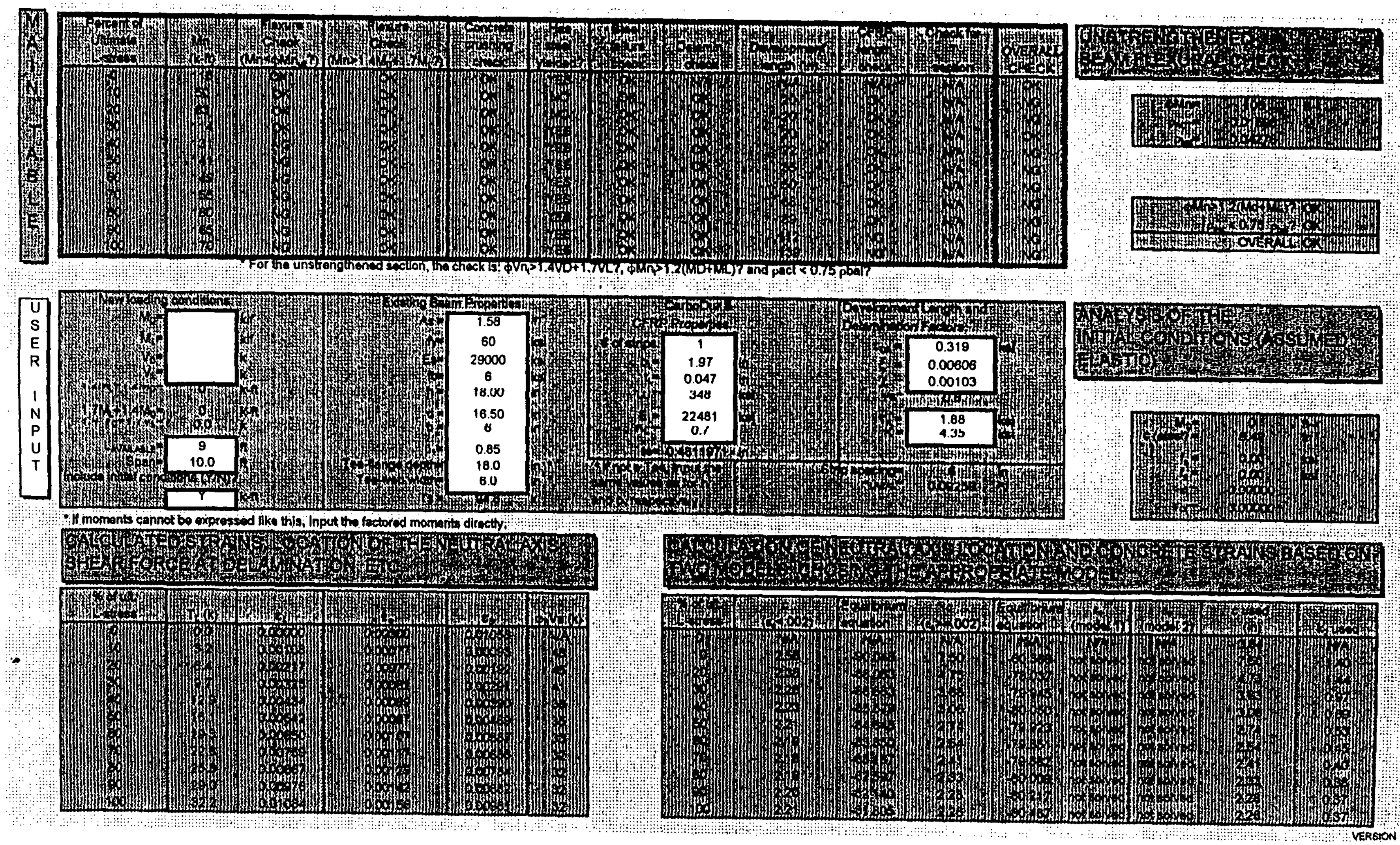

Fig. A11.6 Sika Results for Beam 8

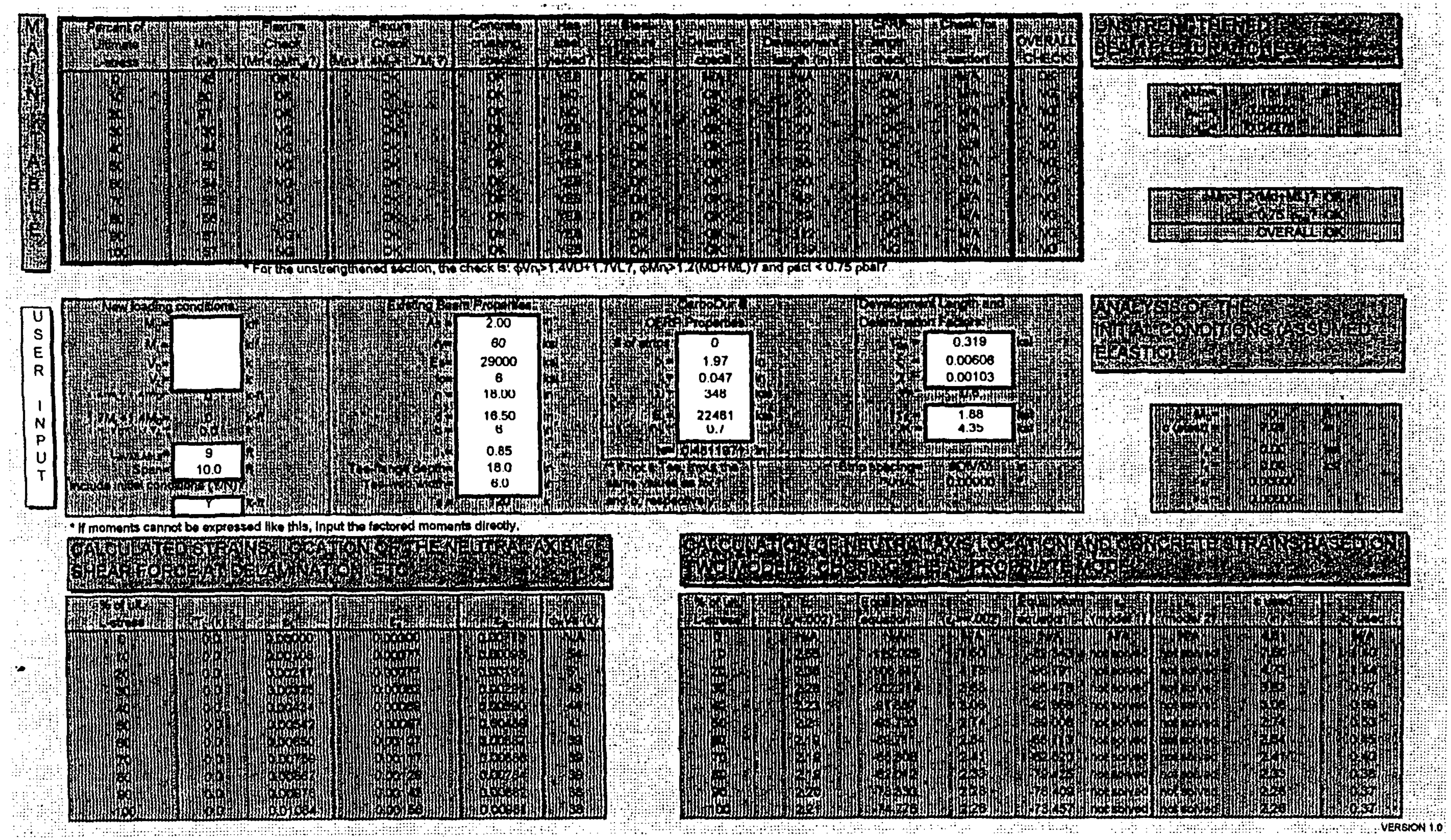

Fig. A11.7 Sika Results for Beam 9A

MAIN TABLE

Percent of Ultimate L-stress	Mn (k-ft)	Flexure Check (Mn>ϕMu ?)	(Mn>1.4MD+1.7ML ?) Flexure Check	Concrete crushing check	Has steel yielded?	Bias failure check	Delamin. check	Development length (in)	CFRP length check	Check for section	OVERALL CHECK
0	45	OK	OK	OK	YES	OK	NA	NA	NA	NA	OK
10	[illegible]	OK	OK	OK	NO	OK	OK	[illegible]	OK	NA	[illegible]
20	[illegible]	OK	OK	OK	NO	OK	OK	[illegible]	OK	NA	[illegible]
30	[illegible]	OK	OK	OK	YES	OK	OK	[illegible]	OK	NA	[illegible]
40	[illegible]	[illegible]	OK	OK	YES	OK	OK	[illegible]	OK	NA	[illegible]
50	[illegible]	NG	OK	OK	YES	OK	OK	[illegible]	OK	NA	NG
60	[illegible]	NG	OK	OK	YES	OK	OK	[illegible]	OK	NA	NG
70	[illegible]	NG	OK	OK	YES	OK	OK	[illegible]	OK	NA	NG
80	[illegible]	NG	OK	OK	YES	OK	OK	[illegible]	OK	NA	NG
90	[illegible]	NG	OK	OK	YES	OK	OK	[illegible]	[illegible]	NA	NG
100	203	NG	OK	OK	YES	OK	OK	[illegible]	[illegible]	NA	NG

* For the unstrengthened section, the check is: $\phi V_n > 1.4VD+1.7VL$?, $\phi M_n > 1.2(MD+ML)$? and $\rho act < 0.75\ \rho bal$?

UNSTRENGTHENED BEAM FLEXURAL CHECK

ϕMn	[illegible]	[illegible]
[illegible]	0.0202	[illegible]
[illegible]	0.0427	[illegible]

ϕMn>1.2(MD+ML)? OK
ρact < 0.75 ρbal ? OK
OVERALL OK

USER INPUT

New loading conditions:

M_D =		k-ft
M_L =		k-ft
V_D =		k
V_L =		k
[illegible]	0	k-ft
1.7ML+1.4MD =	0	k-ft
[illegible]	0.0	k
Lavalue =	9	ft
Span =	10.0	ft
Include initial conditions (Y/N)?	Y	

Existing Beam Properties:

As =	2.00	in²
fy =	60	ksi
Es =	29000	ksi
f'c =	6	ksi
h =	18.00	in
d =	16.50	in
b =	6	in
β1 =	0.85	
Tee-flange depth =	18.0	in
Tee-web width =	6.0	in
[illegible]	[illegible]	k

CarboDur® CFRP Properties:

# of strips =	1	
[illegible]	1.97	in
[illegible]	0.047	in
[illegible]	348	ksi
[illegible]	22481	ksi
[illegible]	0.7	
[illegible] = 0.48107		in

* If not a Tee, input the same values as for b and h, respectively.

Development Length and Delamination Factors:

[illegible]	0.319	ksi
[illegible]	0.00606	
[illegible]	0.00103	
[illegible]	[illegible]	
[illegible]	1.88	ksi
K =	4.35	ksi

Stirrup spacing = 8 in
[illegible] = 0.08258 in

* If moments cannot be expressed like this, input the factored moments directly.

ANALYSIS OF THE INITIAL CONDITIONS (ASSUMED ELASTIC)

Init. Mom.	[illegible]	[illegible]
[illegible]	[illegible]	[illegible]
[illegible]	0.00	[illegible]
[illegible]	0.50	[illegible]
[illegible]	0.00000	
[illegible]	0.00000	

CALCULATED STRAINS, LOCATION OF THE NEUTRAL AXIS, SHEAR FORCE AT DELAMINATION, ETC.

% of ult. L-stress	T (k)	ε_c	ε	ε_s	ϕ Vd (k)
0	0.0	0.00000	[illegible]	[illegible]	NA
10	[illegible]	[illegible]	[illegible]	[illegible]	[illegible]
20	[illegible]	[illegible]	[illegible]	[illegible]	[illegible]
30	[illegible]	[illegible]	[illegible]	[illegible]	[illegible]
40	[illegible]	[illegible]	[illegible]	[illegible]	[illegible]
50	[illegible]	[illegible]	[illegible]	[illegible]	[illegible]
60	[illegible]	[illegible]	[illegible]	[illegible]	[illegible]
70	22.5	[illegible]	[illegible]	[illegible]	40
80	[illegible]	[illegible]	[illegible]	[illegible]	[illegible]
90	29.0	0.00975	[illegible]	[illegible]	40
100	32.2	0.01084	[illegible]	[illegible]	40

CALCULATION OF NEUTRAL AXIS LOCATION AND CONCRETE STRAINS BASED ON TWO MODELS. CHOSING THE APPROPRIATE MODEL.

% of ult. L-stress	c (ε_c<.002)	Equilibrium equation	c (ε_c>=.002)	Equilibrium equation	c (model 1)	c (model 2)	c used (in)	ε_c used
0	NA	NA	NA	NA	NA	NA	[illegible]	NA
10	[illegible]	[illegible]	[illegible]	[illegible]	not solved	not solved	[illegible]	[illegible]
20	[illegible]	[illegible]	[illegible]	[illegible]	not solved	not solved	[illegible]	[illegible]
30	[illegible]	[illegible]	[illegible]	[illegible]	not solved	not solved	[illegible]	0.97
40	[illegible]	[illegible]	[illegible]	[illegible]	not solved	not solved	[illegible]	[illegible]
50	[illegible]	[illegible]	[illegible]	[illegible]	not solved	not solved	[illegible]	[illegible]
60	[illegible]	[illegible]	[illegible]	[illegible]	not solved	not solved	[illegible]	[illegible]
70	[illegible]	[illegible]	[illegible]	[illegible]	not solved	not solved	[illegible]	[illegible]
80	[illegible]	[illegible]	[illegible]	[illegible]	not solved	not solved	[illegible]	[illegible]
90	2.20	107.840	2.28	[illegible]	not solved	not solved	[illegible]	[illegible]
100	2.21	[illegible]	2.28	[illegible]	not solved	not solved	[illegible]	[illegible]

VERSION 1.0

Fig. A11.8 Sika Results for Beam 9B